Quantification of Achilles tendon force and triceps surae muscle energy production during human locomotion: Consideration of monoarticular and biarticular mechanisms

Dissertation
zur Erlangung des akademischen Grades

Dr. phil.
im Fach Sportwissenschaft

eingereicht am 26 May 2023

an der Kultur-, Sozial- und Bildungswissenschaftlichen Fakultät der

Humboldt-Universität zu Berlin

von

Ing.- Biomedizinisch Mohamadreza Kharazi

Prof. Dr. Julia von Blumenthal
Präsidentin der
Humboldt-Universität zu Berlin

Prof. Dr. Claudia Becker
Dekanin der Kultur-, Sozial- und
Bildungswissenschaftlichen Fakultät

Gutachter:

1. Prof. Dr. Markus Tilp

2. Prof. Dr. Wolfgang Potthast

3. Prof. Dr. Bernd Wolfarth

Tag der mündlichen Prüfung: 21. July 2023

Zusammenfassung

Sehnen sind Bindegewebe und übertragen die von einem Muskel ausgeübte Kraft auf das Skelett. Die Beurteilung der Länge und Belastung der Achillessehne (AT) während der Fortbewegung ist wichtig für die Einschätzung des Verletzungsrisikos, die effiziente Interaktion zwischen Muskel und Sehne und die Trainingsplanung. Die derzeitigen In-vivo-Methoden zur Bewertung der AT-Belastung in der Biomechanik-Literatur weisen jedoch bestimmte Einschränkungen auf, die sorgfältig geprüft werden müssen. Ziel der ersten Studie war es daher, die mechanische Belastung und die Dehnungsenergie der AT während der Fortbewegung mit einer präzisen nicht-invasiven Methode zu bewerten. Die Messung der AT-Länge erfolgte unter Berücksichtigung der Krümmung des AT. Elf Teilnehmer wurden angewiesen, mit einer Geschwindigkeit von 1,4 m/s zu gehen und mit Geschwindigkeiten von 2,5 m/s und 3,5 m/s auf einem Laufband zu laufen. Die AT-Länge wurde definiert als die Entfernung zwischen dem Ursprung am Übergang des Musculus gastrocnemius medialis zur Sehne (GM-MTJ) und dem Ansatzpunkt am Fersenbein. Der GM-MTJ wurde dann auf die rekonstruierte Hautoberfläche projiziert, um eine Fehlausrichtung auszugleichen. Die Verschiebungen zwischen Haut und Knochen wurden während einer passiven Drehung (5°/s) des Sprunggelenks bewertet. Die Kraft- und Dehnungsenergie der AT während der Fortbewegung wurde berechnet, indem eine quadratische Funktion an die experimentelle Kraft-Längen-Kurve der Sehne angepasst wurde, die bei maximal willentlichen isometrischen Kontraktionen (MVC) ermittelt wurde. Die maximale Dehnung und Kraft, die die AT erfuhr, wurde von der Geschwindigkeit der Fortbewegung beeinflusst ($p < 0,05$), was zu Dehnungen zwischen 4,0 % und 4,9 % und Kräften zwischen 1,989 kN und 2,556 kN führte. Diese Werte wurden jedoch als unzureichend erachtet, um einen wirksamen Anreiz für die Sehnenanpassung zu bieten.

Die zweite Studie hatte zum Ziel, die Auswirkung der Gehgeschwindigkeit auf die mechanische Leistung und die am Sprunggelenk verrichtete Arbeit zu untersuchen, trotz einer Abnahme des intrinsischen Muskelkraftpotenzials der Muskeln Soleus (Sol) und GM. Die AT-Dehnung und -Kraft wurden mit der in der ersten Studie entwickelten Methode bei vier Gehgeschwindigkeiten (langsam 0,7 m.s-1, bevorzugt 1,4 m.s-1, Übergang 2,0 m.s-1 und maximal 2,6±0,3 m.s-1) gemessen. Die mechanische Leistung und Arbeit der AT-Kraft am Knöchelgelenk, der monoartikulären Sol am Knöchelgelenk und der biartikulären Gastrocnemii am Knöchel- und Kniegelenk wurden ebenfalls separat untersucht. Unsere

Ergebnisse zeigen, dass eine Erhöhung der Gehgeschwindigkeit zu einer 21%igen Abnahme der maximalen AT-Kraft bei den höheren Geschwindigkeiten im Vergleich zur bevorzugten Geschwindigkeit führt, wobei die Nettoarbeit der AT-Kraft am Sprunggelenk (ATF-Arbeit) in Abhängigkeit von der Gehgeschwindigkeit zunahm. Zusätzlich trugen eine frühere Plantarflexion, eine erhöhte elektromyografische Aktivität der Sol- und GM-Muskeln und eine Energieübertragung vom Knie zum Sprunggelenk über die biartikulären Gastrocnemii zu einem 1,7- bzw. 2,4-fachen Anstieg der ATF-Nettoarbeit bei der Übergangs- bzw. Höchstgeschwindigkeit bei. Diese Ergebnisse deuten darauf hin, dass der monoartikuläre Sol-Muskel die geleistete kontraktile Nettoarbeit erhöht, während die biartikulären Gastrocnemii durch den Einsatz biartikulärer Mechanismen zur geschwindigkeitsbedingten Erhöhung der Netto-ATF-Arbeit beitragen. Diese Studie liefert erstmals Beweise für die unterschiedliche mechanistische Beteiligung dieser Muskeln an der geschwindigkeitsbedingten Zunahme der Netto-ATF-Arbeit.

Die genaue Bestimmung der AT-Länge und -Belastung erfordert die Berücksichtigung ihrer Krümmung. In der ersten Studie verwendeten wir eine auf Ultraschall und Kinematik basierende Methode, bei der eine Reihe von reflektierenden Folienhautmarkern verwendet wurde, die die AT vom Ursprung bis zur Insertion abdeckten, um diese Krümmung zu berücksichtigen. Ziel der dritten Studie war es, diese Methode zu vereinfachen, indem die Anzahl der Marker reduziert und gleichzeitig eine hohe Genauigkeit beibehalten wurde. Elf Teilnehmer gingen (1,4 m/s) und liefen (2,5 m/s, 3,5 m/s) auf einem Laufband. Die AT-Krümmung wurde mit reflektierenden Folienmarkern gemessen, die mit der AT zwischen dem Ursprung am GM-MTJ (durch Ultraschall geortet) und einem Marker am Fersenbeinansatz ausgerichtet waren. Anschließend wurden die Folienmarker systematisch entfernt und die sich daraus ergebenden Auswirkungen auf die Messung der AT-Länge und -Belastung wurden quantifiziert. Unsere Ergebnisse deuten darauf hin, dass eine Verringerung der Anzahl der Folienmarker um 70 % beim Gehen und um 50 % beim Laufen zu einem marginalen Fehler und somit zu einer vernachlässigbaren Auswirkung auf die Messung der AT-Länge und der maximalen Dehnung in allen Gangphasen und Geschwindigkeiten führen würde.

Abstract

Tendons are connective tissue and transmit the force exerted by a muscle to the skeleton. Assessing the Achilles tendon (AT) length and loading during locomotion is important for estimating injury risk, efficient muscle-tendon interaction, and exercise prescription. However, current in vivo methods to assess the AT strain and loading in the biomechanics literature have certain limitations that require careful consideration. Therefore, the objective of the first study was to evaluate the mechanical loading and strain energy of the AT during locomotion with an accurate noninvasive method. The measurement of AT length was done with consideration of its curvature. Eleven participants were instructed to walk at a speed of 1.4 m/s and run at speeds of 2.5 m/s and 3.5 m/s on a treadmill. The AT length was defined as the distance between its origin at the junction of the gastrocnemius medialis muscle-tendon junction (GM-MTJ) and its insertion point at the calcaneus bone. The GM-MTJ was then projected onto the reconstructed skin surface to compensate for misalignment. Displacements between the skin and bone were evaluated during passive rotation (5°/s) of the ankle joint. The force and strain energy of the AT during locomotion were calculated by fitting a quadratic function to the experimental tendon force-length curve obtained from maximum voluntary isometric contractions (MVC). The maximum strain and force experienced by the AT were influenced by the speed at which locomotion occurred ($p < 0.05$), resulting in strains ranging from 4.0% to 4.9% and forces ranging from 1.989 kN to 2.556 kN. However, these magnitudes were deemed insufficient to be an effective stimulus for tendon adaptation.

The second study aimed to investigate the effect of walking speed on the mechanical power and work done at the ankle joint, despite a decrease in the intrinsic muscle force potential of the soleus (Sol) and GM muscles. The AT elongation and force were measured using the developed method in the first study during four walking speeds (slow 0.7 m.s-1, preferred 1.4 m.s-1, transition 2.0 m.s-1, and maximum 2.6±0.3 m.s-1). The mechanical power and work of the AT-force at the ankle joint, the monoarticular Sol at the ankle joint, and the biarticular gastrocnemii at the ankle and knee joints were also investigated separately. Our findings indicate that an increase in walking speed leads to a 21% decrease in maximum AT-force at the higher speeds compared to the preferred speed, yet the net work of the AT-force at the ankle joint (ATF-work) increased as a function of walking speed. Additionally, an earlier plantar flexion, increased electromyographic activity of the Sol and GM muscles, and knee-to-ankle joint energy transfer via the biarticular gastrocnemii contributed to a 1.7 and 2.4-fold increase in the net ATF-mechanical work in the transition and maximum walking speeds,

respectively. These results suggest that the monoarticular Sol muscle increases contractile net-work done, while the biarticular gastrocnemii contribute to the speed-related increase of net ATF-work through the use of biarticular mechanisms. This study provides first-time evidence for the different mechanistic participation of these muscles in the speed-related increase of net ATF-work.

Accurate determination of AT length and strain requires considering its curvature. In the first study, we used an ultrasound-kinematic-based method that utilized a series of reflective foil skin markers spanning the AT from origin to insertion to consider this curvature. The objective of the third study was to simplify this method by reducing the number of markers while preserving high accuracy. Eleven participants walked (1.4 m/s) and ran (2.5 m/s, 3.5 m/s) on a treadmill. The AT curvature was assessed using reflective foil markers aligned with the AT between the origin at the GM-MTJ (tracked by ultrasound) and a marker at the calcaneal insertion. Subsequently, the foil markers were systematically removed, and the resulting impact on measuring AT length and strain was quantified. Our results indicate that reducing the number of foil markers by 70% during walking and 50% during running would result in a marginal error and, thus, a negligible effect on the AT length and maximum strain measurement across gait phases and speeds.

Table of content

List of figures

List of tables

1. Introduction and literature review

This introduction outlines the primary components of previous research on the Achilles tendon (AT) and biarticular muscles. The hierarchical organization of the AT as a multi-unit structure, as well as the extracellular matrix of the tendon tissue, are initially discussed. Following this, the twisted anatomy of the AT structure and force transmission between triceps surae muscles components were examined. After that, emphasis is placed on the techniques used to measure the strain and loading of the Achilles tendon (AT) during functional activities, as well as the energy storage and recoil of the tendon. Furthermore, the anatomical features and functional significance of biarticular muscles are examined. These insights culminate in the articulation of the purpose of the present thesis.

1.1. Anatomy of Achilles tendon

Tendon primary function is to transfer the muscle-generated force to the bone to provoke motion. Depending on muscle and bone, tendons feature various shapes and sizes (Jozsa & Kannus, 1997). The longest tendons in the human body are in the hands and feet. Tendons in the foot serve not only as force transmitters but also as an elastic energy-saving and recoil mechanism that can regulate the amount of required energy in various movement velocities. The AT is considered the second thickest tendon in the human body, following the patellar tendon (Bohm et al., 2014; F Mersmann et al., 2017). It can transmit the generated forces from the triceps surae muscles to the calcaneus. The calcaneus bone with the superior tuberosity acts as a pully for the Achilles tendon attachment during dorsiflexion (Benjamin et al., 2008). AT is located in the posterior surface of the lower leg, and it's connected with the gastrocnemius next to the middle of the calf and soleus further to the distal part of the leg (Figure 1-1, (Doral et al., 2010)). The average length of the free Achilles tendon is reported to be 56 mm, with a range of 52 to 75 mm, and the cross-sectional area of the free Achilles tendon varies from 70 mm^2 to 40 mm^2 when measured from the distal to the proximal end. (Arampatzis, Karamanidis, & Albracht, 2007; Arampatzis et al., 2010; Bohm et al., 2014). According to a study, the contribution of the soleus and gastrocnemius muscles to the Achilles tendon varies among individuals (Cumins et al., 1946). Measuring the exact degree of contribution can be challenging due to the changing orientation of the tendon fibers. Out of 100 cadaver specimens, 52 showed that the soleus contributed 52% and the gastrocnemius contributed 48% of the fibers to the Achilles tendon. In 35% of specimens, both muscles contributed equally, while in 13%,

the gastrocnemius contributed more than 60% (Cumins et al., 1946). The Achilles tendon fibers are not aligned parallel to each other but are instead twisted around each other at a 90-degree angle, which allows the tendon to withstand greater stress. This unique twisted fiber structure is believed to contribute to the energy storage and recoil mechanism of the Achilles tendon (Maffulli, 1999). Finite element analysis was used to create a model of the rotational structure of the Achilles tendon. The non-uniform displacement was reduced by 85% by eliminating the differential muscle force and by 35% by eliminating the rotational structure (Handsfield et al., 2017). O'Brien et al. (O'Brien, 2005) stated that the highest stress in the Achilles tendon occurs between 20 and 50 millimeters above its insertion into the calcaneus.

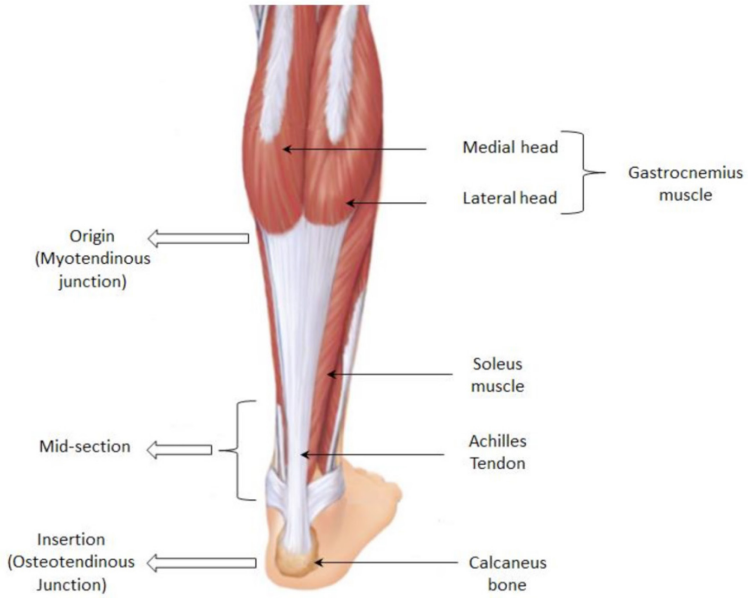

Figure 1-1 The anatomy of the Achilles tendon

The perimysium vessels at the musculotendinous junction, the periosteal vessels at the osteotendinous junction, and the capillary system surrounding the tendon are the three sources of vascular supply for the AT. The tendon middle is less vascularized than the proximal and distal tendon ends, creating a relatively avascular region where injuries are more common (Chen et al., 2009). Nerves from the attaching muscles and small fasciculi from cutaneous nerves, particularly the sural nerve, supply the AT and the surrounding paratenon with neural supply (Andres et al., 1985; Stilwell Jr, 1957). The tendon is relatively neuronal and has few nerve endings (Lian et al., 2006; Schubert et al., 2005).

1.1.1. Composition of tendon

Tendon is a connective tissue composed of densely collagen fibers packed in an opaque substance, including water (60–80% of the total wet weight), collagen (65–86% of the dry weight, mainly type I collagen 95–98%), proteoglycans (1–5%), elastin (1–2%) and 0.2% inorganic components (Kannus, 2000; Li et al., 2013). The anatomy of the tendon has been reviewed and reported frequently (Benjamin et al., 2008; Handsfield et al., 2016; Kannus, 2000). For instance, the shape of the extensor tendons is usually more flattened, whereas the flexor tendons are more roundish or oval (Benjamin et al., 2008). Like other tendons in the human body, AT also has a well-organized hierarchical structure. From the bottom-up, the most minor and primary entities are the collagens. By bounding three collagen molecules together, the triple-helix rods will form. Five tropocollagen make a microfibril, and they are connected by covalent bonds forming fibrils, and with the combination of them, fibers will form (Handsfield et al., 2016). The next higher level of hierarchical tendon structure is the fascicles and the tertiary bundles surrounded by the epitenon that make the whole tendon (Figure 1-2, (Screen et al., 2004)). In addition, AT has a paratenon that surrounds the entire tendon, and it has been suggested to facilitate the tendon healing progress (Müller et al., 2018).

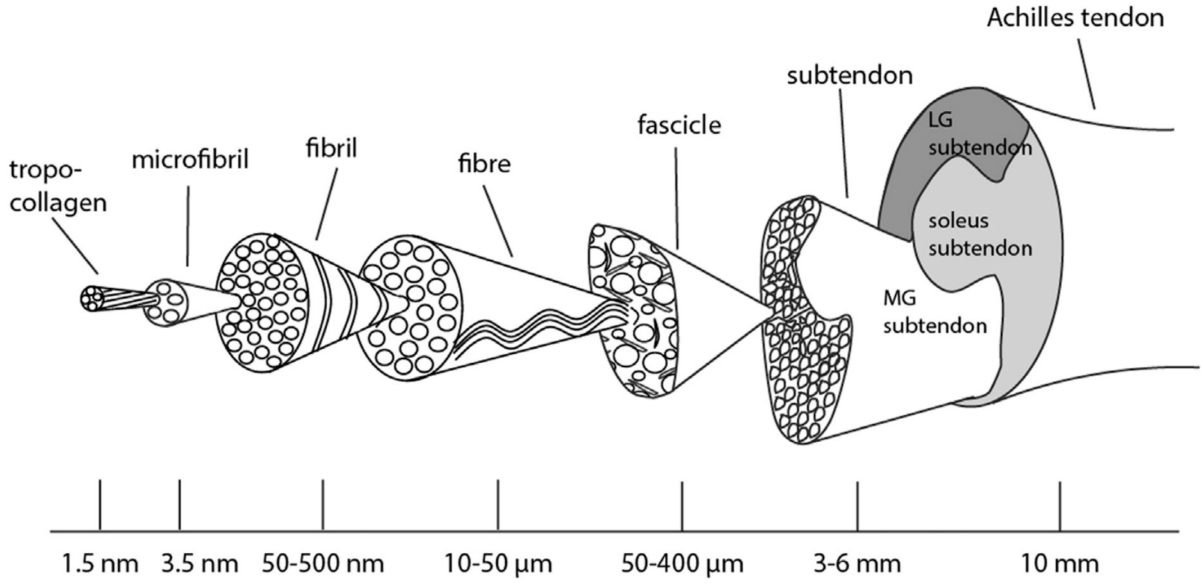

Figure 1-2 The hierarchy of the Achilles tendon. MG refers to medial gastrocnemius, and LG refers to lateral gastrocnemius adopted from (Handsfield et al., 2016).

1.1.2. Extracellular matrix (ECM)

Proteoglycans, glycoproteins, and elastin make up the ECM. The vascularized myotendinous and osteotendinous junctions supply nutrition and oxygen to the tendon tissue, which has

almost no vessels (Ballal et al., 2014). A dense ECM with parallel-aligned, slightly crimped collagen type I fibers makes up healthy native tendon tissue, as shown in Figure 1-3 (Ballal et al., 2014). Other collagens, such as II, III, V, VI, IX, and XI, are also present but in much lower concentrations than collagen I. In contrast, collagen type I represents about 95% of the tendon collagen dry weight (Riley, 2005). After acute exercise, collagen synthesis rises from 1% at rest to 2-3%, lasting 2–3 days (Heinemeier et al., 2003). As demonstrated in the rabbit AT, the collagen fibrils are bio-generated in activated tenocytes. They have precursor structures like procollagen filaments with a 30–60 nm length excreted to the ECM (Santander et al., 1999). Intermediate fibril lateral fusion produces linear and lateral growth (Silver et al., 2003). The interaction of quantitatively minor fibrillar collagens and proteoglycans controls fibrillogenesis (Zhang et al., 2005). The formation of a strong tendon or ligament tissue necessitates the transformation of viscous collagen macromolecule assemblies into solid, sturdy, and energy-storing components. Therefore, the collagen molecules must be cross-linked end to end within a fibril.

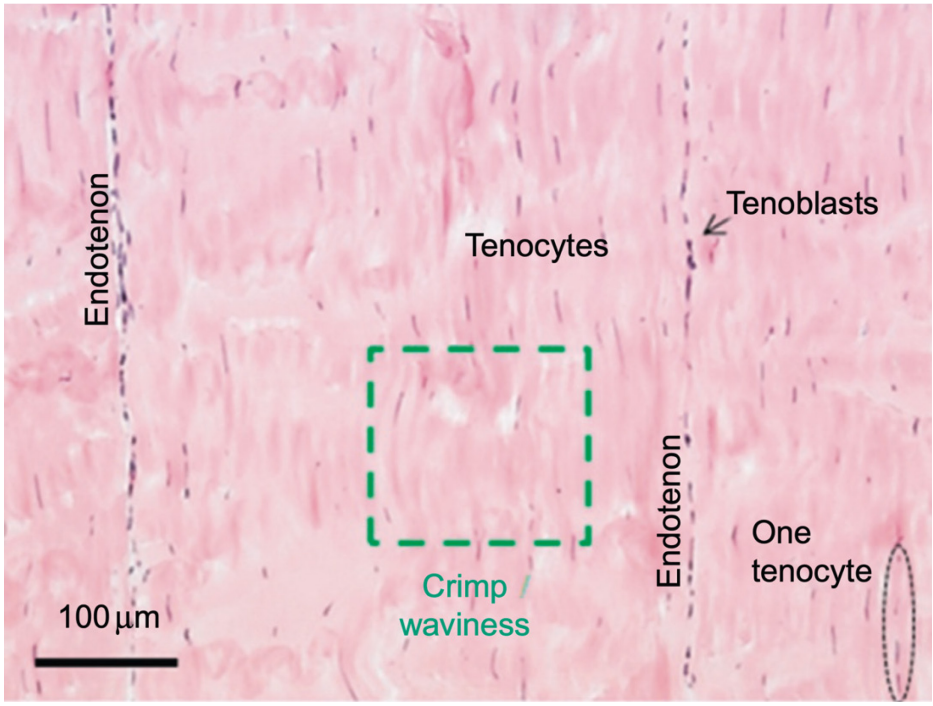

Figure 1-3 A typical histological section of rabbit AT (100 magnification) showing cellular-rich endotenon, tenoblasts, tenocytes, and the waviness (crimping) of the collagen fibers (adopted from (Buschmann et al., 2014)).

Two modes suggested that the extracellular matrix would transmit external strain to the tendon cells: (a) cell deformation and (b) shear stress caused by fluid flow (Lavagnino et al., 2003). Loss of collagen crimp and an increase in fiber recruitment were seen with increasing strain (Schatzmann et al., 1998) which almost certainly leads to a rise in the number of deformed

cells composition (Arnoczky, Lavagnino, et al., 2002). Fluid flow-induced shear stress appears to be another mechanism of external strain transmission to tendon cells that affects cellular responses and cell deformation (Lavagnino et al., 2008). Lavagnino et al. (Lavagnino et al., 2008) reported that strain rate mediates fluid flow-induced shear stress and observed decreased catabolic cell responses with increased strain rate. Additionally, it appears that gender impacts the mechanical and morphological characteristics of the tendon, with lower stiffness and Young's modulus values reported for the tendon aponeurosis of women compared to men (Kubo et al., 2003).

1.1.3. Muscular attachment

The triceps-surae muscles contain soleus (Sol), gastrocnemius medialis (GM), and gastrocnemius lateralis (GL) shared AT that is inserted on the posterior side of the calcaneus bone (Figure 1-4). The gastrocnemii muscles lie superior to the Sol, and biarticular muscles (medial and lateral heads of Gastrocnemius) cross the knee and ankle joint. However, both heads of the gastrocnemii muscles are subject to functional shortening, and the medial head is thicker (Cohen, 2009). It's been reported that the volume of the GM relative to the total volume of the triceps surae muscle is 26% and about 12% for GL (Albracht et al., 2008). In comparison, the majority of triceps surae volume (62%) is allocated to the soleus muscle (Albracht et al., 2008).

Some tendons, such as AT in humans (Yin et al., 2021), have sub-section tendons originating from different muscles. Term sub-tendon refers to grouped fascicles within the AT that can be traced back to the origin from either soleus or gastrocnemii muscles. The extension of both gastrocnemii muscle bellies come together and form a tendon combined with aponeurosis on the anterior side of the forces (O'Brien, 2005). This tendon then merges with the AT of the soleus. The joined tendon to the soleus musculotendinous junction calls the free part of the AT. The muscular attachment of the triceps surae to the AT is illustrated in Figure 1-4.

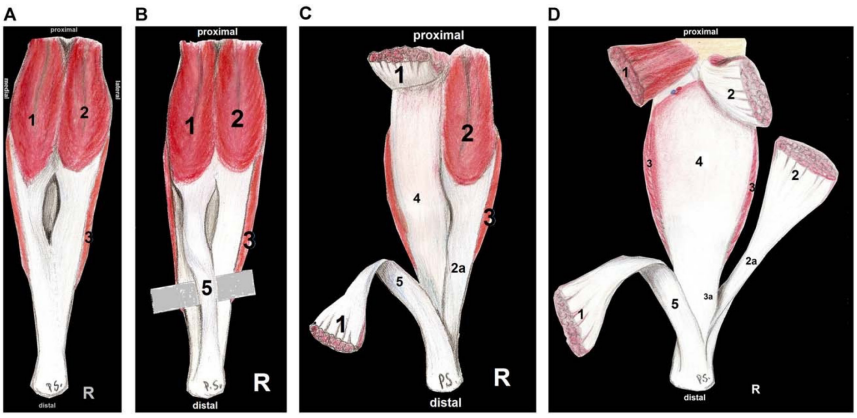

Figure 1-4 (A-D) Posterior view of the stages of dissection of the right Achilles tendon. (1) gastrocnemius muscle medial head, (2) gastrocnemius muscle lateral head, (2a) fibers from the lateral head of the gastrocnemius, (3) soleus muscle, (3a) fibers from the soleus muscle, (4) aponeurosis of the soleus muscle, and (5) medial head of the gastrocnemius muscle (Szaro et al., 2009)

The fascicles of the AT are parallel proximally and rotated distally, which makes the AT a spiral structure. The Soleus muscle is connected to the AT directly. Therefore, the tendon's mechanical behavior follows the soleus muscle activation pattern (i.e., monoarticular muscle). On the contrary, the tendon of the gastrocnemii muscles has an extended tendinous portion that is thin and flat and lies posteriorly to the soleus. The muscle-tendon-junction of the gastrocnemii to the tendon is loose proximally and then gradually tightness distally (Blitz & Eliot, 2007).

The fiber bundles of the Achilles tendon also have a rotational structure, as was previously mentioned. The soleus fibers make up the deep layer of the Achilles tendon, the gastrocnemius medialis fibers make up the superficial medial aspect, and the gastrocnemius lateralis fibers make up the superficial lateral aspect, where the soleus fibers confluence with the gastrocnemius aponeurosis. The gastrocnemius and soleus fiber bundles rotate as the tendon descends to its insertion, with individual differences in the amount of rotation (Ballal et al., 2014; Edama et al., 2015; Szaro et al., 2009). The loading circumstances and the rotational structure probably cause differential loading within the Achilles tendon. The non-uniform displacement of the tendon fibers seen using B-mode ultrasound and ultrasound elastography supports this theory. During walking, ultrasound elastography has demonstrated that the superficial layer of the Achilles tendon moves less than the deep layer of the tendon and that this difference grows as walking speed rises (Franz et al., 2015). However, evidence suggests that the myotendinous structures of the triceps surae muscle-tendon units (MTUs) are not independent but are mechanically connected (Bojsen-Møller et al., 2010; Finni et al., 2017). The force transmission through the contiguous extra-muscular connective tissue structures

influences the mechanical linkage of adjacent MTUs during muscle contraction (Huijing, 2009; Kinugasa et al., 2013), and promotes a synchronous movement of connective tissues between the triceps surae muscles (Bojsen-Møller et al., 2010; Finni et al., 2017). The tendon inter-fascicular matrix is highly elastic and stiff (~50% of the tendon fascicles), and inter-fascicle sliding may strain it, facilitating force transmission within the tendon (Maas & Finni, 2018). The force transmission mechanisms through the connective tissue network of the MTUs may redistribute the forces within the Achilles tendon, minimizing peak stresses (Maas & Finni, 2018), thus reducing regional displacement gradients. Previous studies have reported similar Achilles tendon force-elongation curves and tendon stiffness, measured at either the gastrocnemius or soleus muscle-tendon junctions (Morrison et al., 2015; Obst et al., 2016), which were not dependent on ankle angle or the rest length of the Achilles tendon (Ackermans et al., 2016; Morrison et al., 2015). In a study conducted by Arampatzis et al. (Arampatzis, Mademli, et al., 2007), there was a symmetrical shortening of the triceps surae muscles during maximum voluntary contractions.

1.2. Quantification of Achilles tendon strain

In addition to helping to define physiologic loading conditions for in vitro experiments and tissue-engineered constructs, a thorough understanding of in vivo tendon strains with noninvasive methods is crucial for determining injury mechanisms, informing surgical reconstructions, and optimizing rehabilitation protocols. Measuring in vivo musculoskeletal soft tissue strain patterns during functional movements is vital to facilitate scientific advancements and inspire novel therapeutic therapies. In 1847, Wertheim showed that the stress-strain relationship in soft tissues is not following a Hookean linear law (Wertheim, 1847). More than one century later, Fung found the first evidence of soft tissue viscoelasticity, which brought insight into soft tissue deformation in response to the applied loading (Fung, 2013). It was suggested that tissue viscoelasticity influences the soft tissue's deformation, strain, and strain rate (Haut, 1983).

By permitting the assessment of the elongation of the muscle fibers, tendon, and aponeurosis individually, in vivo strain measurements also offer crucial insights into the operation of the muscle-tendon system (Cronin & Lichtwark, 2013). Force-velocity muscle contraction is made possible by measurements of muscle fiber lengths and velocities during movement. According to ultrasound studies, the tendon may serve as a buffer against overall muscle-tendon unit stretching, causing stresses in the different tissues rather than a change in the overall length of

the muscle-tendon unit (Cronin & Lichtwark, 2013). There is a trade-off involved in the muscle architecture to generate forces. On the one hand, shorter muscle fibers require less energy for activation, while on the other hand, longer fibers are necessary to maintain an appropriate shortening velocity.

Moreover, the energetic cost of muscle activation is also influenced by the strain rate of the tendon, which regulates the temporal characteristics of the mechanical work produced by the muscle (Lichtwark & Wilson, 2008). During the propulsion phase of human walking and running, the tendon shortens at a higher rate relative to the whole muscle-tendon unit, maintaining the muscle in an isometric mode to generate force in optimal condition (Bohm et al., 2021; Fukunaga et al., 2001; Mian et al., 2007). The findings of these studies highlight the crucial role of in vivo tendon strain measurement in enhancing our understanding of the biomechanics of the muscle-tendon complex. Such measurements provide valuable insights into the mechanisms underlying energy storage and release during muscle contraction, power amplification, and energy absorption in response to perturbations (Roberts & Azizi, 2011). Consequently, the quantification of the tendon strain is essential for advancing our knowledge of the musculoskeletal function and informing the design of interventions individually for preventing or treating musculoskeletal injuries and disorders (Arampatzis et al., 2020).

Tendon strain is a metric used to quantify the extent of deformation of a tendon in response to applied loads. It is defined as the ratio of the change in length of the tendon to its original or reference length, expressed as a percentage (Equation 1-1).

$$\epsilon = \frac{l - l_0}{l_0} \times 100 \qquad \text{Equation 1-1}$$

Where the l is the instantaneous length of the tendon and the l_0 is the reference length of the tendon. The reference length of the tendon is the slack length to which zero forces are applied to the tendon. The methods concerning the measurement of the tendon slack length are inconsistent in the biomechanics literature. Therefore, careful examination of the l_0 definition is required when comparing tendon strains across the literature.

1.2.1. During static conditions

Typically, B-mode ultrasonography frames are gathered while an individual acts, such as isometric plantarflexion. The displacement of an anatomical landmark, frequently the muscle-tendon junction of the gastrocnemius, can then be manually tracked throughout the stack of ultrasound images. It is thus possible to calculate tendon length by having end-point displacements and the movement at the calcaneus insertion. This technique has been modified

to assess the relative stretch and displacement throughout the tendon and aponeurosis (Arampatzis, Stafilidis, et al., 2005; Karamanidis & Arampatzis, 2005). The muscle-tendon junction tracking method has revealed new information on the impact of gender (Kubo et al., 2003), injury (Child et al., 2010), training (bohm, 2015), and age on tendon strain, stiffness, and elastic modulus (bohm, 2015). Arampatzis et al. (Arampatzis et al., 2008; Arampatzis, Stafilidis, et al., 2005) reported the effect of the joint rotation and the curvature of the AT on its elongation and strain, the reliability and validity of this method were also validated against the magnetic resonance imaging technique (Barfod et al., 2015). The maximal strain experienced by the Achilles tendon during a maximal voluntary contraction (MVC) ranges from 4% to 9%. Additionally, the elongation or lengthening of the tendon during MVC has been reported to range from 13 to 25 mm. (Arampatzis et al., 2008; Arampatzis, Karamanidis, Morey-Klapsing, et al., 2007; Arampatzis et al., 2020).

Freehand ultrasound scanning is another ultrasound method to measure the length of the tendon during a static position. This technique combines conventional user-operated B-mode ultrasound imaging and motion capture cameras to reconstruct the anatomical structure of the tendon (Treece et al., 1999). As the transducer is moved or "swept" over the region of interest to generate a stack of arbitrarily oriented successive 2-D ultrasound pictures, the position and orientation of the transducer in 3-D space are recorded using a motion capture device. Using a rigid body calibration approach, each successive 2-D picture location is converted into a global coordinate system to generate a reconstructed 3-D volume. This volume is then utilized for object segmentation, surface rendering, and volumetric registration (Gee et al., 2004; Prager et al., 1998; Treece et al., 1999). However, it's been reported that measuring human AT length in vivo is more reliable using skin markings than the ultrasound freehand reconstruction method (Brouwer et al., 2018). Comparing the freehand ultrasound method to measure AT volume with MRI images (30.6±5.8 m^3)showed an overestimation of, length and average cross-section area of 0.3±0.7 mm and 0.3±.42 $mm^{2,}$ respectively (Devaprakash et al., 2019). Although, the freehand ultrasound method is unsuitable for strain measurement because the ultrasound probe should sweep alongside the AT for each time frame. Pizzolato et al. 2020 used freehand ultrasonography with a combination of finite element methods to estimate the strain and forces in the AT during static and functional tasks (Pizzolato et al., 2020).

1.2.2. During dynamic conditions

The process of tendon adaptation is initiated by strain on the tendon (Bohm et al., 2014; Magnusson et al., 2010). In vivo measurement of the AT strain is vital to firstly find the adaptational threshold and secondly to quantify the strain energy storage and recoil of the tendon during dynamic tasks. Thus, gaining a deeper understanding of how tendons undergo strain during dynamic movements is imperative. Several strain assessment techniques during locomotion are introduced in the biomechanics literature, ranging from manually tracking musculotendinous junctions (Magnusson et al., 2003; Werkhausen et al., 2018) to ultrasound-assisted 3D motion capture (Barber et al., 2009) to finite element modeling (Pizzolato et al., 2020; Shim et al., 2014). All the approaches to measure the tendon strain in vivo during a dynamic task such as walking/running, jumping, and cycling are also feasible during static/isometric tasks but not vice versa.

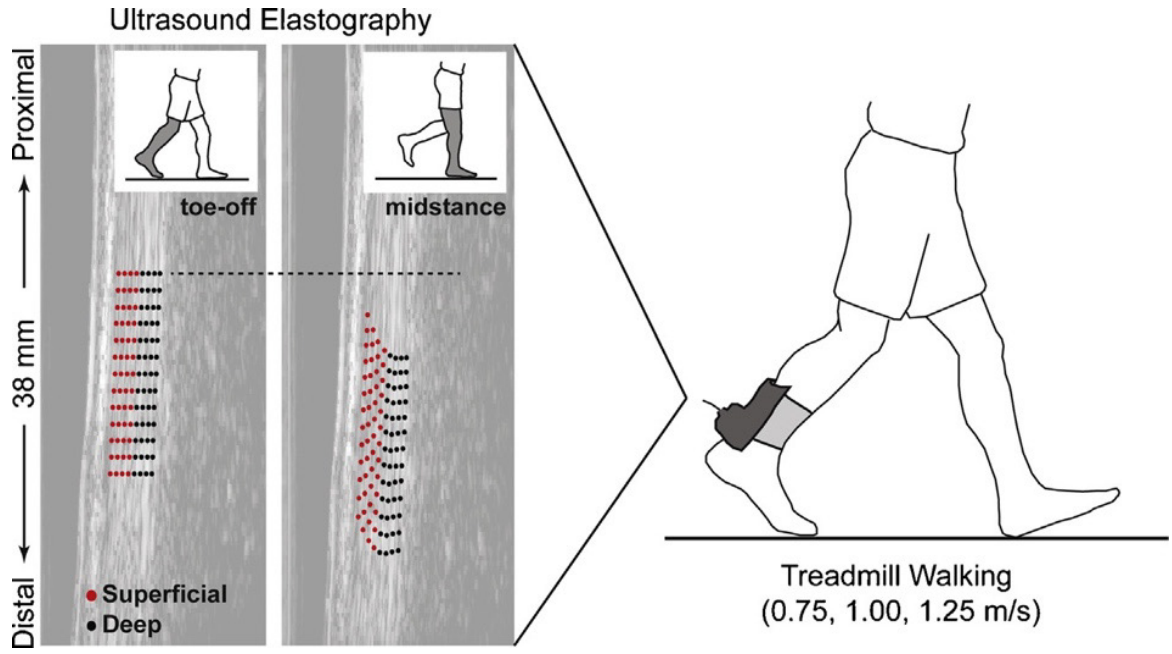

Figure 1-5 Ultrasound elastography speckle tracking method to evaluate the Achilles tendon strain during human walking (image adapted from (Franz et al., 2015)).

Ultrasound speckle tracking is another method used to evaluate in vivo strain of the tendon during functional tasks (Franz et al., 2015; Franz & Thelen, 2015). Since its introduction in 1991, the word "elastography" has grown to refer to a wide range of techniques for assessing tissue stiffness, including ultrasound, among other methods (Ophir et al., 1991). The displacement of speckle patterns obtained from tissue in undeformed and deformed states is tracked using the phase information inherent in ultrasound radiofrequency (RF) data (Varghese, 2009). The estimation of strain fluctuations inside tissue is therefore made possible

by the spatial differentiation of displacement data (O'Donnell et al., 1994). Applying elastography to tendinous tissue presents substantial obstacles during functional tasks because the results are difficult to interpret of this method limited applicability to functional loading scenarios. However, because the major direction of tissue motion is parallel to the skin surface, which has an intrinsically lower resolution in ultrasonography, tracking displacements during physiological tendon loading can be challenging (Bohs & Trahey, 1991; Ophir et al., 1991). With the same methodology, Franz et al. 2015 (Franz et al., 2015) showed a non-uniform longitudinal displacement of the AT during walking. They found the superficial elongation of the AT elongated higher by 0.4 to 1.1 mm during the stance phase at different walking speeds (Figure 1-5). Another frequently used method to measure the AT length and strain in vivo during functional tasks is a combination of the ultrasound and motion capture system (Lichtwark et al., 2007; Lichtwark & Wilson, 2005; Matijevich et al., 2018; Rasske & Franz, 2018; Suzuki et al., 2019). In this approach, the ultrasound tracks the displacement of the muscle-tendon junction, and the motion capture system tracks the insertion of the AT on the calcaneus bone. The tracked positions in a stack of the ultrasound images then transfer to the global coordinate system (i.e., same as the motion capture coordinate system). Then, the length and strain of AT can be measured as the Euclidian distance between AT insertion and its origin. The AT maximal strain levels during walking and running with the mentioned methodologies range between 4.6 to 9.0% during running (Lai et al., 2015; Lai et al., 2018; Lichtwark et al., 2007) and 4.0 to 4.3 % during walking (Lai et al., 2014; Lichtwark et al., 2007; Lichtwark & Wilson, 2006). Neuromusculoskeletal modeling has recently been used to estimate the strain on free part of the AT. The peak strain in the free part of the AT of trained runners ranged from 7% during walking to almost 14% during running at a speed of 5 m/s (Devaprakash et al., 2022). The latter value is close to the failure strain of 15% observed in vitro (Schechtman & Bader, 1997). However, there is a nearly two-fold difference between these strain values, which may be due to differences in calculation methods or because of the former study, (Lai et al., 2015; Lai et al., 2014; Lai et al., 2018; Lichtwark et al., 2007; Lichtwark & Wilson, 2006) tracked the muscle-tendon junction of the medial gastrocnemius (GM-MTJ) in relation to the calcaneus insertion. From a methodological point of view, differences in the AT strain (e.g., consideration of AT curvature, projection of GM-MTJ to the skin surface, and the artifact introduced by skin movements on top of the calcaneus at the insertion of AT (Lichtwark & Wilson, 2005) during human walking and running should be considered the biomechanical study to maintain the accuracy of the measurements. For instance, neglecting the curve shape of the AT can introduce significant error in AT length and strain measurements (Arampatzis et

al., 2008; Fukutani et al., 2014; Stosic & Finni, 2011). According to these research, it is essential to consider the AT curvature when calculating the tendon length and strain. Thus, a need to have simple, accurate, noninvasive method to quantify the AT strain by considering of mentioned source of errors during human locomotion is sensible.

1.3. Quantification of Achilles tendon loading

Since tendon structures resemble springs, their tensile stiffness may be adjusted to the mechanical conditions in which they function, rising in response to chronic loading and falling in reaction to chronic unloading. The AT is the body strongest tendon and is subjected to significant stresses in both daily activities and athletics. The maximal AT tendon loading varies among biomechanics literature, ranging between ~200-3800 N (Arampatzis, Stafilidis, et al., 2005; Hansen et al., 2003; Maganaris et al., 2008; Muramatsu et al., 2001). This inter-study variation is mainly due to methodological differences. One main parameter that influences methods is the antagonistic muscle effect on the moment of the ankle, and the second is different reference points of muscle-tendon junction. Running can cause the AT to transport up to 110 MPa in each step, according to in vivo tests of tendon force (Komi et al., 1992). This stress surpasses the ultimate tensile tendon stress of 100 MPa, implying that the Achilles tendon might tear in a single stride in real life (David et al., 1978; Shadwick, 1990). The following sections will discuss in vivo measurement of the AT loading with direct, inverse dynamic, and musculoskeletal modeling approaches.

1.3.1. Direct measurements

Human tendon force has been directly measured in vivo using implantable sensors. These sensors often operate according to tissue deformation, resulting in changes to their electric signals. However, in vivo, measuring the AT force remained challenging due to methodological complications during normal human locomotion. More than three decades ago, Komi et al. (Komi, 1990) used a buckle-type transducer to measure the tendon strain and forces in vivo during human walking and running. He found the maximum exerted force on the AT of 3750 N during running at a speed of 3.9 m/s. The force of the AT reaches 9 kN during running at a speed of 6 m/s, which is about 12.5 times higher than the body weight. If the AT cross-section area is 0.81 $cm^{2,}$ then the maximum stress would be 11100 N/cm^2, which is well above the ultimate tensile strength of the tendon (Butler et al., 1984). Almost ten years later, Finni et al. (Finni et al., 1998) suggested a novel optic fiber technique to measure the AT forces

in vivo during functional tasks. They found the maximum AT forces ranged between 750 N to 2360 N while the walking speed at 1.1, 1.5, and 1.8 m/s evidencing a high intrasubject variability. The average cross-sectional area of the AT was 74±25 mm^2 for all individuals, which makes the maximum stress during walking 21±9.3 $N.mm^2$ on the AT. The results showed the average rate of fore development increased by 32% by the progress of walking speed from slow to fast. However, the maximum AT force did not change significantly.

1.3.2. Inverse dynamic approaches

The traditional method for analyzing movement is the Newton-Euler inverse dynamics approach. This technique assumes that the foot, shank, and thigh are rigid segments joined by body joints (Winter, 2009). It determines the total joint moments, powers, and intersegmental forces by inserting ground reaction forces and observed or estimated segmental accelerations into equations of motion ($\bar{F} = m\bar{a}$, $\bar{M} = I\bar{\alpha}$) (Kaufman, 1999; Siegler & Liu, 1997; Winter, 2009). The analysis starts at the foot and then solves for the ankle joint intersegmental force and net ankle moment, followed by the shank and then the thigh to compute the net joint moment and joint intersegmental force at the knee and hip. This method has the benefit that it does not require modeling of segments proximal to the thigh, such as the trunk segments, to compute the net joint moment and joint intersegmental force at the ankle, knee, and hip. Additionally, a least-squares approach can be used to estimate the net joint moments and forces in the presence of noisy data (Kuo, 1998).

The joint contact force is calculated by adding the joint intersegmental force (which is obtained directly from the traditional inverse dynamics method) and the compressive joint force caused by muscle forces and forces in the soft tissues of the joint. An additional method is used to estimate the compressive joint force, which involves breaking down the net muscle moments (obtained from the inverse dynamics approach) into individual muscle moments using static optimization (Zajac et al., 2002). The standard mathematical approach to solve the optimization problem is to minimize the following mathematical (Equation 1-2):

$$\phi(f) = \sum_{i=1}^{n} \left(\frac{f_i}{w_i}\right)^{\alpha} \qquad \text{Equation 1-2}$$

Where f_i is the force value, w_i is the weight factor (i.e., usually the contribution of the muscle regarding its cross-section area), α is greater than one (i.e., usually is 3), n is the number of muscles in the model, and $\phi(f)$ is the generalized forces acting on the joint. A numerical method would generally be conducted to solve this equation, especially if the model is more

complex (Buchanan & Shreeve, 1996; Davy & Audu, 1987). Yettram et al. (Yettram & Camilleri, 1993) used an optimization method to calculate the exerted force on the calcaneus during quiet human standing.

Decomposing the net joint moments into individual muscle moments or muscle forces using static optimization has been used for a long time (Hardt, 1978; Pedotti et al., 1978), but it can be problematic when studying muscle coordination (Hatze, 2000; Kautz et al., 2000). One issue is the low confidence in the optimization criterion inherent in this approach (Herzog, 1996; Herzog & Leonard, 1991). Additionally, most of these methods are unable to predict co-contraction among antagonistic muscles (Binding et al., 2000; Herzog & Leonard, 1991).

Another limitation of the traditional inverse dynamics method is related to the uncertainty in estimating mechanical energy expenditure by muscles. This uncertainty arises due to the inter-compensation caused by biarticular muscles and the recoiled elastic strain energy (Aleshinsky, 1986; Caldwell & Forrester, 1992). While attempts can be made to address these effects in calculating mechanical energy expenditure (Broker & Gregor, 1994; Kautz et al., 1994), significant problems remain (Neptune & Van Den Bogert, 1997). Although net joint moments/powers can be computed using inverse dynamics and then decomposed into individual muscle contributions through static optimization, it is impossible to determine individual muscle contributions to segment and joint acceleration and joint intersegmental forces. This is because the Newton-Euler equations for leg segments are incomplete and do not include equations of motion for the head, arms, and trunk (HAT). The force generated by a leg muscle affects the acceleration of all segments, including the HAT, which affects the acceleration of leg segments. As a result, the Newton-Euler equations for leg segments alone cannot be used to decompose the acceleration of a segment, such as a leg segment, into the individual muscle or net joint moment contributions. This significantly limits the traditional inverse dynamic ability to identify the role of individual muscles contribution in different tasks (Andriacchi et al., 2005).

1.3.3. Musculoskeletal modeling and simulations (forward dynamic)

The crucial aspect of comprehending muscle coordination is determining how individual muscles contribute to the movement of the body segments and objects that come into contact with the body. To achieve this, it is important to identify the instantaneous contributions of individual muscles to the acceleration and power of the segments. Multiple methods exist to obtain these instantaneous contributions, either through individual muscles or net joint

moments. However, each approach requires a complete set of dynamical equations of motion of the entire body, essentially a dynamical model of the body (Delp & Loan, 2000).

To determine the individual muscle contributions to the movement of the body segments, the net joint moments calculated through traditional inverse dynamics can be decomposed into individual muscle forces. These forces can then be applied to the dynamic model of the whole body. To decompose the net joint moments, a musculoskeletal model of muscle moment arms can estimate through a scaling calibration process and static optimization methods. The optimization criterion for the net joint moment decomposition can vary, such as minimizing muscle fatigue, stress, or peak forces. When muscle forces are estimated, joint contact forces can also be computed, and the individual muscle contributions can be found.

Simulations are not required if a dynamical model is available and the inputs, such as the net joint moments or muscle forces, are known to calculate the instantaneous contributions of individual net joint moments or muscle forces to the accelerations and power of a segment. At every stage of the motion, the computations may be done individually. Due to probable discrepancies between the dynamical characteristics of the model and the applied net joint moments or muscle forces, the resulting accelerations and powers could not match the anticipated motion. Dynamical simulations incorporating models of individual muscles can provide an even greater understanding of muscle coordination. By including models for muscle and tendon in the whole body dynamical model, the simulation can test for compatibility between measured kinematics, kinetics, and EMG patterns not only with the model of the body segments but also with the models of muscle, tendon, and muscle moment arm properties (Hatze, 1977, 1980).

The major challenge in dynamic simulation is to match the measured experimental kinematics, kinetics, and EMG parameters to the pattern of the muscle excitation estimated by the model. There are two main forward dynamic approaches used to generate muscle excitation trajectories for simulations, both of which use optimization theory and a dynamical model to find the muscle excitations that produce desired trajectories (Zajac, 1993). One approach involves specifying the objective of the motor task, and the optimization algorithm finds the muscle excitations that fulfill this objective (Raasch et al., 1997; Van Soest & Casius, 2000). The other approach measurements are obtained from subjects performing the task, and the optimization algorithm finds the muscle excitations that match the simulated trajectories to the measurements as closely as possible, regardless of whether energy is minimized to the extreme or not (Neptune & Hull, 1998).

The construction of a generic model of muscle and tendon based on a few architectural parameters is common (Delp et al., 1990), but the available anatomical, physiological, and musculotendon paths data for determining these parameters is limited (Delp et al., 1990; Murray et al., 1926; Zajac & Winters, 1990). In addition, techniques and data for describing body-segmental mass and inertial properties concerning subject-specific information are not available (Hatze & Baca, 1993; Sarfaty & Ladin, 1993). Consequently, sensitivity studies based on simulations should be structured to determine the most appropriate data for the model. On top of these limitations, difficulties in determining the precise moment arms of biarticular muscles (Pal et al., 2007) and the active and passive force-length characteristics of individual muscles make it challenging to accurately determine the specific muscle excitations in forward dynamic model simulations (Zajac et al., 2002).

Mentioned attempts show a high level of importance of in vivo, noninvasive approaches to quantify the AT mechanical properties. The importance of noninvasive methods for quantifying mechanical loading on the AT during walking and running is highlighted by the high incidence of tendon injuries and their impact on individuals health and performance (Child et al., 2010; Erickson et al., 2014; Hess et al., 1989; Huttunen et al., 2014; Kvist, 1994; Falk Mersmann et al., 2017; Obst et al., 2018; Yin et al., 2021). By accurately quantifying tendon loading, clinicians and researchers can better understand the biomechanics of muscle-tendon interaction, optimize training programs, and develop effective prevention and treatment strategies for tendon injuries (Arampatzis et al., 2020; Karamanidis & Epro, 2020). To date, no accurate in vivo method with noninvasive approaches exist to quantify the AT forces. Differences in the AT force measurement approaches may partly explain the variation between the reported values in the literature.

1.4. Energy storage and recoil in Achilles tendon

By definition, a spring element behaves in a relatively straightforward manner. When a force is applied, the spring shortens, and it will return to its resting shape when removed. Materials can behave like springs, like a rubber band, when loaded in tension or compression, like a rubber ball. Both loading types play crucial roles in nature. Elastic strain energy is a sort of energy that springy materials retain during deformation; this energy is released during rebound (i.e., recoil). The stiffness of the material and the degree of deformation affect how much energy is retained. The human kinetic and potential energy is the lowest during running because the hip passes over the supporting foot. Furthermore, the leg joints are mostly bent at this stride

time, thus maximizing the ground reaction forces. The lost kinetic and potential energy will be stored as elastic strain energy in the AT at this time and then restored immediately as an elastic recoil (Alexander, 1991). The triceps surae muscles then lengthen during a saving period and, in the second half of the stance phase, shorten as the contractile elements generate forces (Alexander, 1991). It is reported that the AT can store about 35% of the total kinetic and potential energy as strain energy and then recoil to the skeletal system when needed (Ker et al., 1987b). In 2005, Ishikawa et al. (Ishikawa et al., 2005) showed gradual AT lengthening in the first half of the stance phase during walking and then rapidly recoiling in the second half. However, later, Roberts et al. (Roberts & Azizi, 2011) proposed three scenarios of energy storage and tendon recoil. 1) Tendons momentarily store energy from the body or a segment before releasing it back into the body. In this scenario, the metabolic energy will consume more economically during running, hopping, and walking. 2) The mechanical energy generated by a muscle contraction is stored in a tendon. In this scenario, the power in the needed joint will amplify, such as jumping, acceleration incline running, and ballistic feeding. 3) Tendon stores energy from the skeletal system and then releases it to function on muscles that are actively extended to absorb energy. In this scenario, the power in the target joint will attenuate during activities like decline running, deceleration, and landing (Figure 1-6).

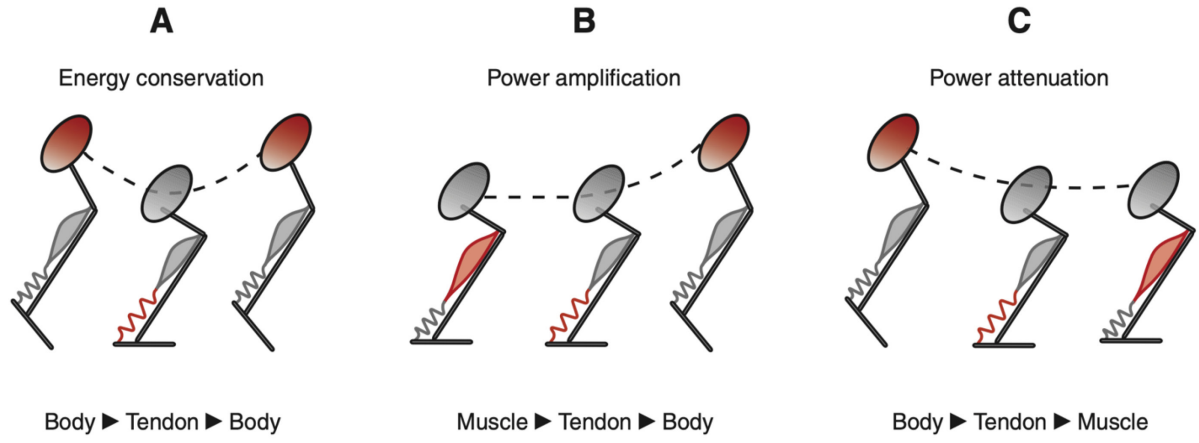

Figure 1-6 (A) shows a schematic of how the direction of energy flow determines mechanical function in muscle-tendon systems. When elastic structures store and recoil cyclic changes in the body's mechanical energy, mechanical energy is conserved (i.e., reduced muscle work). (B) Tendons loaded by the direct work of muscle contraction can quickly release that energy to the body. Muscle power can be increased if energy is released more quickly than stored. (C) Rapid loss of mechanical energy can cause it to temporarily be stored as elastic strain energy, which can then be released to exert force on working muscles. This mechanism may function by decreasing the peak power input to muscles.

Because of the stretch and recoil of the Achilles tendon during walking, the triceps surae muscles in humans can perform almost isometrically (i.e., at constant length) during walking (Fukunaga et al., 2001; Lichtwark et al., 2007). The isometric behavior of the muscle can advantage the walkers and runners in both economy (Fenn, 1924) and muscle force production (Roberts et al., 1997). Investigations on human hopping have also shown a significant increase in muscle activity for a given force production when individuals hop on exceptionally soft surfaces, undermining efficient elastic-energy storage (Moritz & Farley, 2005). Lai et al. (Lai et al., 2014) quantified the contribution of the AT elastic strain energy to the positive work done by the muscle-tendon-unit (MTU) increased by 19% for soleus and 13% for gastrocnemius, as the running speed increased from 2.0 m/s to more than 8.0 m/s. They have concluded that the human ankle plantar-flexor muscle prioritizes energy storage and recoil over muscle fiber work at high running speeds. They showed a reduction of positive ankle plantar-flexor fiber muscle work after 5.0 m/s of running speed in both soleus and gastrocnemius muscles. Hof et al. (Hof et al., 2002) showed a constant increase in the positive work of soleus and gastrocnemius by increasing the running speed in the range of 2.7 and 5.4 m/s. They found the contribution of the tendon to total MTU-positive work is 59% and 77% for soleus and gastrocnemius, respectively. In line with Sasaki and Neptune (Sasaki & Neptune, 2006), they estimated 28 J and 45.3 J AT energy storage and recoil during running in the range of 2.4 m/s to 5.39 m/s. Farris and Sawicki (Dominic James Farris & Gregory S Sawicki, 2012) also found that AT is responsible for 57% of the total MTU-positive work for gastrocnemius during running at 2.0 m/s.

The studies, as mentioned earlier, did not account for the knee joint contribution to the generated forces (Fraysse et al., 2009) at the AT via gastrocnemii muslces, and a possible energy transfer from knee to the ankle joints. Previously, the benefits of biarticular muscles during variant human activities (M. Bobbert et al., 1986; Bobbert & van Ingen Schenau, 1988; Gregoire et al., 1984; Jacobs et al., 1996; van Ingen Schenau, 1989; van Ingen Schenau et al., 1985; van Ingen Schenau et al., 1987) and the benefits of strain energy recoil of tendons (Alexander & Bennet-Clark, 1977; Kümmel et al., 2018; Lai et al., 2014) have been extensively discussed. However, their specific roles during human walking and running at high speeds have not been explored yet. A deeper understanding of tendon mechanical properties, including force, strain, and strain energy, along with the role of biarticular muscles in transferring energy in adjutant joints, could significantly enhance our fundamental knowledge of the economy of human walking and running (i.e., especially in high speeds). This knowledge, in turn, could

contribute to developing strategies for improving human locomotor performance, designing exoskeletons and robots, and preventing/rehabilitating muscle-tendon injuries.

1.5. Biarticular muscles

The complex movements of the human leg require the coordination of multiple joints. The torques produced by these joints come from the combination of forces generated by muscles that act on one joint (monoarticular) and those that span two joints (biarticular). Monoarticular muscles can adjust the force on a single joint depending on neural signals, while biarticular muscles coordinate the forces between joints based on their moment arms. This inherent coordination between joints provided by biarticular muscles is likely advantageous, as the leg morphology has evolved over a long period of time (Chiel & Beer, 1997; Nishikawa et al., 2007). The biarticular muscles are found to cover a wide range of functions in animals, such as dampening impact-related oscillations in horses (Wilson et al., 2001), allowing for energy transfer in distal hindlimbs of turkey, wallaby, and goat or generating positive work in dog and goat forelimbs (Biewener, 2016; Carroll & Biewener, 2009). Unlike the human leg, where biarticular muscles control the flexion and extension of adjutant joints, the biarticular muscle in guinea fowl extends both the hip and knee joints. Additionally, during the stance phase of the guinea fowl movement, this muscle undergoes a stretch-shortening cycle (Carr, Ellerby, & Marsh, 2011; Carr, Ellerby, Rubenson, et al., 2011).

In humans, biarticular muscles have been found to coordinate joint movements, improve the economy of dynamic tasks (i.e., by transferring energy) and secure the zig-zag configuration of the leg against joint overextension (van Ingen Schenau et al., 1987). These commonly known functions are extended by an explicit role of biarticular muscles in controlling the center of mass angular momentum for balance and swing (Schumacher et al., 2020). This thesis section will aim to deliver a brief structure and functional relevance of biarticular muscles.

1.6. Structure of biarticular muscles

The structure and characteristics of a muscle play a crucial role in its capacity to produce force and regulate the length of its fibers in response to the stretching of the tendon (Biewener & Roberts, 2000). A muscle with short pinnate fibers and long tendons is ideal for efficient force production through elastic recoil, while a muscle with longer contractile fibers and short tendons is better suited for generating higher work/power output and controlling the joint

stiffness when subjected to external perturbations (Biewener & Roberts, 2000; Carroll & Biewener, 2009).

The fiber-tendon length ratio of a muscle plays a critical role in determining its contraction dynamics and functional capabilities (Wakeling et al., 2011). The data driven from a musculoskeletal model (Rajagopal et al., 2016) show the biarticular muscle generally has a longer muscle-tendon unit (MTU) compared to monoarticular muscles (Schumacher et al., 2020). This is because biarticular muscles are defined as muscles that cross more than one joint or segment, resulting in a need for longer tendons and contractile fibers in their MTU (Figure 1-7). Understanding the functional contribution of biarticular muscles in generating torques at the joints they span is essential, and their moment arms play a crucial role in this regard. The values of the biarticular moment arm are varied among literature depending on the joint angles (Arnold et al., 2000; Buford et al., 1997; Németh & Ohlsén, 1985; Rugg et al., 1990; Visser et al., 1990; Wretenberg et al., 1996). The biarticular gastrocnemii muscles moment arm at the ankle ranged from 3 to 7cm (Maganaris et al., 1998, 2000; Rasske et al., 2017), while its knee moment arm was in the range of 1 to 4cm (Buford et al., 1997; Spoor et al., 1990). For biarticular thigh muscles, hip moment arms were generally greater than knee moment arms (Cleather et al., 2015). These results are consistent with the previously suggested moment-arm ratios of gastrocnemii (ankle-to-knee ratio: 2:1), hamstring (hip-to-knee ratio: 2:1), and RF (hip-to-knee ratio: 4:3) (Winter, 2009). As far as the author knowledge, there is no connection between the lever-arm of monoarticular and biarticular joints and/or any functional benefits one may have. However, it appears that the energy tends to directed toward the joints with a longer lever arm (Lombard, 1903).

1.7. Mechanics and functional importance of the biarticular muscles

Withstanding or overcoming gravitation is a crucial prerequisite for mobility in both human and animals. Leg joints (hip, knee, and ankle) are frequently synchronized during ground contact such that they go a through flexion/extension cycle during different functional tasks (Cleland, 1867; Ivanenko et al., 2007). Because of the zig-zag shape of the leg, biarticular leg muscles are pulled at one joint while being released at the other joint simultaneously (van Ingen Schenau, 1989). Regardless of the full range of motion of the leg, the length of the biarticular muscle-tendon unit is nearly constant (Dominic James Farris & Gregory S Sawicki, 2012). A distinct function of the biarticular muscle-tendon unit (MTU) is that it can convey mechanical work/power to adjacent joints while creating minimal mechanical work/power (M. Bobbert et

al., 1986; Cleland, 1867; Jacobs et al., 1996; Lombard, 1903; Minetti & Alexander, 1997; Prilutsky et al., 1996; Prilutsky & Zatsiorsky, 1994; Prilutsky, 2000; van Ingen Schenau et al., 1985; van Ingen Schenau et al., 1987). The synchronization of muscles during the extension of the hip, knee, and ankle involves the activation of both single and double-joint opposing muscles, such as Gluteus maximus vs. rectus femoris (RF) and Vastii vs. Gastrocnemii. This coordination can exchange mechanical work/energy between the joints (Lombard, 1903; Wells, 1988). Given that the muscles on the proximal segments of the leg have bigger volumes and, thus, a greater ability produce mechanical work/power than those on the distal segments in both humans (Alexander & Ker, 1990) and animals (Gambaryan, 1974).

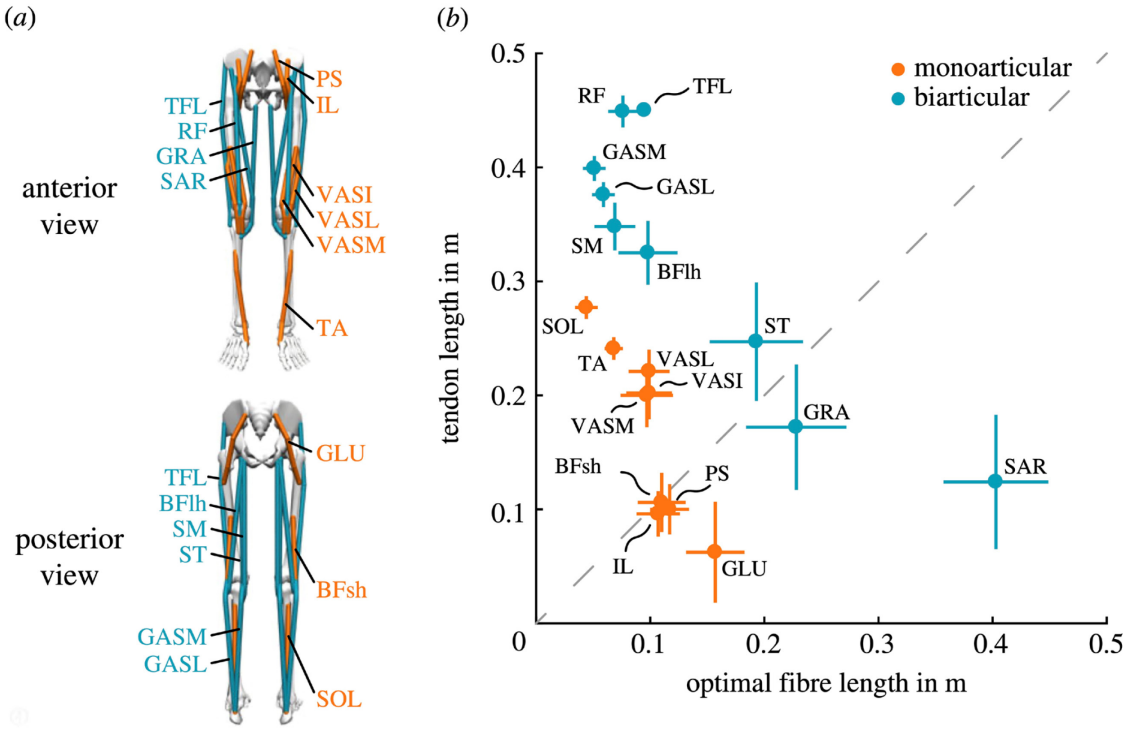

Figure 1-7 (a) Lower limb muscles are categorized into biarticular (cyan) and monoarticular (orange) muscles. (b) The mean and standard deviation of tendon and muscle fiber lengths were generated based on data from Rajagopal et al. (Rajagopal et al., 2016). Muscle abbreviations: soleus (SOL), vastus lateralis (VASL), gastrocnemius medial head (GASM), vastus medialis (VASM), semimembranosus (SM), rectus femoris (RF), vastus intermedius (VASI), gastrocnemius lateral head (GASL), psoas major (PS), biceps femoris long head (BFlh), tibialis anterior (TA), gluteus maximus (GLU), iliacus (IL), semitendinosus (ST), biceps femoris short head (BFsh), tensor fasciae latae (TFL), gracilis (GRA) and sartorius (SAR). The figure is adopted from Schumacher et al. (Schumacher et al., 2020).

In cat locomotion (Prilutsky et al., 1996) and human landing (Prilutsky & Zatsiorsky, 1994), the estimated energy transported by biarticular muscles from distal to proximal joints ranges from 22 to 39% of total negative work at the ankle. In the leg extension phase of locomotion, the contribution of energy transferred from the knee-to-ankle was reported to be 7-14% in cat

locomotion (Prilutsky et al., 1996), 7% in human jogging (Prilutsky & Zatsiorsky, 1994), 28% in human sprinting (Jacobs et al., 1996), 23% (Prilutsky & Zatsiorsky, 1994) and 25% (M. Bobbert et al., 1986; Jacobs et al., 1996) in human vertical jumping. Therefore, during extension, moments are produced at the ankle, knee, and hip during the stance phase of locomotion as well as in landing and jumping. Coactivation of one-and-two joint agonists (Gastrocnemii vs Vastii and RF vs Gluteus maximus) and activation of Gastrocnemii and RF muscles allow bigger proximal muscles to compensate for a limited mechanical capacity of distal muscles to do mechanical work. The same energy transfer mechanism can also be seen in animals such as cats (Prilutsky et al., 1996), dogs (Carrier et al., 1998), goat (Biewener, 2016; Carroll & Biewener, 2009), turkeys, wallabies (Biewener, 2016), frogs (Lombard, 1903; Lombard & Abbott, 1907) and kangaroos (Alexander & Vernon, 1975). Achieving the same mechanical work/power outcome without using biarticular muscles would necessitate activating two monoarticular muscles and subjecting them to shortening/lengthening contractions, which would come at a higher cost (Elftman, 1939b). Experimental testing done by Wells (Wells, 1988) showed that employing biarticular muscles while walking resulted in mechanical energy cost reductions ranging from 7 to 29%, with an average of 11.6%. These findings suggest the function of biarticular muscle is to lower the cost of movement. It's also shown the forces generated by the biarticular muscles can have a significant transverse component which is essential to shift the center of pressure forward (Hof, 2001).

1.7.1. Biarticularity during jumping

Jumping is a common ability shared by a diverse range of animals, including humans, by quickly extending a set of legs. The mechanism of jumping has been conducted on various species, such as fleas (Bennet-Clark & Lucey, 1967), locusts (Bennet-Clark, 1975), frogs (Calow & Alexander, 1973; HIRANO & ROME, 1984; Lutz & Rome, 1994) bushbabies, bonobos (Scholz et al., 2006), rabbits (Gushue et al., 2005), other prosimians (Günther et al., 1991; Günther, 1985), and human (Bobbert & van Ingen Schenau, 1988; Dowling & Vamos, 1993; Fukashiro & Komi, 1987; Gregoire et al., 1984; Pandy et al., 1990; van Ingen Schenau et al., 1987). Two distinct mechanisms enable all these species to perform jumping. First, the energy saving and recoil mechanism in the series of elastic elements of distal plantar flexors muscle-tendon (Alexander, 1995; Dawson & Taylor, 1973; Ker et al., 1987a; Lichtwark & Wilson, 2005; Mo et al., 2020) and second is due to the mechanism of biarticular muscle that transfers the energy from more proximal to distal joints (Fukashiro & Komi, 1987; Gregoire et al., 1984; Pandy et al., 1990; Scholz et al., 2006). According to Gregoire et al. (Gregoire et al.,

1984), proximal-to-distal power transfer effectively converts rotational motion into translation of the body center of mass. This is said to be achieved by the timely activation of the RF and gastrocnemii right before takeoff. According to Bobbert and van Ingen Schenau (Bobbert & van Ingen Schenau, 1988), when the knee begins to extend, the trunk angular acceleration reduces, which causes power to be transmitted from the hip to the knee. Similar to this, activation of gastrocnemii just prior to liftoff will transmit forces produced by the vastii and other knee extensors to the ankle joint (Bobbert & van Ingen Schenau, 1988). As a result, the lack of biarticular muscles would result in the human musculoskeletal system having bigger (and thus heavier) ankle plantar flexors and knee extensors (Pandy & Zajac, 1991). A similar so-called "endless chain" of energy transfer from proximal to distal joints appears to happen in frogs (Calow & Alexander, 1973; Lombard, 1903). A recent study on desert kangaroo rats found that approximately 48% of the work done at the ankle joint during vertical jumps was transferred from the proximal to distal muscles through the biarticular ankle extensor (Schwaner et al., 2018). In jumping dogs, this proximal to distal joint energy transfer contributed to 34% of the positive work produced by the hindlimb and 27% of the total positive work produced by both forelimbs and hindlimbs (Gregersen & Carrier, 2004).

Nonetheless, there is no evidence to support the transfer of mechanical work and power from the knee to the hip (i.e., from distal to proximal joints) during human or animal jumping (M. Bobbert et al., 1986; Bobbert & van Ingen Schenau, 1988; Carrier et al., 1998; Gregersen & Carrier, 2004; Gregoire et al., 1984; Lombard, 1903; Lombard & Abbott, 1907; Pandy & Zajac, 1989; Pandy & Zajac, 1991; Schwaner et al., 2018). It is worth noting that a study on bonobo vertical jumping (Scholz et al., 2006) suggested the possible transfer of mechanical energy from the quadriceps knee extensor to the hip joint through the hamstring muscles. However, this finding contradicts the earlier studies. It may be due to the overestimation of hip moments (due to the inverse dynamic approach) or the underestimation of hip mass muscles in their proposed methodology.

Jumping in humans includes extending joints in a proximodistal sequence, which is well-known for maximum-height jumps (M. Bobbert et al., 1986; Bobbert & van Ingen Schenau, 1988; Pandy & Zajac, 1991). This sequence requires high net joint moments that must be produced at high extension velocities at the distal joints, particularly at the ankle joint (Prilutsky, 2000). Around the ankle joint, the instantaneous power output, which is the product of the net joint moment and joint angular velocity, can reach values as high as 2500 W (Bobbert & van Ingen Schenau, 1988). This was significantly higher than reported during isometric maximal voluntary contraction of 214 W (FUGL-MEYER et al., 1982). It has been argued that

biarticular muscles, such as gastrocnemii, are well-suited for delivering this power (Alexander, 1995; Hof et al., 2002; Kurokawa et al., 2001; Nikolaidou et al., 2017). This is because when the knee is extending, the gastrocnemii muscle length remains close to optimum, and its contraction velocity remains relatively low, even when the ankle extends rapidly. Consequently, the biarticular muscles can generate a significant force and power output around the ankle joint (Bobbert & van Ingen Schenau, 1988). In 1986, Bobbert created a mathematical model to determine the contribution of elastic energy recoil and biarticularity in one-legged jumping (M. F. Bobbert et al., 1986). The ankle joint generated a total of 110 J of energy during one-legged jumping. Of this total, 33 J came from contractile muscle elements, 28 J from the biarticular mechanism, and 49 J from tendon energy storage and recoil. Based on these findings, it can be concluded that the transfer of work/power from the proximal to the distal joint plays a significant role in the high net peak work/power at ankle joint.

1.7.2. Biarticularity during locomotion

Bi-quadrupeds locomotion is thought to be energy efficient (Alexander, 1991; Kar et al., 2003; Rosendo & Iida, 2016; Silva & Machado, 2006) and capable of covering long distances (Kar et al., 2003; Pons, 2008) in a wide range of variant environments (Buschmann et al., 2015; Lee et al., 2020). One of the reasons for this is the exploitation of passive structures in the legs. During specific stages of movement, elastic energy is accumulated in the tendons and ligaments, which is subsequently discharged when its needed (Alexander, 1984, 1988; Alexander, 1991; Alexander & Bennet-Clark, 1977; Babič, 2012; Ker et al., 1987a; Wang et al., 2011). Over the years, numerous researchers have suggested that energy transfer between joints is another factor contributing to the efficiency of locomotion (Carr, Ellerby, & Marsh, 2011; Cleland, 1867; Elftman, 1939b; McGowan et al., 2005; van Ingen Schenau, 1989; van Ingen Schenau et al., 1985; van Ingen Schenau et al., 1987; Whittle, 2014). The most effective technique for reducing total mechanical energy expenditure (Aleshinsky, 1986) or positive and negative work done by all muscles is to generate force through biarticular muscles since its belly length change is less than monoarticular muscles (Prilutsky, 2000).

To avoid whole body rotation in human and animal during locomotion, the direction of the body center of gravity should be approximately aligned with the line of action of the resultant of the ground reaction forces (Winter, 1995). Quadrupeds have their center of gravity positioned in front of the hip and knee joints to a greater extent than bipeds, which enables them to push off with their hind legs during jumping, sprinting, and galloping (Alexander & Ker, 1990). On the other hand, in humans, the line of action is mostly directed towards the

trunk and passes between the hip and knee joints with occasional variations on both sides (Winter, 1995). Consequently, quadrupeds rely more heavily on their biarticular hamstrings and less on the monoarticular RF muscle than humans (Prilutsky, 2000). These differences could explain the variations in the two species relative size of these biarticular muscles. Cheetah is an extraordinary example, where the hamstring is also connected to the calcaneus by a strong tendon (Hudson et al., 2011). The triarticular hamstring biceps femoris muscle assists the animal in achieving the required combination of a net hip-extending, knee-flexing, and plantar flexing moment to become the fastest sprinter specie on the planet (Hudson et al., 2012).

During human locomotion in the second phase of the swing, it should be noted that the hamstring muscles are contracting while the hip and knee are both extending (Perry & Davids, 1992). This causes the hamstrings to produce a flexor moment at the knee and an extensor moment at the hip. The knee moment opposes the direction of knee rotation, leading the hamstrings to produce energy at the hip and absorb energy at the knee (Prilutsky & Zatsiorsky, 1994). However, as the overall change in length of the hamstrings is minimal, they neither absorb nor produce energy. In this scenario, the hamstrings can be viewed as an "energy strap" that helps facilitate energy transfer from the tibia to the pelvis, thereby aiding hip extension. During the first half of the swing, the two joints of the RF muscle can also be analyzed similarly. It was found that in the push-off phase of human locomotion, the RF and gastrocnemius muscles transfer mechanical energy from the proximal joints of the leg to the distal joints, aiding in the extension of the distal joints (Prilutsky & Zatsiorsky, 1994).

Conversely, during initial contact and the first half of the stance, they transfer energy from the distal to proximal joints, facilitating dissipation of the body mechanical energy. The amount of energy transferred by biarticular muscles varies depending on the activity, ranging from 17.3±9.1 J in the running to 178.6±45.6 J in squat jumping (Prilutsky & Zatsiorsky, 1994). During the shock-absorbing phase, however, it's the opposite. The biarticular muscles transfer energy from the distal joints to the proximal joints, ranging from 1.5±1.6 J in shock-absorbing phase of running to 18.6±4.2 J in stance phase of running (Prilutsky & Zatsiorsky, 1994). This energy transfer mechanism has significant functional implications because the muscles on the proximal links of the lower extremity are larger and more capable of producing mechanical work than those on the distal links (Alexander & Ker, 1990). The reason for the proximal muscles ability to produce more work is due to their longer fibers, shorter tendons, and larger cross-sectional areas compared to distal muscles (Alexander & Ker, 1990; Schumacher &

Wolff, 1966). This even distribution of muscles along the leg results in a lower moment of inertia concerning the hip joint, which acts as a "suspension point" for the leg, allowing for more efficient movement with less energy expenditure (Elftman, 1939a).

2. Purpose of the thesis

Precise quantification of the AT strain, strain energy, and force in vivo using noninvasive approaches poses methodological challenges. Current methods in the biomechanics literature have certain limitations that require careful consideration (Finni & Vanwanseele, 2023; Zhang et al., 2020). Using inaccurate methods to quantify AT strain, strain energy, and force can hinder our understanding of AT loading and the functional participation of the triceps surae muscles for power and energy production during human locomotion. Repetitive loading of the AT within a specific strain range (4.5 to 6.5 %) is an effective stimulus for increasing AT stiffness, AT cross-sectional area, and Young's modulus (Arampatzis, Karamanidis, & Albracht, 2007; bohm, 2015). Previous studies suggested that during running, the maximum strain of the AT is ranged between 4.6-9.0 % (Lai et al., 2015; Lai et al., 2018; Lichtwark et al., 2007) and the AT-force is ranged between 3 to 5 kN (Almonroeder et al., 2013; Baxter et al., 2021; Lai et al., 2015; Lai et al., 2018; Lichtwark et al., 2007). The above literature suggests that both AT strain and force during running are sufficient to initiate adaptive responses in the AT mechanical and morphological properties. On the other hand, several studies have failed to detect any significant differences in the AT stiffness between trained runners and untrained controls (Arampatzis, Karamanidis, Morey-Klapsing, et al., 2007; Hansen et al., 2003; Karamanidis & Arampatzis, 2005; Kubo et al., 2010; Wiesinger et al., 2016). To the best of my knowledge, no scientific research discusses this deficit. The biomechanics literature contains limited information on the in vivo quantification of the AT strain energy during locomotion, such as walking and running. This is due to the fact that the majority of investigations in this field have relied on inverse dynamic and musculoskeletal modeling approaches, resulting in a lack of direct measurement.

It has been discovered that the ankle joint is responsible for a sizeable amount (between 40 and 50 percent) of the mechanical work generated in the lower extremities when walking. (D. J. Farris & G. S. Sawicki, 2012; Novacheck, 1998). Additionally, it has been noted that walking speed, mechanical power, and work done at the ankle joint are all positively correlated. (D. J. Farris & G. S. Sawicki, 2012; Lai et al., 2015). These studies provide evidence for the ankle joint crucial contribution to the mechanical power and work required for walking, highlighting the significance of the plantar flexor muscles as a major source of energy generation for walking. The monoarticular Sol generates the most significant part of the mechanical power and work at the ankle joint during walking (Neptune et al., 2008). The biarticular GM and GL

muscles generate moments in both the ankle and knee joints. Thus, power and energy can be transferred from the more proximal monoarticular vastii muscles to the ankle joint (M. Bobbert et al., 1986; Gregoire et al., 1984; van Ingen Schenau et al., 1987). This allows biarticular muscles to control the redistribution and transmission of mechanical force and energy across crossing joints, allowing them to be effective at the needed joint (Cleland, 1867; van Ingen Schenau, 1989). However, the function of the biarticular gastrocnemii muscles at the ankle and knee joints during high walking speeds and the possible modulation of biarticular mechanisms with increasing walking speeds to enhance power and work production at the ankle joint is currently unknown.

The AT length is often calculated as the linear distance between the AT origin at the gastrocnemius medialis muscle-tendon junction (GM-MTJ) and the AT insertion (i.e., the notch at the calcaneus bone). This method assumes that the AT follows a straight line and does not change its alignment, i.e., curvature, during the movement tasks. The AT features a concave curvature that can alter during contractions and functional movements (Maganaris et al., 2000). In study 1, we provided a method to consider the AT curvature for the AT length determination using a line of reflective foil markers (i.e., self-adhesive retro-reflective tape circles with a 5 mm diameter). The foil marks covering the AT from origin to insertion are positioned at regular spatial intervals on the skin. The AT curvature must be considered to measure AT length and strain accurately. However, utilizing several foil markers requires more experimental work due to the increased hardware need (i.e., the number of cameras for marker tracking) and time-intensive post-data processing. However, when used in a diagnostic approach to monitor the mechanical demand of a tendon and control for strain ranges to stimulate adaptation (4.5% to 6.5%), a simplified AT length assessment using a reduced marker-set may be appropriate to detect the AT length and strain magnitudes. However, it is yet to be determined how many foil markers are necessary for a correct AT length measurement during movement.

The objectives of the current thesis were to address the identified gaps in the existing literature by pursuing the following goals: (1) in vivo measurement of the AT strain and force during walking and running using a noninvasive method. (2) Exploring the compensatory role of the monoarticular soleus muscle and biarticular gastrocnemii muscles in human high walking speeds. (3) Measuring the AT length under consideration of its curvature using a modified number of foil markers compared to the proposed method in study 1.

1. The purpose of the first study was to introduce a new in vivo noninvasive method to quantify the AT strain, force, and strain energy. To accomplish this, we employed a novel method to measure AT length during walking and running with consideration of the curve-path shape of

the AT using foil skin markers, the projection of the GM-MTJ to the skin surface as well as the artifact introduced by skin movements relative to the calcaneus bone on top of the AT insertion. Subsequently, based on a tendon force-elongation relationship as a calibration measure established experimentally during maximum voluntary isometric contractions, tendon force, and strain energy were determined. We hypothesized that a) both the GM-MTJ projection to the skin surface and the b) relative movement of skin to the calcaneus bone (i.e., insertion of the AT) can introduce a significant inaccuracy to the AT length and strain, c) AT force and strain during running would not be sufficient to induce adaptation of the AT, d) The results of our direct assessment of the energy storage and release of the AT during walking and running may exhibit differences when compared to previous methodologies.

2. The second study aimed to examine how the monoarticular soleus and biarticular gastrocnemii muscles contribute to mechanical power and work at the ankle joint across a range of walking speeds (slow: 0.7, preferred: 1.4, transition from walking to running: 2.0 and maximum walking speed: 2.6±0.3 m/s). We used the developed method in the first study to measure the AT elongation, strain, and forces during walking speeds. The mechanical power and work of the AT-force at the ankle joint and, separately, the mechanical power and work of the monoarticular soleus at the ankle joint and the biarticular gastrocnemii muscles at the ankle and knee joints were determined. We hypothesized that an increase in contractile net work production of the soleus muscle and an increased contribution of biarticular mechanisms of the gastrocnemii muscles would result in a continuous increase of net mechanical work at the ankle joint from slow to maximum walking speed.

3. Finally, the third study aimed to investigate the feasibility of simplifying the developed method in Study 1 for measuring the AT length by means of reducing the number of foil markers at the path of AT while maintaining accuracy. The study determined the error in the AT length and maximum strain caused by the removal of markers from the curved length compared to the length calculated with all possible markers used in Study 1. We hypothesized a significant inaccuracy in the AT length measurement across gait phases, gait modes (walking vs. running), and gait speeds of the AT length without considering the curve shape compared to AT curved approach. We further hypothesized that the AT length and strain could be determined with a tolerable error by a reduced marker-set, i.e., fewer markers than all available markers.

3. First study: Quantifying mechanical loading and elastic strain energy of the human Achilles tendon during walking and running

Authors:

Mohamadreza Kharazi [1,2]
Sebastian Bohm [1,2]
Christos Theodorakis [1,2]
Falk Mersmann [1,2]
Adamantios Arampatzis [1,2]

[1] Department of Training and Movement Sciences, Humboldt-Universität zu Berlin, Germany.
[2] Berlin School of Movement Science, Berlin, Humboldt-Universität zu Berlin, Germany.

Published in:
Scientific Reports, 2021, 11:5830. doi.org/10.1038/s41598-021-84847-w.
(reprinted with permission by Nature)

3.1. Abstract

The purpose of the current study was to assess in vivo Achilles tendon (AT) mechanical loading and strain energy during locomotion. We measured AT length considering its curve-path shape. Eleven participants walked at 1.4 m/s and ran at 2.5 m/s and 3.5 m/s on a treadmill. The AT length was defined as the distance between its origin at the gastrocnemius medialis myotendinous junction (MTJ) and the calcaneal insertion. The MTJ was tracked using ultrasonography and projected to the reconstructed skin surface to account for its misalignment. Skin-to-bone displacements were assessed during a passive rotation (5°/s) of the ankle joint. Force and strain energy of the AT during locomotion were calculated by fitting a quadratic function to the experimentally measured tendon force-length curve obtained from maximum voluntary isometric contractions. The maximum AT strain and force were affected by speed ($p < 0.05$, ranging from 4.0 to 4.9% strain and 1.989 to 2.556 kN), yet insufficient in magnitude to be considered as an effective stimulus for tendon adaptation. Besides the important tendon energy recoil during the propulsion phase (7.8 to 11.3 J), we found a recoil of elastic strain energy at the beginning of the stance phase of running (70–77 ms after touch down) between 1.7 ± 0.6 and 1.9 ± 1.1 J, which might be functionally relevant for running efficiency.

3.2. Introduction

Tendons cannot generate force actively, yet their elastic behavior upon loading influences the muscle-tendon unit's function during locomotion. The human Achilles tendon (AT) length changes during functional tasks as walking, running, jumping, or cycling is important to understand the interaction between muscle and tendon (Dick & Wakeling, 2017; Kümmel et al., 2018; Lichtwark & Wilson, 2005), assess tendon loading, and examine tendon's elastic strain energy (Ishikawa et al., 2005; Lai et al., 2014). The AT's reported maximum strain values during running are between 4.6 and 9.0% (Lai et al., 2015; Lai et al., 2018; Lichtwark et al., 2007) and between 4.0 to 4.3% during walking (Ishikawa et al., 2005; Lai et al., 2014; Lichtwark et al., 2007; Monte et al., 2020). Corresponding AT force values ranged from 3.06 to 4.64 kN during running (Almonroeder et al., 2013; Werkhausen et al., 2019) and about 2.63 kN during walking (Giddings et al., 2000). These results suggest substantial mechanical loading of the AT during human locomotion. The AT can adapt to external mechanical loading by increasing its stiffness, elastic modulus and size (Bohm et al., 2015; Wiesinger et al., 2015). Loading-induced alteration of tendon properties is a biological mechanism to maintain the functional integrity of the muscle-tendon unit and to keep tendon mechanical loading in a

physiological range during functional tasks (Arnoczky, Tian, et al., 2002; Wang et al., 2013). Repetitive loading of the AT with a strain magnitude between 4.5 and 6.5% has been evidenced as an effective mechanical stimulus, improving AT mechanical properties (Arampatzis, Karamanidis, & Albracht, 2007; Arampatzis et al., 2010; Bohm et al., 2014). This tendon strain range is commonly reached at about 90% of a voluntary maximum isometric contraction of the adjacent muscle, which results in AT forces between 2.34 and 3.69 kN (Arampatzis, Karamanidis, Morey-Klapsing, et al., 2007; Arampatzis et al., 2010; Bohm et al., 2014).

Although the above mentioned reports of AT strain and force during running indicate sufficient AT loading for the initiation of adaptive alterations in tendon properties (Almonroeder et al., 2013; Lai et al., 2015; Lai et al., 2018; Lichtwark et al., 2007), most studies, which compared the AT mechanical properties between runners and untrained controls were not able to detect any differences between the two groups (Arampatzis, Karamanidis, Morey-Klapsing, et al., 2007; Karamanidis & Arampatzis, 2005; Kubo et al., 2010; Wiesinger et al., 2016). Furthermore, in the longitudinal study of Hansen et al., no significant changes in AT's mechanical properties were observed after nine months (78 sessions) of running training (Hansen et al., 2003). In addition to a shorter loading duration (i.e., during running) that may explain this discrepancy (estimates of loading vs. lack of adaptive response) (Arampatzis, Karamanidis, & Albracht, 2007; Arampatzis et al., 2010; Bohm et al., 2014) , these findings might also result from the methodological approaches used in vivo assessment of AT strain during locomotion. Previous in vivo approaches used for assessing AT length during functional tasks either calculated AT length using a simple planimetric model (Lai et al., 2015; Lichtwark et al., 2007) or did not consider the AT's concave curvature in their measurements (Dick et al., 2016; Lichtwark & Wilson, 2005, 2006). There is evidence that considering the AT as a straight line between calcaneus (insertion) and gastrocnemius medialis (GM) myotendinous junction (MTJ, origin) results in an underestimation of the AT length and substantial errors (up to 78%) of the AT length changes (Fukutani et al., 2014).

The instantaneous curved length of the AT can be obtained using a line of reflective markers attached to the skin from the tuber calcanei to the MTJ of the GM (Arampatzis et al., 2008; De Monte et al., 2006). Although this method has been validated by comparing the outcomes with accurate AT length measurements from magnetic resonance imaging (Fukutani, 2014), it has not been applied to assess AT length during locomotion. The neglect of AT's curvature during locomotion could result in a 3.4 mm error when the ankle rotates from 30° in plantar flexion to 15° in dorsiflexion (Fukutani et al., 2014). Considering an average AT rest length of 200 mm would cause a significant strain error of 1.7%. During dynamic functional tasks, two more

issues may introduce errors in such AT length measurements. First, the original position of the GM MTJ is not aligned with the reflective markers attached to the skin surface and, therefore, for an accurate AT length measurement, the identified position of the MTJ should be projected to the skin (Figure 3-1 a). Secondly, the attached marker at the calcaneus that defines the AT insertion represents the underlying bones' movement. However, the relative movement of the skin to the bone can introduce important artifacts in the measurements and should be considered. Therefore, the skin's potential displacement relative to the bone underneath the calcaneus marker that defines the AT insertion can also introduce errors in the AT length measurement (Lichtwark & Wilson, 2005).

The elastic strain energy recoil of the AT during the propulsion phase of walking and running is a well-known mechanism within the muscle-tendon unit, which increases the efficiency of muscle output power (Ishikawa et al., 2005; Lai et al., 2014; Monte et al., 2020). The contribution of the elastic strain energy recoil to the muscle-tendon unit's positive work is greater compared to the work produced by the muscle fascicles alone (Ishikawa et al., 2005; Lai et al., 2014; Monte et al., 2020). However, there are also indications of AT elastic strain energy recoil during the early stance phase of running (Komi, 1990), which is not well understood. Komi et al. (Komi, 1990), using an implanted transducer around the AT, measured in vivo AT forces during running and found an apparent decrease of AT force after heel contact, particularly in rearfoot runners, indicating an energy recoil of the AT directly after touchdown. Considering that in this phase, the fascicles of the triceps surae muscles actively shorten (Bohm et al., 2019; Lai et al., 2018; Lichtwark et al., 2007), it can be argued that the contractile elements do not absorb this elastic strain energy recoil from the AT and, thus, it might be an additional important source of energy for human running.

The current study aimed to assess the AT's mechanical loading and strain energy during walking and running. For this purpose, we measured the AT length during walking and running using a new in vivo approach, which considers the tendon curve-path shape using skin markers, taking into

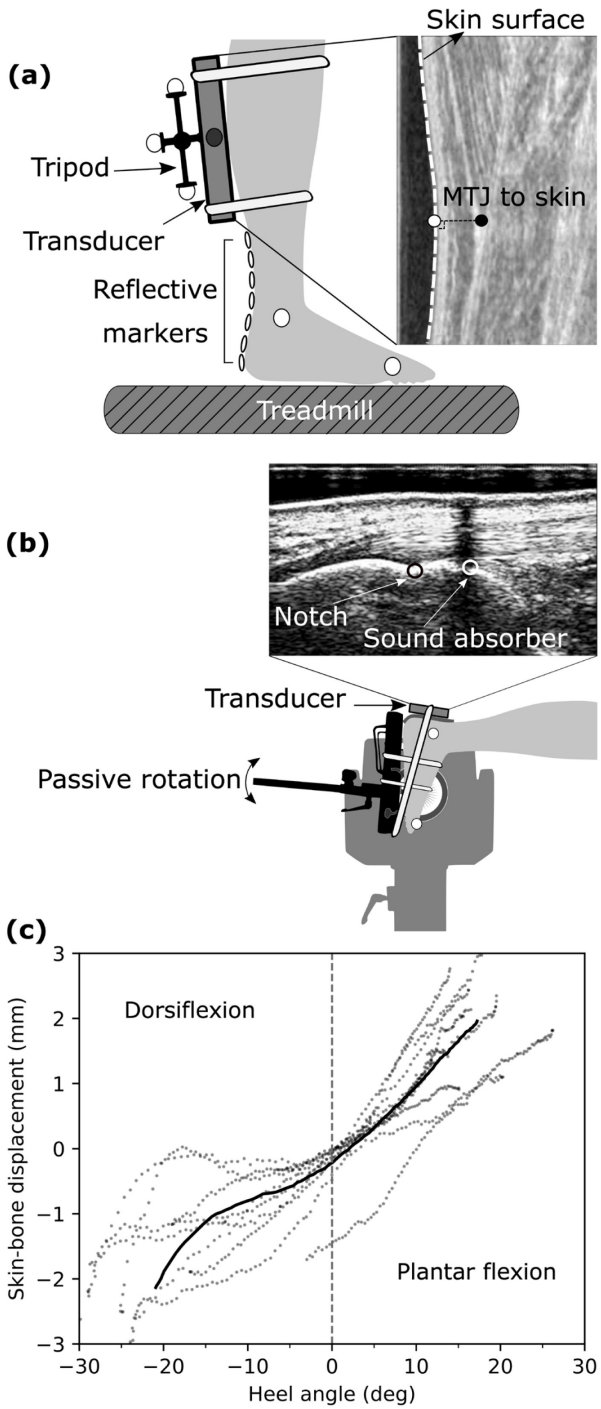

Figure 3-1 (a) Experimental setup for determining Achilles tendon (AT) length during gait. (a) Reflective foil markers on the skin were used to reconstruct the curve-path shape of the AT. The position of the gastrocnemius medialis myotendinous junction was projected to the skin surface, and the coordinates of the ultrasound images were transformed to the global coordinate system using a marker tripod attached to the ultrasound probe. (b) A three-centimeter ultrasound probe was placed on top of the calcaneus bone and a sound-absorptive marker in-between to measure the differences in calcaneus bone displacements (notch) and the skin (absorber marker) displacements as a function of the heel to shank angle. (c) Average (solid line) and individual (filled dots) data of skin-to-bone displacements vs. heel angle. Positive heel angles represent plantar flexion, and negative ones are dorsiflexion (eleven participants with three repetitions)

account the projection of the MTJ to the skin surface as well as potential movements of the skin relative to the calcaneus bone. Tendon force and strain energy were then calculated based on an experimentally determined tendon force–elongation relationship. We hypothesized a relevant contribution of the MTJ projection to the skin and skin-to-bone displacement on the AT length. Further, we expected lower levels of tendon strain during locomotion, as previously reported, insufficient in magnitude to serve as a stimulus for the adaptation of AT mechanical properties. Finally, we hypothesized a functional relevant recoil of tendon elastic strain energy to the body at the beginning of the stance phase during running.

3.3. Results

The non-normal distribution of all data was rejected significantly ($p = < 0.001$). A significant gait speed effect was found on stance-time and cadence ($p < 0.001$) but not on swing-time ($p = 0.436$, Table 3-1). Comparing semi-automatic versus manual tracking of the MTJ position, the variance accounted for (VAF) were $93 \pm 0.4\%$, $97 \pm 0.1\%$ and $97 \pm 0.5\%$, and the adjusted r-squares were 0.96 ± 0.02, 0.99 ± 0.008 and 0.98 ± 0.02 ($p < 0.001$) during walking, slow running and fast running, respectively, evidencing high conformity of the developed algorithm with manual tracking (Figure 3-2). The average root-mean-square error (RMSE) of the skin-to-bone displacement on the AT length during gait was between 0.92 and 1.09 mm. The average RMSE of the projection of the MTJ to the skin surface and AT length was between 1.9 and 2.1 mm (Table 3-2). The SPM-analysis (statistical parametric mapping) showed significant effects ($p < 0.001$) of both skin-to-bone displacement and the projection of the MTJ to the skin on the AT length-measurement during walking and running (Figure 3-3). The significant differences between AT length and length without considering the skin-to-bone displacement were in walking, mainly at the beginning of the swing phase (Figure 3-3). During running, there were significant differences in both stance and swing phases (Figure 3-3). The effects of MTJ projection to skin were more prominent and expanded in the whole gait cycle (Figure 3-3).

We found a significant effect of gait speed on maximum AT strain ($p = 0.043$), force ($p = 0.025$), strain energy ($p = 0.008$) and strain energy recoil during the propulsion phase ($p = 0.007$, Table 3-3). The post hoc analysis showed significant differences in maximum strain, force, strain energy and energy recoil during the propulsion phase between walking and fast running ($p = 0.023$, $p = 0.018$, $p = 0.016$, $p = 0.014$, respectively) as well as between slow running and fast running ($p = 0.023$, $p = 0.018$, $p = 0.016$, $p = 0.014$, respectively). At the beginning of the stance

phase, the initial strain energy recoil did not show significant differences ($p = 0.635$) between slow and fast running (Table 3-3).

The maximum tibialis anterior (TA) EMG activity during the stance phase was not significantly different between the three gait speeds ($p = 0.128$). A significant effect of gait speed on maximum GM and soleus (Sol) EMG activity was found ($p < 0.001$). The pos thoc analysis revealed a significant difference between walking and slow running ($p < 0.001$) and walking and fast running ($p < 0.001$) for

Table 3-1 Duration of the stance and swing phases and cadence during walking and running (average value ± standard deviation). *Statistically significant gait effect (p < 0.05). # Statistically significant differences (post hoc analysis) to fast running (p < 0.05). ^ Statistically significant differences (post hoc analysis) to slow running (p < 0.05).

	Walking (1.4 m/s)	Slow running (2.5 m/s)	Fast running (3.5 m/s)
Stance (ms) *	605 ±47 # ^	330 ±36 #	279 ±19
Swing (ms)	437 ±33	436 ±45	423 ±32
Cadence (gait cycles/s) *	1.7 ±0.1 # ^	2.3 ±0.1#	2.5 ±0.1

Sol and GM muscles. The post hoc comparisons between slow and fast running revealed a significant difference ($p = 0.001$) only for the Sol muscle (Table 3-3).

3.4. Discussion

In order to assess the mechanical loading and strain energy of the AT during walking and running, we measured AT length using a new in vivo approach, which considers the tendon curve-path shape, taking into account the offset between MTJ and skin surface and the potential movements of the skin relative to the calcaneus bone at the AT insertion marker. Further, we developed a novel algorithm to track the MTJ position from the ultrasound image sequences that showed high conformity with a manual analysis. The of video frames analyzed for walking was on average 1912 ± 411 pictures and for running between 1324 and 1407 pictures for ten gait cycles.

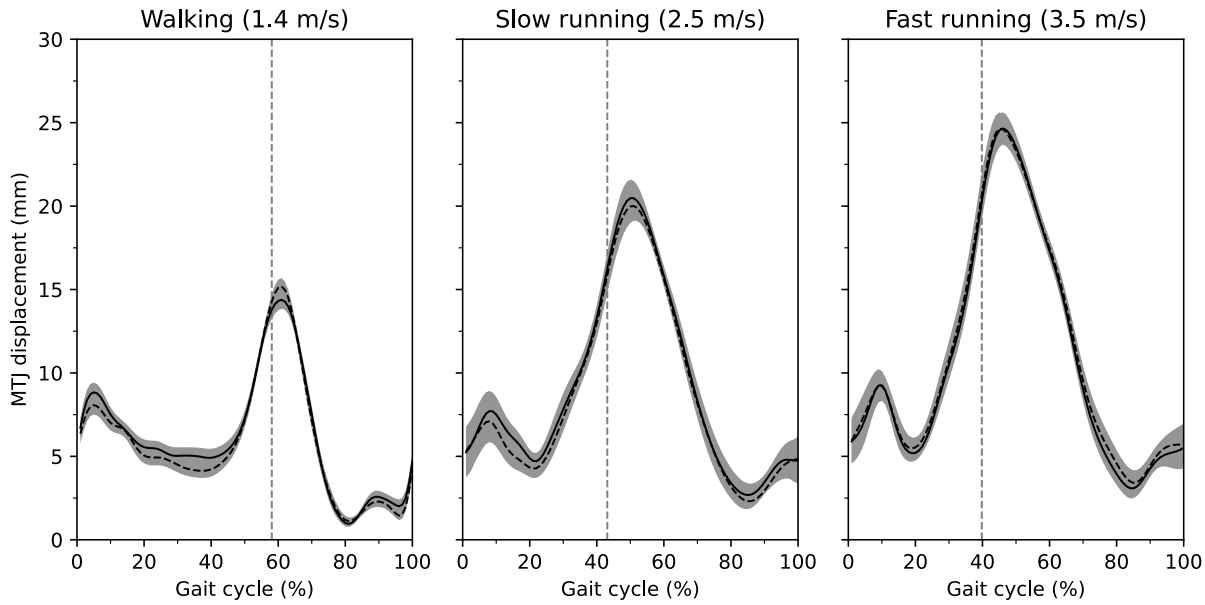

Figure 3-2 Displacement of the gastrocnemius medialis myotendinous junction using the self-developed semi-automatic algorithm compared to the manual tracking for walking, slow running, and fast running. The x-axis is normalized to the gait cycle. The gray highlighted areas are the standard errors. The gray dashed vertical line separates the contact and swing phase (average of seven participants with three gait cycles).

Table 3-2 Contribution of skin-to-bone displacement and projection of MTJ to the skin surface on the AT length as means of the root mean square error (average value ± standard deviation).

	Walking (1.4 m/s)	Slow running (2.5 m/s)	Fast running (3.5 m/s)
Skin-Bone (mm)	0.92 ±0.57	1.08 ±0.61	1.09 ±0.53
MTJ projection (mm)	1.90 ±0.90	2.00 ±0.80	2.10 ±0.80

The average time needed for the manual tracking of one video was 7.9 h for walking and 5.4 h for running trials. The time for the analysis using our algorithm was considerably reduced to 17 min for walking and 13 min for running (i.e., including manual adjustment), giving evidence for essential improvements of the MTJ tracking's time-efficiency without a decline in the quality of the outcome.

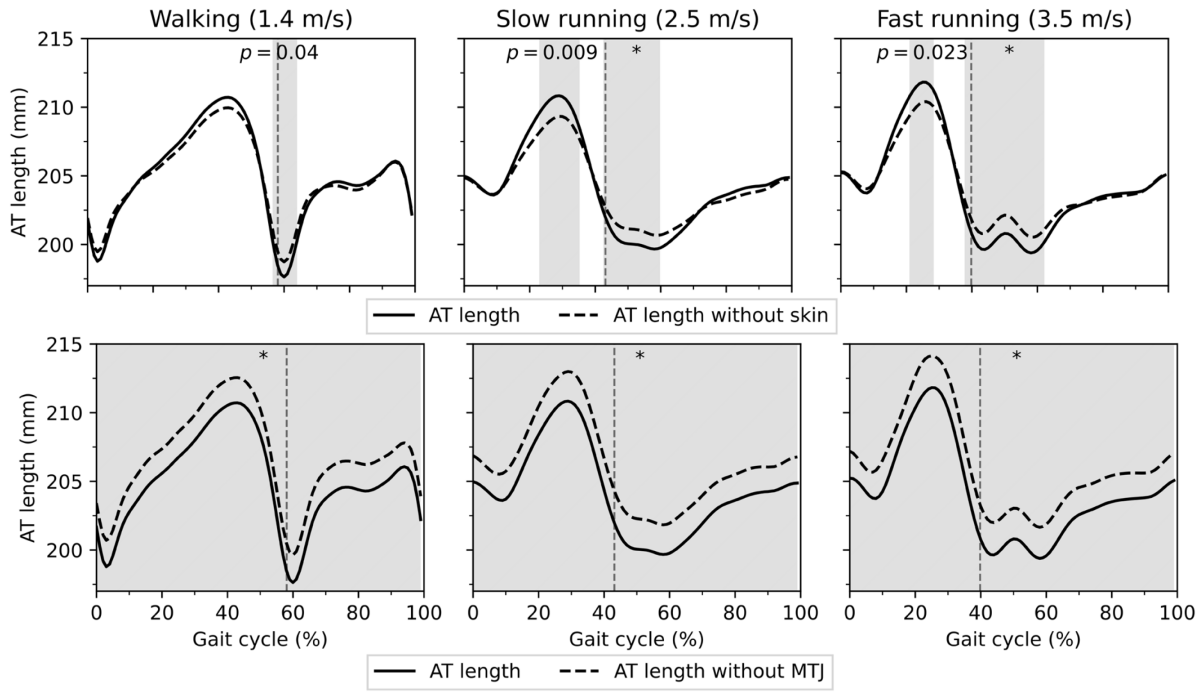

Figure 3-3 The first row shows the contribution of the skin-to-bone displacement to AT length; the second row shows the contribution of the projection of the MTJ to the skin surface to AT length. AT length: The length of AT considering its curve-path shape, skin-to-bone displacement and the projection of the myotendinous junction (MTJ) to the skin surface. AT length without skin: AT length considering its curve-path shape and the projection of the MTJ to the skin surface. AT length without MTJ: The length of AT considering the curve-path shape and skin-to-bone displacement; the x-axis is normalized to the gait cycle. The filled gray areas indicated a significant difference between methods as result of the SPM paired t-test. The gray dashed vertical lines separate the contact and swing phases. The '*' sign indicates the p-value < 0.001. Otherwise, the exact p-values are annotated in the figure. (the average of eleven participants with ten gait cycles). The maximum tendon force and elongation during the isometric MVCs were 5.523 ± 0.552 kN and 14.0 ± 2.5 mm, respectively. The adjusted r-square from the force–elongation of the quadratic equation (Equation 3-5) was, on average, 0.98 ± 0.01 ($p < 0.001$), and the average values of the two constants a and b were 8.7 and 181, respectively. Strain, force, strain energy, and the EMG activity of the three investigated muscles during walking and running are depicted in Figure 3-4.

The AT morphology features a variable curvature that changes during muscle contraction (Kinugasa et al., 2018; Maganaris et al., 2000). Therefore, the consideration of the AT curved shape is crucial for the investigation of in vivo conditions (Harkness-Armstrong et al., 2020). A reconstruction of the AT curvature using skin markers is a practical and valid approach to address this issue (Arampatzis et al., 2008; De Monte et al., 2006; Fukutani et al., 2014). Our findings indicate that the misalignment of the MTJ and the markers on the skin as well as the skin-to-bone displacement are two important error sources that affect AT length measurements during locomotion when using this approach. The MTJ projection effect on the AT length was

significant during the whole gait cycle in both walking and running. The RMS differences between AT length and AT length without MTJ projection, which depicts the contribution of the MTJ projection to the skin surface, were on average, 2.0 mm (across gait speeds), resulting in 1.01% of AT strain.

The contribution of the skin-to-bone displacement was lower compared to the MTJ projection. However, the RMSE was 1 mm on average, indicating 0.45% inaccuracy on AT strain, thus a notable effect on AT length and strain.

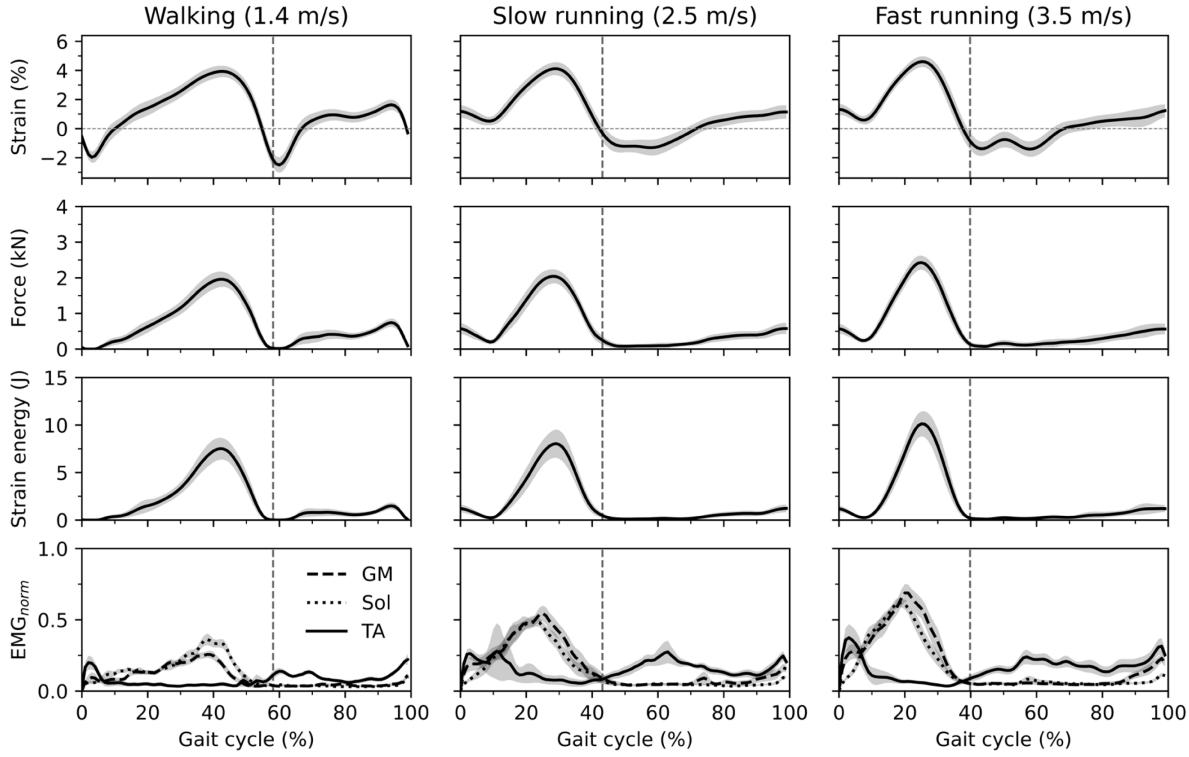

Figure 3-4 Achilles tendon (AT) strain, force and strain energy as well as EMG activity of the gastrocnemius medialis (GM), soleus (Sol) and tibialis anterior (TA) muscle during walking (1.4 m/s), slow running (2.5 m/s), and fast running (3.5 m/s). The gray highlighted area around the curves indicates the standard error. The x-axis is normalized to the gait cycle. The gray dashed vertical line separates the contact and swing phase (average of eleven participants with ten gait cycles).

As expected, the maximum strain values in all gait conditions occurred during the stance phase and close to the beginning of the propulsion phase. Shortly after take-off, strain drops rapidly to its minimum value and again increases with a moderate slope until the end of the gait cycle. The maximum strain values were, on average, between 4.0% during walking and 4.9% during running, corresponding to 51 and 62% of the strain achieved during the MVCs. Earlier studies (Lai et al., 2015; Monte et al., 2020) reported

Table 3-3 Peak values of strain, force and strain energy of the Achilles tendon (AT) as well as maximum normalized EMG activities of the gastrocnemius medialis (GMnorm), soleus (Solnorm), and tibialis anterior (TAnorm) during walking and running. Furthermore, elastic strain energy recoil during the propulsion phase and at the initial part of the stance phase is presented (average value ± standard deviation). *Statistically significant gait effect ($p < 0.05$). # Statistically significant differences (post hoc analysis) to fast running ($p < 0.05$). ^ Statistically significant differences (post hoc analysis) to slow running ($p < 0.05$).

	Walking (1.4 m/s)	Slow running (2.5 m/s)	Fast running (3.5 m/s)
$Strain_{max}$ (%) *	4.0 ±1.2 #	4.5 ±1.3 #	4.9 ±1.2
$Force_{max}$ (kN) *	1.989 ±0.0684 #	2.284 ±0.0536#	2.556 ±0.0540
$Strain\ energy_{max}$ (J) *	7.8 ±3.7 #	9.5 ±4.3 #	11.3 ±4.1
Propulsion recoil (J) *	7.8 ± 3.9 #	9.1 ± 4.4 #	11.3 ± 4.3
Initial recoil (J)	_	1.88 ±1.10	1.71 ±0.65
GM_{norm} *	0.31 ±0.09 # ^	0.68 ±0.15	0.8 ±0.2
Sol_{norm} *	0.38 ±0.11 # ^	0.61 ±0.13 #	0.73 ±0.11
TA_{norm}	0.27 ±0.13	0.54 ±0.55	0.5 ±0.27

maximum AT strain values of 3.9 to 4.4% during walking at velocities of 1.25 to 1.4 m/s. These values are very close to the maximum strain we found (4.0%) in the current study at 1.4 m/s walking velocities. During running, we depicted 4.5% to 4.9% of maximum AT strain at speeds of 2.5 and 3.5 m/s. Most of the earlier reports about the maximum AT strain during running are based on calculations using a simple planimetric model of the gastrocnemius or/and the soleus muscle-tendon unit (Lai et al., 2015; Lai et al., 2018; Monte et al., 2020). In those planimetric models, the length of the tendon was calculated by subtracting muscle fascicle length projected in the direction of the line of force application from the MTU length. The reported maximum tendon strain values using the soleus muscle-tendon unit

ranged from 6.0 to 8.0% at velocities from 2.0 to 4.0 m/s. For the gastrocnemius medialis muscle-tendon unit Lichtwark et al. (Lichtwark et al., 2007) found at 2.1 m/s running velocity maximum strain values of 5.5% where Monte et al. (Monte et al., 2020) reported strains of 3.5 to 4.0% at running velocities of 2.8 and 3.6 m/s. Further, Lai et al. (Lai et al., 2018) calculated maximum tendon strains of 2.0 to 3.0% at velocities of 2.0 to 4.0 m/s.

The repetitive strain of tendons is a crucial mechanical stimulus that regulates cell function. It affects the expression of growth factors and the synthesis of matrix proteins (Arnoczky, Tian,

et al., 2002; Lavagnino et al., 2003; Yang et al., 2004), determining tendon plasticity (Arampatzis, Karamanidis, & Albracht, 2007; Bohm et al., 2014; Wiesinger et al., 2015).

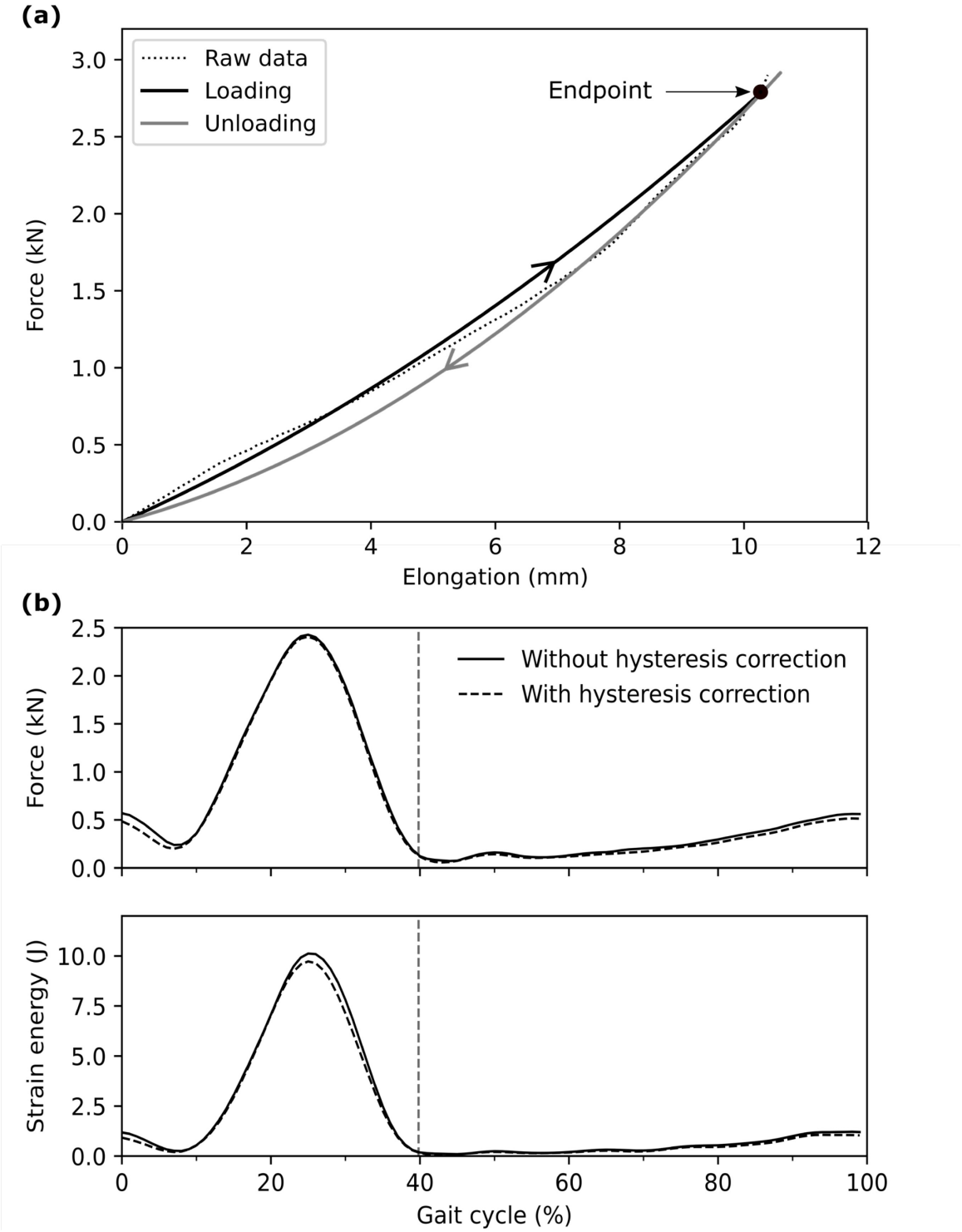

Figure 3-5 (a) Experimentally assessed Achilles tendon (AT) force–elongation relationship during maximum voluntary contractions (Raw data) and the modeled force–elongation curve during loading and unloading (eleven individuals with ten gait cycles. (b) AT force and AT strain energy with and without hysteresis

consideration during fast (3.5 m/s) running. The x-axis is normalized to the gait cycle. The gray dashed vertical line separates the contact and swing phase.

Previous studies examining the effects of submaximal running on AT mechanical properties reported similar AT stiffness between runners and untrained individuals in young and old adults (Arampatzis, Karamanidis, Morey-Klapsing, et al., 2007; Karamanidis & Arampatzis, 2005) and no adaptive effects of long-time running training on the AT properties (Hansen et al., 2003). Considering that the effective mechanical stimulus for tendon adaptation in terms of strain magnitude ranges between 4.5 and 6.5% strain and long duration of loading (i.e., 3 s) (Arampatzis, Karamanidis, & Albracht, 2007; Bohm et al., 2014; Pizzolato et al., 2019), our findings indicate that submaximal running does not provide sufficient tendon loading magnitude for triggering improvements of the AT mechanical properties and may explain the lack of observable effects in the former studies. The found maximum AT strain of 4.0 to 4.9% during the stance phase of walking and running was very short in duration. The time interval where AT strain exceeded 4.5% in five individuals during slow running and seven individuals during fast running on average 90 ± 40 ms for both running speeds. These results indicate a very short duration of AT strain above the reported threshold and less compared the recommended longer duration per repetition (i.e., 3 s) for an effective loading stimulus for tendon adaptation (Falk Mersmann et al., 2017). The average strain during the stance phase was for walking 1.9% and for running ranged from 2.2 to 2.4%, indicating low mechanical loading on the AT and insufficient to trigger additional adaptive responses. Therefore we can argue that in both conditions, walking and submaximal running, the applied mechanical loading on the AT is likely too low to initiate anabolic tendon responses (Pizzolato et al., 2019). The assessed maximum AT force in the current study was for walking 2.7 and for running between 3.2 and 3.5-times of body weight. These values are significantly lower than predictions based on musculoskeletal models, which reported maximum AT forces of 3.9 of body weight during walking (Giddings et al., 2000) and between 5 and 7 of body weight during running (Almonroeder et al., 2013; Lee et al., 2019). These discrepancies might be a result of musculoskeletal model limitations, for example, the difficulties in the prediction of activation dynamics using optimization methods (Ait-Haddou et al., 2004; Jinha et al., 2006) for muscle force predictions, which is more evident during rapid movements (Neptune & Kautz, 2001). Further, the missing individual muscle and tendon properties for all involved muscles and the non-consideration of all possible forces that contribute to the resultant ankle joint moment (e.g., ligaments, bones) in the musculoskeletal models increase the model limitations.

It has been generally accepted that one of the primary roles of the tendon in vertebrates is to store energy during stretching and recoil during shortening (Alexander, 1984; Alexander, 1991). Our results showed an average maximum elastic energy recoil during the propulsion phase of 7.8 J during walking, which increased to 9.5 and 11.3 J during slow and fast running. Although the pos thoc analysis resulted in a statistically significant difference of elastic strain energy recoil only in fast running compared to walking and slow running, the positive effect of gait speed on the energy storage and recoil during locomotion is notable and in agreement with earlier studies (Lai et al., 2015; Lai et al., 2014; Monte et al., 2020). During the push-off phase of walking and running, almost the whole AT strain energy is returned to the human system (at take-off, the AT strain energy is very close to zero). It is well accepted that this recoil of energy reduces the plantar flexor muscles mechanical work (Shadwick, 1990) to accelerate the body's center of mass in the desired movement direction (Voigt et al., 1995). The average assessed maximum AT force of 1.989 kN in the current study during walking is very close to the reported values measured with the optic fiber method (~ 1.7 kN) at a similar walking velocity (Ishikawa et al., 2005) and consequently, the elastic energy recoil is also close to our assessment. During running, we found AT tendon forces between 2.284 to 2.556 kN. These values are significantly lower compared to tendon force estimations using inverse dynamics and musculoskeletal model approaches (3.06 to 4.64 kN (Almonroeder et al., 2013; Werkhausen et al., 2019)). These differences result in differently calculated tendon strain energy storage and recoil values. In our study and using the experimentally assessed quadratic function of the tendon force–length curve, we found significantly lower values in the energy recoil during the propulsion phase of running than studies using an inverse dynamics approach and musculoskeletal modeling (Lai et al., 2014). Lai et al. (Lai et al., 2014) reported an AT energy recoil during the propulsion phase of 27.7 and 38.7 J, at running speeds of 2.1 and 3.5 m/s, respectively. These values are about three times higher than in the current study with 9.2 and 11.2 J at 2.5 and 3.5 m/s of running speed, respectively. In the inverse dynamics approach by Lai et al. (Lai et al., 2015), the passive forces transmitted by ligaments, by bone-to-bone contacts and by soft tissues around the ankle joint are not considered, and therefore the calculated muscle forces might be overestimated, resulting in an overestimation of the tendon strain energy.

Our results also demonstrated elastic strain energy recoil directly after the touchdown during running. The recoil of strain energy in this initial stance phase (i.e., 70 to 76 ms) was between 1.7 and 1.9 J. These values are 15 to 20% of the maximum AT strain energy during the stance phase. Therefore, they might be functionally relevant. We can exclude that this initial strain energy

recoil might be dissipated by the muscle contractile elements of the triceps surae muscle because in the investigated running velocities, the fascicles of all three muscles of the triceps surae show an active shortening (Bohm et al., 2019; Lai et al., 2014; Lichtwark et al., 2007). We interpret this finding as the recoil of AT tendon elastic strain energy to the body in this initial phase of stance right after touchdown. This phenomenon (i.e., a decrease of AT force and recoil of elastic strain energy after heel contact) has not been mentioned in the literature, and, therefore, the functional consequences for the running task are not known. Komi et al. (Komi, 1990), using a force transducer that was surgically implanted in the AT, reported a decrease of AT force directly after the touchdown in rearfoot running and suggested an association with the reduction of TA EMG activity. As the foot contacts the ground, the TA muscle showed a high EMG activity, indicating an active control of the initial plantar flexion through muscular force. The reduction of the AT force after heel contact decreases the internal resultant ankle joint moment, supporting the TA function as a regulator of the ankle joint during the initial part of the stance phase. However, it is difficult to explain the resulting functional consequences of the AT elastic energy recoil in this initial phase because it is unclear where this energy is returned. A recoil of AT strain energy must not necessarily increase the mechanical work/power at the ankle joint but can, for example, be absorbed by the TA tendinous tissues (Maharaj et al., 2019) or by the elastic structures of the foot arch (Kelly et al., 2015; Ker et al., 1987b) and stored as elastic strain energy.

We measured the force–elongation relationship of the AT using MVCs with a slow rate of the force application. The participants completed five trials of isometric ramp contractions, steadily increasing effort from rest to the maximum in ~ 5 s resulting in an average tendon loading rate of 1.076 ± 0.456 kN/s. Using the individually assessed force–elongation relationship, we calculated the AT force during walking and running. During the stance phase in the investigated conditions, the AT loading rate ranged from 16.5 to 20.0 kN/s and was significantly higher compared to the MVCs. Tendons, as biomaterials, are viscoelastic, and, therefore, the differences in the loading rate may influence the accuracy of the tendon force assessment during the walking and running trials. However, tendon hysteresis is ~ 10% (Bennett1 et al., 1986; Pollock & Shadwick, 1994), indicating minor damping components in the tendon properties. Ker et al. (Ker, 1981) found that loading frequencies from 0.22 to 11 Hz (loading rate from 0.580 to 31.240 kN/s) did not affect the youngs modulus of the tendon and, therefore, we can assume a negligible effect of loading rate on tendon dynamics during physiological activities like walking and running. More recently, Rosario and Roberts et al. (Rosario & Roberts, 2020) investigated tendon strains at loading rates between 10 and 80 MPa/s and

predicted a change from slow to fast loading of 0.16% strain on the human AT during running, evidencing a minor effect of loading rate on tendon dynamics. Based on these reports, we can argue that the loading rate differences between the MVCs and the investigated locomotor activities did not significantly affect the AT force and strain energy assessment.

Further, both the loading and unloading phases of AT force were assessed from the same force–elongation curve during MVC trials, and the effect of hysteresis in the unloading phase was not considered. To examine the impact of the hysteresis effect on both AT force and AT strain energy, we assumed a 10% hysteresis, as it is the reported order of magnitude in most studies (Bennett1 et al., 1986; Ker, 1981; Pollock & Shadwick, 1994). For that reason, we determined the two coefficients (a and b) of the Equation 3-5 for the unloading phase based on the following constraints: (a) force–elongation curve during the unloading phase will reduce the strain energy by 10%, and (b) both force–elongation curves (loading and unloading) will end in the same point (Figure 3-5a). The two constant coefficients of the unloading curve were reached by solving two equations with two unknown variables. The choice of appropriate coefficients in the recalculation of force and strain energy was based on the first derivative of the AT length. If the first derivative was negative, the unloading curve's coefficients were used; otherwise, the standard force–elongation curve was used (Figure 3-5b). The contribution of hysteresis to AT force and strain energy was assessed using RMSE, which resulted in a negligible effect of 46 N and 0.2 J in forces and energy, respectively (i.e., 1.9% of the maximum AT force or strain energy).

In conclusion, in this study, we introduced a new in vivo assessment of the AT mechanical loading and strain energy during locomotion, demonstrating that when taking into account the curvature of the AT using skin markers, the projection of the MTJ to the skin and skin-to-bone displacement are two methodological issues that significantly influence the AT length measurement. We found that the AT mechanical loading during submaximal running is lower than previously reported and inadequate to initiate an adaptation of tendon mechanical properties, which explains at least partly the reported absence of significant differences in the AT mechanical properties between runners and non-runners. Finally, we provided the first evidence of an elastic strain energy recoil at the beginning of the stance phase during running, which might be functionally relevant for running economy.

3.5. Methods

3.5.1. Experimental design

Eleven adults (one female) with an average height of 177 ± 6 cm, body mass of 74 ± 9 kg, and age 29 ± 3 years participated in this study. All participants gave written informed consent to the experimental procedure, which was approved by the ethics committee of the Humboldt-Universität zu Berlin (HU-KSBF-EK_2018_0005) and followed the standards of the Declaration of Helsinki. The participants were in full health, and none of them reported neuromuscular or skeletal impairments in the past year. After a familiarization phase, the participants walked (1.4 m/s) and ran (2.5 m/s and 3.5 m/s) with randomized order on a treadmill (Daum electronic, ergo_run premium8, Fürth, Germany) whereby AT length was determined experimentally by integrating kinematics and ultrasound analysis. AT length was defined as the distance between the origin (i.e., the most distal junction) of the GM and the insertion on the tuber calcanei.

During gaits, marker-based motion capture was used to track the position of the insertion point, represented by a marker that was placed over the tuber calcanei as well as joint kinematics (Figure 3-1a). The potential skin-to-bone displacement was assessed while the foot was passively rotated (5°/s) throughout the full range of motion from plantar flexion to dorsiflexion by means of ultrasonography (Figure 3-1 b). Ultrasound was used to detect the MTJ, and the transducer position was tracked by the motion capture system using a mounted marker tripod (Figure 3-1 a). To assess the AT's curved path, small foil markers were placed on the skin covering the AT path on the line from the defined origin to the insertion (Figure 3-1 a). The MTJ position was then projected to the skin sur- face (Figure 3-1 a) and mapped to the global coordinate system to assess AT length during gait (i.e., from projected MTJ over the curved foil marker path to the insertion). Force and strain energy of AT during locomotion were assessed by fitting a quadratic function to the experimentally measured force–length curve of the AT based on individual maximum voluntary isometric contractions (MVC). During gait, the AT force was assessed by applying coefficients of the quadratic function to the AT elongation values obtained during locomotion. The AT tendon strain energy during walking and running was calculated by integrating tendon force over tendon elongation.

3.5.2. Kinematics and gait cycle determination

Kinematic data of the right leg were assessed using six reflective markers (14 mm in diameter) placed on the tip of the toe, medial and lateral epicondyle, on a line from greater-trochanter to lateral epicondyle as well as medial and lateral malleolus. 3D-trajectories of all markers were captured in real-time with 14 Vicon (Version 1.7.1, Vicon Motion Systems, Oxford, UK) cameras (4× MX T20, 2× MX-T20-S, 6× MX F20, 2× MX F40, 250 Hz). A fourth-order low pass and zero-phase shift Butterworth filter with a cut-off frequency of 12 Hz was applied to the raw marker trajectories (including foil markers). A one-minute warm-up and familiarization phase with the treadmill in each of the three speeds was considered before the captured trials, which included at least twelve stride cycles for each speed. During walking, the foot touchdown was determined as the heel marker's instant minimal vertical position and during running as the first peak of the knee joint angle (i.e., extension) (Dingwell et al., 2001). The take-off was defined as the reversal of the toe marker's anterior-posterior velocity during walking and as the second peak of the knee joint angle during running.

3.5.3. Measurement of the AT length during gait

The point of insertion of the AT, defined at the notch of the tuber calcanei of the calcaneus bone (Kongsgaard et al., 2011), was detected in sagittal plane ultrasound scans. The origin of the AT was determined as the most distal position of the GM MTJ, obtained by transversal and sagittal ultrasound scans. A T-shaped 60 mm ultrasound transducer (Aloka UST-5713T, Hitachi Prosound, alpha 7, Japan) operating at 146 Hz was fixed over the GM MTJ with a customized, flexible plastic cast. A gel pad was used to account for surface unevenness. The ultrasound device was time-synchronized with the motion capture system using a manual analog trigger signal. The AT curved path was elaborated by placing reflective foil markers on the skin that directly cover the AT (Arampatzis et al., 2008; De Monte et al., 2006). Depending on the position of the MTJ on the shank length, varying number (i.e., from 5 to 9) of reflective plane foil markers with 5 mm in diameter and 20 mm interval gap were placed on the path of AT from the defined insertion point to the last possible position below the plastic cast. Note that the ultrasound probe was then oriented in extension to this line. The curved path's length was calculated as the sum of the vectors, which was defined by the position of two consecutive foil markers.

An image-based tracking algorithm was developed to determine the position of the MTJ from the ultrasound videos (MATLAB, version 9.6. Natick, Massachusetts: The MathWorks Inc).

The procedure included a multi-updating template-matching technique with 33 manually defined templates. These 33 templates were rectangular windows covering the area around the MTJ and were defined in the first gait cycle, distributed equally in time throughout the stance and swing phase. The created templates then served to detect the MTJ during the subsequent steps (10 step cycles of the right leg on average). The ultrasound images were first cropped to a region of interest (in the range of MTJ displacement) and were convolved with a gaussian (3*3 kernel size) filter to reduce noises. By sweeping each template on the cropped image, the maximum value of normalized 2D cross-correlation was detected as the position of MTJ. Each template auto-updates itself under specific criteria until the next manually defined template occurs. The criteria of the auto-updating template were defined as Equation 3-1and Equation 3-2:

$$\mathrm{d} = \sqrt{(X_n - X_{n-1})^2 - (Y_n - Y_{n-1})^2} < T_1 \qquad \text{Equation 3-1}$$

$$D = \sqrt{(X_n - X_c)^2 - (Y_n - Y_c)^2} < T_2 \qquad \text{Equation 3-2}$$

where $\boldsymbol{X_n}$ and $\boldsymbol{Y_n}$ are the coordinates of the best-matched position (MTJ coordination) in the current frame, $\boldsymbol{X_{n-1}}$ and $\boldsymbol{Y_{n-1}}$ are the best-matched position in the previous frame, $\boldsymbol{X_c}$ and $\boldsymbol{Y_c}$ are the coordination of the best-matchedd position in the last accepted frame (i.e., the last frame that template was auto-updated), $\boldsymbol{T_1}$ and $\boldsymbol{T_2}$ are the thresholds defined in pixels (in our case was 5 and 10 pixels, respectively), d is the Euclidean distance between the best-matched position of the current frame and the previous, $\boldsymbol{D}$ is the Euclidean distance of the matched position between the current frame and the last accepted frame. If $\mathbf{d}$ and $\boldsymbol{D}$ were below the thresholds, then the updated template was accepted and used for the next frame. If the criteria were not fulfilled, the last accepted template was used for the next frame. Visual inspection of all frames was conducted afterward to verify the automatic tracking results, and corrections were made if necessary. When an inappropriately tracked MTJ position was deleted, the gap was filled by linear interpolation. In case the interpolation was unacceptable, the position of the MTJ was defined manually.

A custom 3D-printed marker tripod was fixed to the ultrasound transducer. The calibration of the ultrasound images with respect to the tripod was done by digitizing the four corners of the transducer's protective front layer. A coordinate system was defined (P) on the center-left side of the protective front layer. The gap between the left edge side of the protective front layer to the first piezoelectric sensor underneath was determined by subtracting the plate's width from the ultrasound image's width divided by two. This gap size was then verified with an x-ray

image of the transducer. The coordinate system (t) on the transducer (defined by a mounted tripod) was then adjusted accordingly. Another coordinate system (2D) was determined with the origin located at the first pixel (top left) of the ultrasound image (U). To map the MTJ position from the ultrasound image to the global coordinate system, a global transformation matrix ($^{V}_{U}T$) was used. This matrix was created by multiplicating the three transformation matrixes in Equation 3-3 (Craig, 2005).

$$^{G}_{U}T = {}^{G}_{t}T \times {}^{t}_{P}T \times {}^{P}_{U}T \qquad \text{Equation 3-3}$$

$^{P}_{U}T$ is the transformation matrix to transform the coordinate systems from the ultrasound image [U] to the protective front face of the transducer [P], $^{t}_{P}T$ is to transform the coordinate system of the protective front face of the transducer to tripod [t] and $^{V}_{t}T$ transfer the tripod coordinates to the global system [G] (i.e., defined by the motion capture). In this way, the detected MTJ position from the ultrasound images could be projected to the global coordinate system by Equation 3-4:

$$P_V = {}^{G}_{U}T \times \begin{bmatrix} P_{ux}.scale \\ P_{uy}.scale \\ 0 \\ 1 \end{bmatrix} \qquad \text{Equation 3-4}$$

where P_V is the transformed MTJ position to the global coordinate system, P_{ux} and P_{uy} are the detected MTJ position in the vertical and horizontal direction in the ultrasound images, respectively, and *scale* is the pixel to millimeter scale-factor for the US image (i.e., 4.3 in our case). For the projection of the MTJ to the skin surface, a double threshold-to-intensity gradient of the image was utilized. Then a spline curve was fitted to the detected edges of the skin surface, and the position of the MTJ was transferred to the fitted curve via the shortest distance. The kinematic and ultrasound recordings obtained to account for potential displacements of the reflective calcaneus marker above the defined insertion point (notch at tuber calcanei) were captured in two separate sessions due to spatial constraints around the ankle (i.e., only a reflective marker or an ultrasound probe could be mounted above the calcanei at the same time). In the first session, the participants lay prone on a dynamometer bench (Biodex Medical, Syst. 3, Inc., Shirley, NY) while their foot was fixed to the dynamometer footplate. Three trials were recorded while the foot was rotated passively by the dynamometer (5°/s) from 30° plantar flexion to the individual maximum dorsiflexion angle (Figure 3-1b). A sound-absorptive skin-adhesive marker was placed about 5 mm above the identified insertion point on the skin. A three-centimeter ultrasound transducer (My Lab60, Esaote, Genova, Italy, 37 Hz) was attached

above the calcaneus bone over the insertion of the AT in a sagittal plane. The skin position was detected in the ultrasound images by registering a shadow line as the sound absorptive marker's effect, and the notch identified the bone's position as a fixed bony landmark (Figure 3-1b). The skin position relative to the bone was tracked throughout the full range of motion from plantar flexion to dorsiflexion. In the second session, the ultrasound probe was removed, and reflective markers were placed precisely on the same positions as during the treadmill session, i.e., epicondyle (lateral and medial), malleoli (lateral and medial), between the first and the second metatarsal and on the defined insertion point (i.e., notch). Then the ankle joint was again passively rotated under the same conditions by the dynamometer. The heel angle (i.e., the created angle between the two vectors, first the knee joint center and ankle joint center and the second the heel and ankle joint center) was calculated and matched to the angle given by the dynamometer observed in the first session. Finally, the differences between skin and bone positions measured in the ultrasound images were converted to millimeters, and a spline curve was fitted to the skin-to-bone displacement versus heel angle (Figure 3-1c). The individual error model was then used to correct potential skin-to-bone movements as a function of the heel angle during gaits. The average maximum displacement of the skin relative to the bone was 2.30 ± 0.95 mm in plantar flexion and 1.90 ± 0.69 mm in dorsiflexion during the ankle's passive rotation.

3.5.4. Measurement of muscle electromyographic activity

Surface electromyographic (EMG) data of the TA, GM and Sol was measured during walking and running using a wireless EMG system (Myon m 320RX, Myon AG, Baar, Switzerland) operating at a sampling frequency of 1000 Hz. The EMG signal was processed using a fourth order high-pass Butterworth zero-phase shift filter with a 50 Hz cut-off frequency, a full-wave rectification, and a low-pass zero-phase shift filter of 20 Hz cut-off frequency. The resultant EMG signal was then normalized to the maximum processed EMG obtained during individual MVCs.

3.5.5. Assessment of AT strain, force and energy during gait

AT strain during walking and running was calculated by dividing the measured AT length by the AT resting length determined during the relaxed state in 20° plantar flexion, where AT slackness has been reported previously (De Monte et al., 2006). A force–elongation relationship of the AT was determined in a separate experiment, combining dynamometry and

ultrasound measurements to calculate AT's force and strain energy during locomotion. Participants performed five isometric plantar flexion ramp MVCs (~5 s gradual increase of force) while their knee was fully extended, and the ankle angle at rest was set to the neutral position (tibia perpendicular to sole). Misalignments of the ankle axis of rotation and dynamometer axis during the MVCs, as well as gravitational and passive moments, were considered through inverse dynamics (Arampatzis, Morey-Klapsing, et al., 2005). The effect of antagonistic muscle co-activation on the resultant joint moment during the MVCs was taken into account with an established procedure (Mademli et al., 2004). During contractions, the AT force was calculated by dividing the ankle joint moment by the AT's lever arm, which was determined using the tendon excursion method (An et al., 1984). As suggested previously, the tendon lever arm changes during the contractions were corrected (Maganaris et al., 1998). The corresponding elongation of the AT during the five trials for each participant was assessed with a 10 cm linear ultrasound probe fastened over the GM MTJ. The position of the MTJ visualized by ultrasound was tracked in the ultrasonographic images with the semi-automatic tracking algorithm described above. The effects of unavoidable ankle joint rotation during the MVCs that cause displacements of the MTJ on the tendon elongation was corrected by subtracting the MTJ displacement tracked during a passive rotation of the ankle (full range of motion at 5°/s) (Arampatzis et al., 2008) with respect to the ankle joint angle changes during the MVCs. The tendon force–elongation relationship of the five trials of each participant was averaged to achieve excellent reliability. A quadratic function (Equation 3-5) was fitted to obtain the individual force–elongation relationship of the AT and then was used to assess AT force during gaits:

$$F = a * l^2 + b * l \qquad \text{Equation 3-5}$$

where **F** is the AT's force during gaits, **a** and **b** are quadratic function coefficients, and ***l*** is the elongation of the AT during gait. The AT force's strain energy during walking and running was calculated by integrating the AT force over the measured AT elongation (we omitted the elongations below the resting length) using Equation 3-6.

$$E = \int F.\, dl = \int (a * l^2 + b * l).\, dl = \frac{1}{3} a.l^3 + \frac{1}{2} b.l^2 + c \qquad \text{Equation 3-6}$$

where **E** is the AT's strain energy during gait, and **c** is the constant of integration. The maximum value of the AT strain energy during the stance phase is the total amount of elastic energy stored. Tendon energy recoil during the propulsion phase of walking and running was calculated as the difference between the AT maximum strain energy and the energy at take-

off. The AT's elastic energy recoil at the beginning of the stance phase of running was calculated as the difference of the AT strain energy between the touchdown and its first local minimum after touchdown.

3.5.6. Statistics

The semi-automatic MTJ tracking algorithm's validity was tested by comparison to manual tracking (i.e., an experienced research assistant student did all the manual tracking of the MTJ). Displacements of the MTJ position in the longitudinal direction were assessed with the parameter VAF and the Pearson correlation coefficient (r) for seven participants in three gait cycles of all gait speeds. SPM one-way repeated measures analysis of variance (ANOVA) was used to find if there is a main effect of skin-to-bone displacement or projection of MTJ to the skin surface to AT length. If a significant main effect was found, an SPM paired t-test was used to investigate the significant difference between methods. In addition to SPM, we also used RMSE between different methods of AT length calculations.

A one-way repeated-measures analysis of variance (ANOVA) was performed to examine the effects of gait speed on maximum AT strain, force and strain energy as well as strain energy recoil during the propulsion phase and during the initial part of the stance phase. The same ANOVA has been used for the EMG activity in GM, Sol and TA and temporal gait parameters such as stance-time, swing-time and cadence. A pairwise t-test with Benjamini–Hochberg corrected p-values were used for post hoc analysis (adjusted p-values are reported) in case of significant main effects. The normal distribution of the data was tested with the Shapiro–Wilk test. The level of significance for all statistical tests was set to $\alpha = 0.05$.

3.6. Acknowledgments

We thank our colleague Arno Schroll for his help during the data analysis. We acknowledge the German Research Foundation (DFG) support and the Open Access Publication Fund of the Humboldt-Universität zu Berlin.

3.7. Author contributions

M.K. participated in designing the methods, carried out the experiments and data analysis and drafted the manuscript; S.M participated in designing the study and carrying out the experiment; C.T participated in experiment and data acquisition; F.M participated in language

proofing of the manuscript and A. A conceived, designed and coordinated the study and drafted the manuscript. All authors gave final approval for publication.

4. Second study: Contractile work of the soleus and biarticular mechanisms of the gastrocnemii muscles increase the net ankle mechanical work at high walking speeds

Authors:

Mohamadreza Kharazi [1,2]
Sebastian Bohm [1,2]
Christos Theodorakis [1,2]
Falk Mersmann [1,2]
Adamantios Arampatzis [1,2]

[1] Department of Training and Movement Sciences, Humboldt-Universität zu Berlin, Germany.
[2] Berlin School of Movement Science, Berlin, Humboldt-Universität zu Berlin, Germany.

Published in:
Biology, 2023, 12, 872. https://doi.org/10.3390/biology12060872.
(reprinted with permission by MDPI)

4.1. Simple Summary

This study enhances our understanding of how different mechanisms in the triceps surae muscles contribute to increased mechanical power and work at the ankle joint during various walking speeds. The findings reveal that both the soleus (Sol) and gastrocnemii muscles play a role in the speed-related increase of mechanical work at the ankle joint but through distinct energetic processes and mechanisms. The Sol muscle primarily increases contractile work (62%), while the gastrocnemii muscles demonstrate an enhanced contribution through biarticular mechanisms (38%). This knowledge can inform the design of exercise interventions and customized assistance through bioinspired exoskeleton configurations for both healthy individuals and those with pathological conditions.

4.2. Abstract

Increasing walking speed is accompanied by an increase of the mechanical power and work performed at the ankle joint despite the decrease of the intrinsic muscle force potential of the soleus (Sol) and gastrocnemius medialis (GM) muscles. In the present study, we measured Achilles tendon (AT) elongation and, based on an experimentally determined AT force–elongation relationship, quantified AT force at four walking speeds (slow 0.7 $m.s^{-1}$, preferred 1.4 $m.s^{-1}$, transition 2.0 $m.s^{-1}$, and maximum 2.6 ± 0.3 $m.s^{-1}$). Further, we investigated the mechanical power and work of the AT force at the ankle joint and, separately, the mechanical power and work of the monoarticular Sol at the ankle joint and the biarticular gastrocnemii at the ankle and knee joints. We found a 21% decrease in maximum AT force at the two higher speeds compared to the preferred; however, the net work of the AT force at the ankle joint (ATF work) increased as a function of walking speed. An earlier plantar flexion accompanied by an increased electromyographic activity of the Sol and GM muscles and a knee-to-ankle joint energy transfer via the biarticular gastrocnemii increased the net ATF mechanical work by 1.7 and 2.4-fold in the transition and maximum walking speed, respectively. Our findings provide first-time evidence for a different mechanistic participation of the monoarticular Sol muscle (i.e., increased contractile net work carried out) and the biarticular gastrocnemii (i.e., increased contribution of biarticular mechanisms) to the speed-related increase of net ATF work.

Keywords: energy transfer; ankle power; Achilles tendon force; energy storage and recoil; maximum walking speed

4.3. Introduction

Human walking covers a wide range of speeds, from 0.4 to 3.0 $m.s^{-1}$ (Mademli & Arampatzis, 2014; Martin et al., 1992; Nilsson & Thorstensson, 1987). During walking, the mechanical work performed at the ankle joint accounts for 40 to 50% of the total mechanical work carried out in the lower extremities (D. J. Farris & G. S. Sawicki, 2012; Novacheck, 1998). Furthermore, increasing walking speed is accompanied by an increase of the mechanical power and work at the ankle joint (D. J. Farris & G. S. Sawicki, 2012; Lai et al., 2015). These reports give evidence for the relevant contribution of the ankle joint to the necessary mechanical power and work during walking and thus indicate the important role of the plantar flexor muscles as a key source of energy production for walking. The monoarticular soleus (Sol), as the most voluminous muscle of the plantar flexors, generates the most significant part of the mechanical power and work at the ankle joint during walking (Neptune et al., 2008). The biarticular gastrocnemius medialis (GM) and lateralis (GL) muscles generate moments in both the ankle and knee joints. Thus, power and energy can be transferred from the more proximal monoarticular vasti muscles to the ankle joint (M. Bobbert et al., 1986; Gregoire et al., 1984; van Ingen Schenau et al., 1987). With this, biarticular muscles may regulate the redistribution and transfer of mechanical power and energy between the crossing joints to be effective at the joint where required (Cleland, 1867)d(van Ingen Schenau, 1989). Observations in turkeys, wallabies, and goats showed that biarticular muscles primarily transfer energy between two crossing joints, significantly contributing to increased positive work during level locomotion (Biewener, 2016). In running dogs, the contribution of the knee-to-ankle joint energy transfer was reported to be around 49% of the total positive work performed at the ankle joint (Carrier et al., 1998). Two separate mechanisms of the biarticular gastrocnemii muscles can influence the mechanical power and work at the ankle joint, independent of their musculotendinous power and work production (Junius et al., 2017; Prilutsky et al., 1996; van Ingen Schenau et al., 1987). First, an energy transfer between the two joints is possible when the mechanical powers of the gastrocnemii muscles at the ankle and knee joint have opposite signs (energy transfer mechanism). Second, the gastrocnemii can simultaneously absorb (negative) or generate (positive) mechanical power and work at the two crossed joints, thus affecting the redistribution of power and work between the two joints (joint coupling mechanism). The function of the biarticular gastrocnemii muscles at the ankle and knee joints during high walking speeds and the possible modulation of biarticular mechanisms with increasing walking speeds to enhance power and work production at the ankle joint is currently unknown.

It is well known that the energy expenditure per meter distance or the metabolic energy cost of walking as a function of walking speed is characterized by a U-shaped curve, with a minimum at speeds around 1.4 $m.s^{-1}$ (Browning et al., 2006; Cavagna & Kaneko, 1977; Margaria et al., 1963; Ralston, 1958; Zarrugh et al., 1974). Humans' preferred walking speed is very close to the optimum speed that minimizes the metabolic energy cost of transport (Browning et al., 2006; Martin et al., 1992). It is also accepted that humans switch voluntarily from walking to running at speeds around 2.0 $m.s^{-1}$, although the metabolic energy cost of running is higher than that of walking (D. J. Farris & G. S. Sawicki, 2012; Hreljac, 1993; Minetti et al., 1994). The higher metabolic cost of running at 2.0 $m.s^{-1}$ shows that the transition from walking to running is not primarily triggered to minimize the energy costs of locomotion. Noble et al. (Nobel et al., 1973) found that the perception of exertion is lower in a wide range of speeds while walking than during running, yet in the walking-to-running transition speed, the perception of exertion during walking exceeded running and, as a result, humans decided to switch from walking to running. Changes in the activation of the lower extremity muscles may increase the sensation of effort and trigger the transition from walking to running (Prilutsky & Gregor, 2001; Stenum & Choi, 2016). A recent study (McDonald et al., 2022) reported that locomotor control and decision making for a less overburdening walking condition are regulated not only based on the whole-body metabolic cost of walking but also muscle activation with the objective to minimize local muscle fatigue. Minetti et al. (Minetti et al., 1994) suggested that the plantar flexor muscles begin to work inefficiently due to the high contraction velocities at the walking-to-running transition speed. Therefore, humans switch to running to improve the efficiency of the plantar flexor muscles, despite the higher metabolic energy cost. Switching from walking to running at transition speed resulted in a greater force–velocity potential (i.e., decreased fascicle shortening velocity) for the GM muscle (Dominic James Farris & Gregory S Sawicki, 2012) and greater force–length–velocity potential (i.e., operating fascicle length close to the optimal length and decrease fascicle shortening velocity) for the Sol muscle (Lai et al., 2015), which in turn increases the economy of muscle force generation (Biewener & Roberts, 2000). These results further support model predictions from Neptune and Sasaki (Neptune & Sasaki, 2005) that intrinsic contractile properties of the plantar flexor muscles might be responsible for the transition from walking to running.

Nevertheless, humans can walk at higher speeds than the transition speed, despite the above-mentioned decreased potential of the Sol and GM muscles to generate forces (Mademli & Arampatzis, 2014; Nilsson & Thorstensson, 1987; Prilutsky & Gregor, 2001). The impaired muscle force potential at walking speeds of 2.0 $m.s^{-1}$ (Dominic James Farris & Gregory S

Sawicki, 2012; Lai et al., 2015) may suggest lower generated muscle forces at higher walking speeds. Inverse dynamic approaches, however, report greater resultant ankle joint moments in walking speeds around the transition speed (2.0 to 2.1 $m.s^{-1}$) compared to the preferred speed (de David et al., 2015; Lai et al., 2015), indicating an increased muscle force generation of the plantar flexor muscles. The ankle joint moments calculated using inverse dynamics are the result of all forces acting around the ankle joint (i.e., forces of synergist and antagonist muscles, forces transmitted by ligaments, bone-to-bone contact forces, and forces from soft tissues around the ankle joint). Therefore, the calculated maximum ankle joint moments may not represent the moments generated by the plantar flexor muscles at the ankle joint. Using the optic fiber methodology, Finni et al. (Finni et al., 1998) measured similar peak forces in the Achilles tendon (AT) at walking speeds between 1.1 and 1.8 $m.s^{-1}$, indicating an unchanged muscle force generation in this range of speeds. Finni et al. (Finni et al., 1998) did not measure AT forces in walking speeds at 2.0 $m.s^{-1}$, thus possible modifications in the AT force cannot be excluded. To our knowledge, measurements of the AT forces at walking speeds higher than the transition speed have not been conducted yet. Assuming a lower muscle-force generation in the transition and higher walking speeds, and thus lower energy storage and recoil from the AT compared to the preferred speed, we can expect compensatory mechanisms of power and energy production to provide the necessary mechanical power and work at the ankle joint. Using a musculoskeletal model, Neptune et al. (Neptune et al., 2008) found that the monoarticular Sol and the biarticular gastrocnemii increase the net contractile work in the transition speed compared to those close to the preferred one. To our knowledge, this model prediction has not yet been experimentally validated. Furthermore, there is a lack of information concerning the AT elastic energy storage and recoil and the musculotendinous power and work performed by the main plantar flexor muscles at maximum walking speeds.

The purpose of the current study was to investigate the contribution of monoarticular and biarticular mechanisms of the Sol and gastrocnemii muscles to the mechanical power and work at the ankle joint from slow to maximum walking speeds. This knowledge may be useful for designing exercise interventions and bioinspired exoskeleton configurations for customized assistance in healthy and pathological conditions. We used an innovative approach (Kharazi et al., 2021) to measure the AT elongation during walking (Figure 4-1) and, based on an experimentally determined tendon force–elongation relationship as a calibration measure, we quantified the AT force in four walking speeds (slow 0.7 $m.s^{-1}$, preferred 1.4 $m.s^{-1}$, transition 2.0 $m.s^{-1}$, and maximum 2.6 ± 0.3 $m.s^{-1}$). Further, we measured the electromyographic activity

(EMG) of the Sol, GM, and tibialis anterior (TA) muscles, and the AT elastic strain energy storage and recoil were calculated.

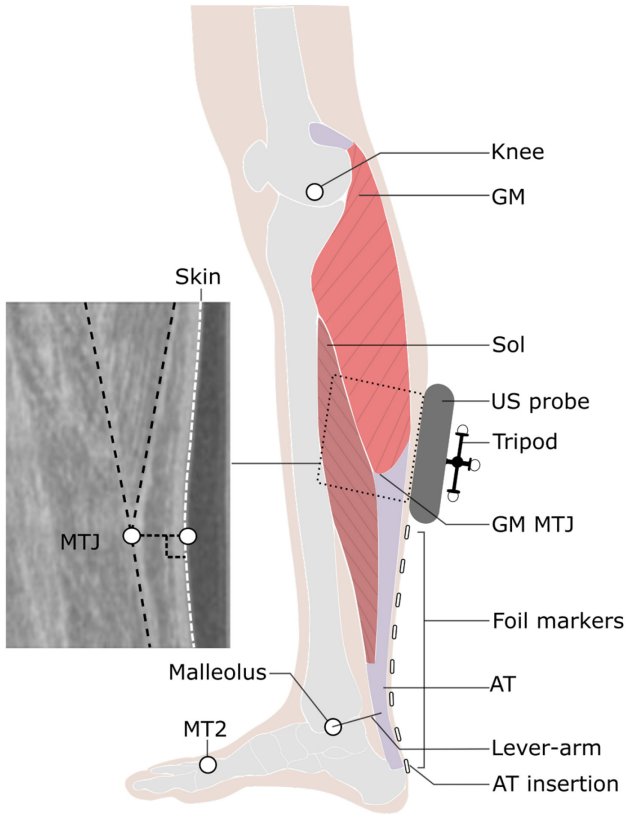

Figure 4-1 Experimental setup for the determination of Achilles tendon (AT) length during locomotion. Reflective foil markers were used to reconstruct the curved shape of the AT. An ultrasound (US) probe was used to detect the movements of gastrocnemius medialis myotendinous junction (GM-MTJ), which was then projected to the skin surface (white dashed line). The tripod markers were used to transfer the detected positions of the GM-MTJ to the global coordinate system (same as the motion capture system). The AT length was calculated as the sum of Euclidian distances from AT insertion (notch of calcaneus bone) between every two consecutive foil markers until the projected position of GM-MTJ to the skin surface. The AT lever arm was defined as the perpendicular distance between the midline of AT curved path and the ankle joint center. MT2: the tip of the second metatarsal; Sol: soleus muscle; Knee: a reflective marker on the epicondyle of the femur.

Finally, we investigated the mechanical power and work of the AT force at the ankle joint and, separately, the mechanical power and work of the monoarticular Sol at the ankle joint and the biarticular gastrocnemii muscles at the ankle and knee joints. We hypothesized that an increase in contractile net work production of the Sol muscle and an increased contribution of biarticular mechanisms of the gastrocnemii muscles would result in a continuous increase of net mechanical work at the ankle joint from slow to maximum walking speed.

4.4. Materials and Methods

4.4.1. Experimental Design

Fifteen healthy individuals (four female) with no record of musculoskeletal disorders (age 28 ± 4 years, height 175.0 ± 7.5 cm, body mass 75.0 ± 9.5 kg) participated in the study. All participants submitted written informed consent to the experimental procedure that was approved by the ethics committee of the Humboldt-Universität zu Berlin (HU-KSBF-EK-2018-0005). The participants were instructed to walk at the speeds of 0.7 $m.s^{-1}$ (slow walking), 1.4 $m.s^{-1}$ (preferred walking), 2.0 $m.s^{-1}$ (transition walking), and their maximum walking speed capacity (2.6 ± 0.3 $m.s^{-1}$) on a treadmill (Daum Electronic, Ergorun Premium8, Fürth, Germany). Experimentally determined individual preferred walking speeds in previous studies ranged between 1.1 and 1.6 $m.s^{-1}$ (Browning et al., 2006; Johnson et al., 2020; Samson et al., 2001), and the walking-to-running transition speed between 1.88 and 2.20 $m.s^{-1}$ (Hreljac, 1993; Margaria et al., 1963; Thorstensson & Roberthson, 1987). Here we used average values of 1.4 and 2.0 $m.s^{-1}$, similar to other studies (Dominic James Farris & Gregory S Sawicki, 2012; Lai et al., 2015), as the main purpose was not to explain why humans decide to walk at their preferred speed or transition from walking to running but to investigate the contribution of monoarticular and biarticular mechanisms to the mechanical power and work at the ankle joint with increasing walking speed. This means that in our study, we investigated the average preferred and transition walking speeds in the included participants. Individual maximum walking speed capacity was determined by gradually increasing the treadmill speed, starting from the transition speed (i.e., 2.0 $m.s^{-1}$), while the participants were instructed to maintain their walking pattern. As soon as the walking pattern could not be maintained and a flight phase was introduced, the earlier selected speed was set as the maximum walking speed.

4.5. 2.2. Kinematics and Electromyographic Activity Measurements

Six reflective markers (14 mm in diameter) were placed on anatomical landmarks, i.e., the tip of the second metatarsal, medial, and lateral epicondyles of the femur, midpoint of a straight line between the greater trochanter and the lateral epicondyle of the femur, and medial and lateral malleolus. One additional reflective foil marker (5 mm in diameter, flat surface) was placed on the insertion of the AT on top of the calcaneus (heel marker, Figure 4-1). The insertion point of the AT was defined as the notch of the calcaneus bone, which was determined by moving a sound absorptive marker underneath an ultrasound probe in the sagittal plane until

the shadow reflection (i.e., caused by sound absorptive marker) crossed the notch. Fourteen Vicon (Version 1.8.1, Vicon Motion Systems, Oxford, UK, 4 MX T20, 2 MX-T20-S, 6 MX F20, 2 MX F40, 250 Hz) cameras were used to capture the 3D trajectories of all markers in real-time. A fourth-order, low-pass, zero-phase shift Butter- worth filter with a cut-off frequency of 12 Hz was applied to the raw marker trajectories. The participants performed a one-minute familiarization on the treadmill for each speed. The touchdown of the foot was determined as the heel marker's instant minimal vertical position (Dingwell et al., 2001). The foot take-off was defined as the sign change in the second metatarsal marker velocity in the anterior-posterior direction (Alvim et al., 2015; Fellin et al., 2010). The ankle joint angle in the sagittal plane was calculated as the angle between the foot (i.e., line crossing the tip of the second metatarsal and calcaneus marker) and shank (i.e., line crossing ankle joint center and knee joint center). Ankle and knee joint centers were defined as the mean point between lateral and medial reflective markers on the malleoli and femur condyles. The knee joint angle in the sagittal plane was calculated as the angle between the femur axis (i.e., the line crossing the lateral knee and greater trochanter reflective marker) and the shank. The ankle and knee joint angles were calculated referencing a neutral quiet stance position (the foot perpendicular to the tibia represents a 0° ankle joint angle; the knee fully extended repre- sents a 0° knee joint angle). Positive values of ankle and knee joint angles constitute ankle plantar flexion and knee flexion. The stance time was calculated as the time duration from the right touchdown and take-off. Accordingly, swing time was calculated from take-off to the next touchdown. Cadence was calculated as a total number of touchdowns divided by the two-fold total time of nine gait cycles. Step length was calculated as the treadmill speed divided by cadence. The duty factor was calculated as the stance time divided by the sum of stance and swing time. A wireless system (Myon m 320RX, Myon AG, Baar, Switzerland) was used to measure the surface EMG activity of the TA, GM and Sol muscles during walking, operating at a sampling frequency of 1000 Hz. A fourth-order high-pass zero-phase shift Butterworth filter with a 50 Hz cut-off frequency, a full-wave rectification, and a low-pass zero-phase shift filter with a 20 Hz cut-off frequency was used to process the raw EMG signal. The resulting EMG signal was normalized to the highest processed EMG value acquired during a maximum voluntary isometric contraction (MVC).

4.6. Measurement of AT Length and Quantification of AT Force and Strain Energy

The origin of the AT was determined as the most distal junction between the AT and the medial head of the gastrocnemius muscle (GM-MTJ), obtained by transverse and sagittal ultrasound scans (Figure 4-1). A 60 mm T-shape ultrasound probe (Aloka UST-5713T, Hitachi Prosound, alpha 7, Hitachi, Japan) with a sampling frequency of 146 Hz was fixed above the GM-MTJ and was tightened firmly with a flexible plastic cast. An ultrasound gel pad was placed between the ultrasound probe and the skin to compensate for the unevenness of the skin surface. The ultrasound and motion-capture systems were synchronized using a 5-volt manual trigger through the ultrasound electrocardiograph channel and motion-capture analog input channel. A semi-automatic image-based tracking algorithm was implemented in a self-developed user interface (MATLAB, version 9.6. Natick, MA, USA: The MathWorks Inc.) to track the position of the GM-MTJ from the stack of ultrasound images. The details of the developed algorithm and its validity compared with manual tracking during human walking and running (i.e., $r2 = 0.97$) were provided earlier (Kharazi et al., 2021). The skin surface was detected using a double threshold-to-intensity gradient provided by the Canny edge-detection function (Canny, 1987). A third-order polynomial curve was then fitted to the detected points on the skin, and the tracked coordinates of the GM-MTJ were perpendicularly (i.e., shortest distance) projected to the fitted curve.

For the transformation of the GM-MTJ to the global motion-capture coordinate system, the four corners of the ultrasound probe's protective plastic rubber were digitized in 3D space using a custom 3D-printed calibration tool in a separate session. A coordinate system was defined on the left-center side of the plastic rubber. The gap between the origin of the specified coordinate system and the first piezoelectric crystal underneath was determined by subtracting the ultrasound rubber plastic width from the ultrasound image width. A custom 3D-printed tripod was mounted on the ultrasound probe, and a coordinate system was defined accordingly. The projected positions of the GM-MTJ on the skin surface were then transferred to the global motion capture coordinate system (for details, see (Kharazi et al., 2021)). Depending on the location of the GM-MTJ, reflective foil markers were placed on the skin in 20 mm intervals from the calcaneus bone (i.e., insertion point of the AT, described above) on the path of the AT to the last possible position below the cast (Figure 4-1). The curved length of the AT was determined as the sum of vectors using the 3D coordinates of every two consecutive foil markers and the GM-MTJ projected to the skin. The strain of the AT was calculated by dividing

the measured AT elongation by the AT length measured at a relaxed state in 20° plantar flexion, where AT slackness has been reported (De Monte et al., 2006). Potential displacements of the skin to the bone underneath the calcaneus marker that defines the AT insertion can also introduce artifacts in the AT length measurement (Lichtwark & Wilson, 2005). In a separate experiment, kinematic and ultrasound measurements were used to measure the displacement of the reflective calcaneus marker above the defined insertion point (notch at tuber calcanei) to account for the potential movements of the skin relative to the calcaneus bone (Kharazi et al., 2021). For this purpose, a sound-absorptive marker was placed between the ultrasound probe and skin close to the bony insertion, and the dynamometer (Biodex Medical, Syst.3, Shirley, NY, USA) passively rotated the ankle joint. The displacement of the calcaneus bone relative to the skin as a function of the heel angle (angle between the line from the calcaneus marker to ankle joint center and the line from the ankle joint center to the knee joint center) was determined and used as a model to correct the AT length during walking as a function of the heel angle. The potential error due to the skin–bone artifact was 0.92 ± 0.57 mm (mean ± standard deviation) on the AT length and 0.45% on AT strain (Kharazi et al., 2021).

In an additional session, an individual force–elongation relationship of the AT was determined. For the measurement of the plantar flexion moment, five ramp MVC (5 s gradual increase of the moment exertion) plantar flexions were performed at a joint angle position of 0° and fully extended knee on a dynamometer. The potential misalignments of ankle and dynamometer axes of rotation during the contractions and gravitational and passive moments were considered by employing an inverse dynamics approach (Arampatzis, Morey-Klapsing, et al., 2005). Further, we considered the effect of coactivation of the antagonistic muscle (i.e., tibialis anterior) on the resultant joint moment during the MVCs using an established EMG-based approach (Mademli et al., 2004). The ankle joint moment was then divided by the AT lever arm to calculate the tendon force. For this purpose, the AT lever arm was calculated using the tendon excursion method and adjusted for the changes in the alignment of the AT during the contractions using the data provided by Maganaris et al. (Maganaris et al., 1998). A 10-centimeter linear ultrasound probe (My lab60, Esaote, Genova, Italy, 25 Hz) was fixed above the GM-MTJ to measure the corresponding elongation of the AT during the five MVCs. The GM-MTJ displacement resulting from ankle joint rotations (i.e., during MVC) was considered by tracking its displacement during a passive rotation (at 5°/s) of the ankle joint (Arampatzis et al., 2008). To achieve excellent reliability, the tendon force-elongation relationship of each participant was averaged from five MVCs (Schulze et al., 2012).

The individual force-elongation relationship of the AT was obtained by fitting a quadratic function (Equation 4-1), which was then used to assess the AT force during walking.

$$F = a * l^2 + b * l \qquad \text{Equation 4-1}$$

where F is the AT force, a and b are the coefficients of the quadratic function, and l is the elongation of AT during the MVCs. Using Equation (1) and the measured AT elongation during the walking trials, we calculated the AT force and then AT elastic strain energy as the integral of the AT force over AT elongation (Equation 4-2) during the stance phase.

$$E = \int F \,.\, dl = \int (a * l^2 + b * l).\, dl = \frac{1}{3} a.l^3 + \frac{1}{2} b.l^2 + c \qquad \text{Equation 4-2}$$

where the E and F are the AT strain energy and force. l is the instantaneous elongation of AT during stance, and c is the constant of the integral. The AT power was calculated as the first time-derivative of the AT elastic strain energy. It is to be mentioned that Equations (1) and (2) do not consider the effect of tendon hysteresis on the assessed AT force and AT strain energy. However, in our earlier study (Kharazi et al., 2021), we estimated a negligible effect of 46 Newton and 0.2 Joule in forces and energy during locomotion, respectively (i.e., 1.9% of the maximum AT force or strain energy).

4.7. Mechanical Power and Work at the Ankle and Knee Joint

The ankle joint moment resulting from the AT force (ATF moment) during walking was calculated as the product of the AT force and the AT lever arm. The instant AT lever arm was measured as the perpendicular distance between the AT line of action and the marker-based ankle joint center during the walking trials (Figure 4-1). The line of action of the AT was assumed at the midpoint of the AT. The distance between the skin surface and the midpoint of the AT was assessed using sagittal plane ultrasound scans and subtracted from the kinematic-based AT lever arm. The ultrasound probe was placed above the AT on the level of the malleoli while participants were seated in a relaxed prone position with their ankle angle set at 0°. The depth between the skin surface and the midpoint of the AT among all individuals was, on average, 5.0 ± 0.3 mm. The mechanical power at the ankle joint from the AT force (ATF power) was calculated as the product of ATF moment and ankle angular velocity. The mechanical work done from the AT force (ATF work) at the ankle joint was calculated as the integral of ATF power over time.

The Sol, GM, and GL muscle forces have been assessed as a fraction of the AT force by using the relative physiological cross-sectional area of the three muscles (i.e., 62% for the Sol, 26 % for the GM, and 12% for the GL) as reported by Albracht et al. (Albracht et al., 2008), assuming the force contribution of each muscle is proportional to its physiological cross-sectional area. The moment generated by the Sol muscle at the ankle joint was calculated as the product of the Sol muscle force (equal to 0.62 of the AT force) and the instantaneous AT lever arm measured during walking. The mechanical power of the Sol at the ankle joint was calculated as the product of the Sol ankle joint moment and ankle joint angular velocity. This Sol mechanical power at the ankle joint is equal to the mechanical power of the Sol muscle-tendon unit (MTU) calculated as the product of the Sol force and Sol MTU velocity (Prilutsky et al., 1996). The ankle mechanical work performed by the Sol was then calculated as the integral of the Sol ankle joint power over time. The GM and GL, as biarticular muscles, can produce or absorb power and energy in both the ankle and knee joints. This means they can redistribute the mechanical power and work performed by their MTUs over the two joints and transfer power and energy from knee-to-ankle joint and vice versa. We investigated the mechanical power and work at the ankle and knee joints by the GM and GL muscles in order to examine their contribution to ankle and knee mechanical power and work and the energy transfer between the two joints during walking. The mechanical power of the GM and GL muscles at the ankle/knee joints was calculated as the product of the ankle/knee joint moment generated from the two muscles and ankle/knee joint angular velocity. The generated moment at the ankle/knee joint by the two muscles was calculated as the product of the GM and GL muscle forces and their instantaneous lever arms. For the ankle joint, the measured AT lever arm was used. The lever arm of the GM and GL at the knee joint were extracted as a function of the knee joint angle using the values reported by Buford et al. (Buford et al., 1997). The mechanical work of the GM and GL muscles at the ankle and knee joints was then calculated as the integral of the GM/GL ankle and knee joint power over time. The sum of the mechanical power/work at the ankle and knee joints of the GM and GL muscles equals the mechanical power/work of the GM/GL MTUs calculated as the product of their forces and MTU velocities (Prilutsky et al., 1996). In the analysis, the sum of the power and work of the GM and GL was used and all muscle kinetics data will be presented as values of the gastrocnemii muscles.

4.8. Statistics

A linear mixed model was used to test for the main effect of walking speed on all investigated outcomes (i.e., spatiotemporal gait parameters, kinematics, EMG, strain, moments, force, and mechanical work). In the linear mixed-effects model, the participants were treated as effects and walking speed as a fixed effect. Linear mixed models are robust against violations of the normality assumption (Jacqmin-Gadda et al., 2007), which was not given for the AT force, AT strain energy, and ATF work, according to the Shapiro–Wilk test applied to the normalized residuals. The significance level was set to $\alpha = 0.05$, and all values are reported as mean ± standard errors. A pairwise Tukey test was performed as a post hoc analysis in case of a significant main effect of speed, and Benjamini–Hochberg-corrected p-values will be reported. The statistical analyses were conducted using R v4.0.1 (R foundation for statistical computing, Vienna, Austria. Packages), where the "nlme" package was used for the linear mixed model and the "emmeans" package for post hoc testing.

Table 4-1 Spatiotemporal gait parameters during the stance phase of walking at slow (0.7 $m.s^{-1}$), preferred (1.4 $m.s^{-1}$), transition (2.0 $m.s^{-1}$) and maximum speed (2.6 ± 0.3 $m.s^{-1}$, Max). All values are presented as mean ± standard error (average of fifteen participants with nine gait cycles). * Statistically significant effect of speed ($p < 0.05$). Each row sharing the same letter does not differ significantly ($p > 0.05$, post hoc analysis).

	Slow (0.7 $m.s^{-1}$)	Preferred (1.4 $m.s^{-1}$)	Transition (2 $m.s^{-1}$)	Maximum (2.6 ± 0.3 $m.s^{-1}$)
Stance time (ms) *	863±27 **a**	601±11 **b**	477±09 **c**	363±11 **d**
Dorsiflexion time (ms)	652±15 **a**	416±20 **b**	229±13 **c**	167±06 **d**
Plantar flexion time (ms)	211±14 **ab**	185±15 **a**	249±19 **b**	197±09 **a**
Swing time (ms) *	490±11 **a**	411±08 **b**	355±06 **c**	316±5 **d**
Step length (m) *	0.47±0.01 **a**	0.7±0.01 **b**	0.83±0.01 **c**	0.89±0.02 **d**
Cadence (steps/s) *	1.49±0.03 **a**	1.98±0.03 **b**	2.41±0.04 **c**	2.95±0.06 **d**
Duty-factor *	0.64±0 **a**	0.59±0 **b**	0.57±0 **c**	0.53±0.01 **d**

4.9. Results

We found a significant main effect of walking speed on all spatiotemporal gait parame- ters (Table 4-1, $p < 0.001$). Both stance and swing time were reduced significantly ($p < 0.001$) at a higher walking speed. Step length and cadence increased as a function of speed ($p < 0.001$), and the duty-factor decreased significantly ($p < 0.001$) with increasing speed; however, it remained above 0.5 (i.e., the threshold for walking) at all walking speeds (Table 4-1). Although the time of the dorsiflexion phase decreased significantly ($p < 0.001$) as a function of speed, the plantar flexion time remained quite preserved (Table 4-1). Ankle and knee joint angles (Figure 4-2B,C), strain (Figure 4-2A), force (Figure 4-2D), and lever arm (Figure 4-2E) of the AT and ankle joint moments generated by the AT force (Figure 4-2F) during the stance phase at all walking speeds are shown in Figure 4-2.

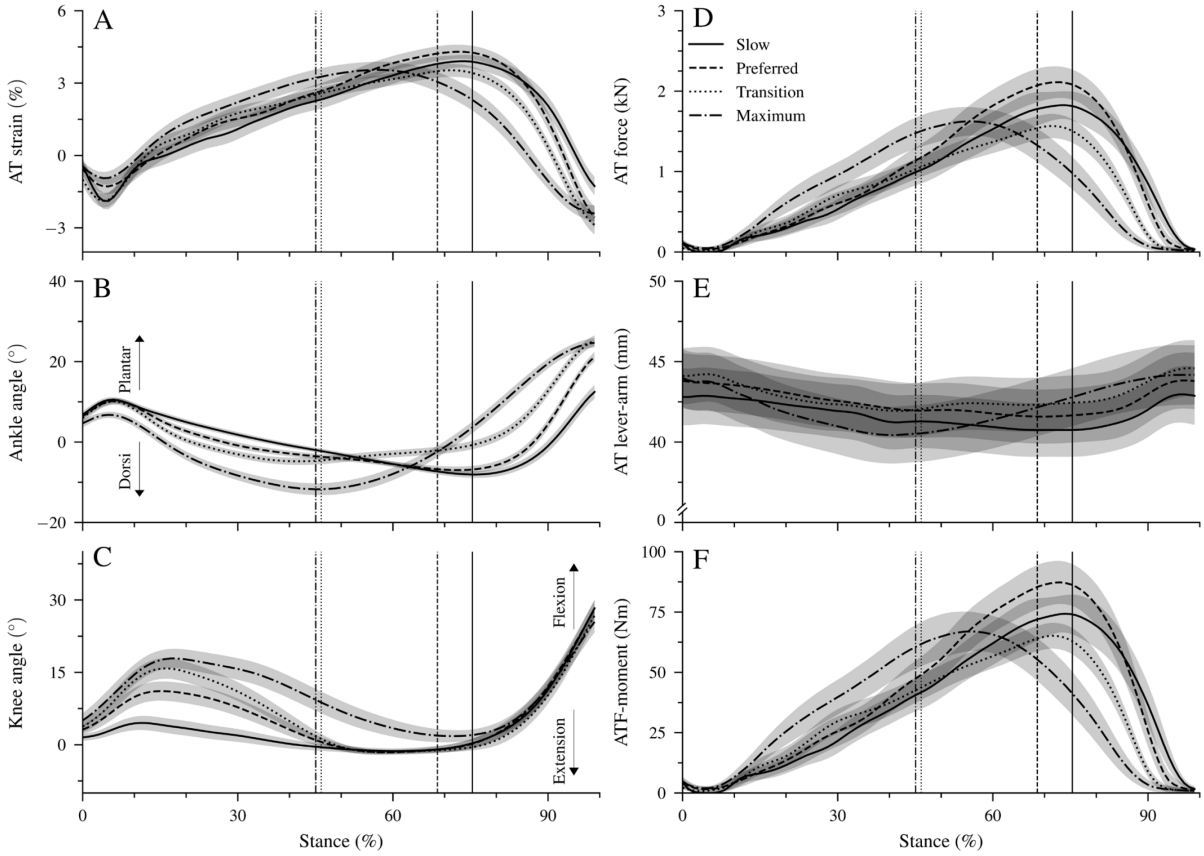

Figure 4-2 Achilles tendon (AT) strain (**A**), ankle and knee joint angles (**B**,**C**), AT force (**D**), AT lever arm (**E**), and moment generated from the AT force at the ankle joint (ATF moment, (**F**) during the stance phase of walking at slow (0.7 m.s−1, Slow), preferred (1.4 m.s−1, Preferred), transition (2.0 m.s−1, transition), and maximum speed (2.6 ± 0.3 m.s−1, Max). The vertical solid, dashed, dotted, and dashed–dotted lines separate the dorsiflexion and plantar flexion of the ankle during walking at slow, preferred, transition, and maximum speed, respectively. The curves and shaded areas represent mean ± standard errors (average of fifteen participants with nine gait cycles).

There was a significant main effect of walking speed on maximum AT strain ($p = 0.014$;Table 4-2) and AT force ($p = 0.005$; Table 4-2). The post hoc comparisons showed a lower maximum AT force in the transition ($p = 0.004$) and maximum walking speed ($p = 0.047$) compared to the preferred one. The maximum AT strain was lower in the transition compared to the preferred speed ($p = 0.017$, Table 4-2) and showed a tendency ($p = 0.058$) towards lower values in the maximum walking speed compared to the preferred one. We found a main effect of speed on the average AT lever arm ($p = 0.003$). The AT lever arm in the transition speed was longer than in the slow ($p = 0.002$) and maximum ($p = 0.020$) walking speeds (Figure 4-2E). However, the differences in the AT lever arms were rather small, with 1 mm between the investigated walking speeds (i.e., 2% of AT lever arm, Table 4-2).

Table 4-2 Peak values of the Achilles tendon (AT) strain and force, average AT lever arm, maximum moment of the AT force at the ankle joint (ATF moment) and average range of motion (RoM) at the ankle joint during the dorsiflexion and plantar flexion phase at slow (0.7 m.s−1), preferred (1.4 m.s−1), transition (2.0 m.s−1) and maximum walking speed (2.6 ± 0.3 m.s−1, Max). All values are presented as mean ± standard error (average of fifteen participants with nine gait cycles). * Statistically significant effect of speed ($p < 0.05$). Each row that shares the same letter does not differ significantly ($p > 0.05$, post hoc analysis).

	Slow (0.7 $m.s^{-1}$)	Preferred (1.4 $m.s^{-1}$)	Transition (2 $m.s^{-1}$)	Maximum (2.6 ± 0.3 $m.s^{-1}$)
AT-strain (%) *	4.1±0.3 **ab**	4.4±0.3 **a**	3.6±0.3 **b**	3.8±0.4 **ab**
AT-force (N) *	1930±190 **ab**	2174±202 **a**	1616±147 **b**	1793±2.3 **b**
AT-lever arm (mm) *	41±1 **a**	42±1 **ab**	43±1 **b**	42±1 **a**
ATF-moment (Nm) *	78±08 **ab**	90±09 **a**	67±05 **b**	74±09 **ab**
Ankle ROM dorsiflexion (°)	15±1 **ab**	14±1 **a**	11±1 **c**	17±2 **b**
Ankle ROM plantar flexion (°)	21±1 **b**	29±1 **a**	30±1 **a**	37±1 **c**

There was a significant main effect of walking speed ($p < 0.001$) on the maximum ATF moment (Table 4-2). Post hoc comparisons demonstrated a lower maximum ATF moment in the transition compared to the preferred ($p = 0.005$, Table 4-2) speed and a tendency for lower values in maximum walking speed ($p = 0.050$). In the slow and preferred speed, the initiation

of the ankle plantar flexion and knee flexion in the second part of the stance phase occurred almost simultaneously (Figure 4-2B,C).

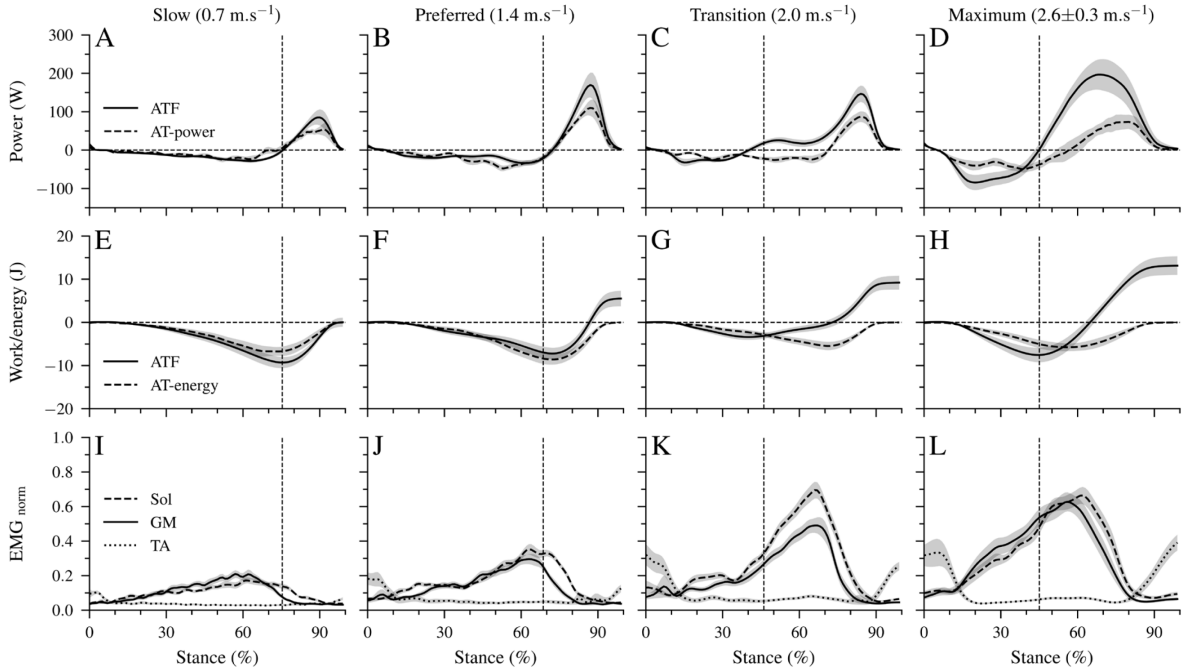

Figure 4-3 Mechanical power (**A**–**D**) and work (**E**–**H**) of the AT force at the ankle joint (ATF power/work), as well as Achilles tendon power (AT power) and elastic strain energy storage and recoil (AT energy). Negative values in the mechanical power indicate energy absorption at the ankle joint during dorsiflexion and AT elastic strain energy storage. Positive power values indicate energy production at the ankle joint during the plantar flexion and elastic AT strain energy recoil. Panel (**I**–**L**) show the electromyographic activity of the soleus (Sol), gastrocnemius medialis (GM), and tibialis anterior (TA) muscles normalized to a maximum voluntary contraction (EMGnorm). All investigated parameters are presented for the stance phase of walking at slow (0.7 $m.s^{-1}$), preferred (1.4 $m.s^{-1}$), transition (2.0 $m.s^{-1}$), and maximum speed (2.6 ± 0.3 $m.s^{-1}$) as mean ± standard error (average of fifteen participants with nine gait cycles). The vertical dashed line shows the separation between dorsiflexion and plantar flexion.

In the two higher walking speeds, the time-wise earlier initiation of the plantar flexion was combined with a knee extension (Figure 4-2B,C). There was a significant effect of speed ($p <$ 0.001) on the range of motion (RoM) at the ankle joint in both the dorsiflexion and plantar flexion phase (Table 4-2). The RoM during dorsiflexion was the lowest in the transition speed, whereas the RoM during plantar flexion was the highest at the maximum speed (Table 4-2). During the simultaneous plantar flexion and knee extension, the knee joint extended by 7.5 ± 1.2° in the transition and by 8.7 ± 1.3° in the maximum walking speeds. The mechanical power (Figure 4-3A–D) and work (Figure 4-3E–H) at the ankle joint from the AT force (ATF power/work) and EMG-activity of Sol, GM, and TA muscles (Figure 4-3I–L) are presented

inFigure 4-3. Speed affected the ATF work during both dorsiflexion and plantar flexion periods ($p < 0.001$, Table 4-3). The ATF work during the dorsiflexion was the lowest in the transition speed, and during the plantar flexion, the highest in the maximum speed ($p < 0.001$, Figure 4-3F,H and Table 4-3). The net ATF work demonstrated a significant main effect of speed ($p < 0.001$) with a continuous increase as a function of walking speed (Figure 4-3E–H and Table 4-3).

Table 4-3 Mechanical work of the Achilles tendon force (ATF work) during dorsiflexion, plantar flexion, and net ATF work at the ankle joint. Achilles tendon energy storage and recoil (AT energy) and normalized maximum electromyographic activity of the soleus (Sol EMG norm), gastrocnemius medialis (GM EMG norm), and tibialis anterior (TA EMG norm) muscles at slow (0.7 $m.s^{-1}$), preferred (1.4 $m.s^{-1}$), transition (2.0 $m.s^{-1}$), and maximum walking speed (2.6 ± 0.3 $m.s^{-1}$, Max). All values are presented as mean ± standard error (average of fifteen participants with nine gait cycles). * Statistically significant effect of speed ($p < 0.05$). Each row that shares the same letter does not differ significantly ($p > 0.05$, post hoc analysis).

	Slow (0.7 $m.s^{-1}$)	Preferred (1.4 $m.s^{-1}$)	Transition (2 $m.s^{-1}$)	Maximum (2.6 ± 0.3 $m.s^{-1}$)
ATF-work dorsiflexion (J) *	-9.6±1.3 **a**	-8.0±1.2 **a**	-4.0±0.7 **b**	-8.1±1.7 **a**
ATF-work plantar flexion (J) *	9.6±2.0 **a**	13.5±2.5 **a**	13.17±2.0 **a**	21.3±3.2 **b**
ATF-work net (J) *	0.0±1.1 **a**	5.5±1.8 **b**	9.19±1.6 **c**	13.2±2.1 **d**
AT-energy (stored/recoiled, J) *	7.2±1.1 **ab**	8.8±1.1 **a**	5.66±0.9 **b**	6.7±1.1 **ab**
Sol EMG $_{norm}$ *	0.20±0.02 **a**	0.39±0.02 **b**	0.73±0.04 **c**	0.77±0.04 **c**
GM EMG $_{norm}$ *	0.25±0.02 **a**	0.35±0.03 **a**	0.61±0.06 **b**	0.71±0.06 **c**
TA EMG $_{norm}$ *	0.13±0.02 **a**	0.22±0.04 **a**	0.38±0.06 **b**	0.51±0.06 **c**

The maximum AT strain energy storage and recoil was also affected by walking speed ($p < 0.05$). The energy storage and recoil were significantly lower in the transition speed ($p = 0.011$) and showed a tendency for lower values in the maximum speed ($p = 0.084$) compared to the preferred one (Table 4-3). The AT strain energy recoil was significantly higher than the net ATF work in the slow ($p < 0.001$) and preferred ($p = 0.01$) speed, while in the two higher speeds, the net ATF work was 1.6 to 1.9-fold greater than the AT energy recoil. The maximum

EMG-activity of all three investigated muscles demonstrated a significant speed effect ($p < 0.001$) with the highest values in the transition and maximum speeds ($p < 0.001$; Table 4-3).

Table 4-4 Negative, positive, and net work of the soleus (Sol work) muscle at the ankle joint, the gastrocnemii muscles (gastro work) at the ankle and knee joints, and the gastrocnemii muscle–tendon unit (Gastro MTU work) at slow (0.7 m.s−1), preferred (1.4 m.s−1), transition (2.0 m.s−1), and maximum walking speed (2.6 ± 0.3 m.s−1, Max). All values are presented as mean ± standard error (average of fifteen participants with nine gait cycles). * Statistically significant effect of speed ($p < 0.05$). Each row sharing the same letter does not differ significantly ($p > 0.05$, post hoc analysis).

		Slow (0.7 $m.s^{-1}$)	Preferred (1.4 $m.s^{-1}$)	Transition (2 $m.s^{-1}$)	Maximum (2.6 ± 0.3 $m.s^{-1}$)
Sol work Ankle	Negative (J) *	-5.9±0.8 **a**	-4.9±0.7 **a**	-2.5±0.4 **b**	-5.0±1.0 **a**
	Positive (J) *	5.9±1.2 **a**	8.4±1.6 **a**	8.1±1.3 **a**	13.1±1.0 **b**
	Net (J) *	0±0.7 **a**	3.4±1.1 **b**	5.7±1.0 **c**	8.1±1.3 **d**
Gastro work Ankle	Negative (J) *	-3.7±0.5 **a**	-3.1±0.5 **a**	-1.5±0.3 **b**	-3.1±0.7 **a**
	Positive (J) *	3.8±0.8 **a**	5.2±1.0 **a**	5.0±0.8 **a**	8.1±1.2 **b**
	Net (J) *	0.1±0.4 **b**	2.1±0.7 **a**	3.5±0.6 **c**	5.0±0.8 **d**
Gastro work Knee	Negative (J) *	-0.6±0.1 **b**	-1.7±0.4 **a**	-2.5±0.5 **a**	-3.4±0.6 **c**
	Positive (J) *	3.4±0.7 **a**	3.3±0.6 **a**	1.8±0.3 **b**	0.9±0.3 **c**
	Net (J) *	2.7±0.7 **a**	1.6±0.5 **a**	-0.6±0.3 **b**	-2.5±0.5 **c**
Gastro MTU work	Negative (J)	-3.9±0.6	-4.2±0.7	-3.0±0.6	-4.6±0.9
	Positive (J)	6.6±1.3	7.9±1.4	5.9±0.9	7.1±1.1
	Net (J)	2.7±1.0	3.7±1.0	2.8±0.7	2.4±0.8

Figure 4-4 shows the mechanical power and work at the ankle joint by the Sol muscle, the mechanical power and work at the ankle and knee joints by the biarticular gastrocnemii muscles, and the total mechanical power and work of the gastrocnemii MTU. The Sol net work increased continuously ($p < 0.001$, Table 4-4, Figure 4-4E–H) with walking speed. The positive

work of the Sol muscle was the highest at the maximum speed, whereas at the transition speed, the negative Sol work was the lowest ($p < 0.001$, Table 4-4). The increased net Sol work at the preferred compared to the slow speed occurred due to an average decrease of negative work and increase of positive work in the preferred speed, though the differences did not reach statistical significance (Table 4-4). The negative and positive work at the ankle and knee joints by the gastrocnemii muscles showed a significant speed effect ($p < 0.001$, Table 4-4). The negative work at the ankle joint was the lowest in the transition speed, and the positive work was the highest in the maximum walking speed ($p < 0.001$, Table 4-4). Between the other speeds, neither the negative nor the positive work showed any statistically significant ($p > 0.05$) differences (Table 4-4). The net mechanical work at the ankle joint from the gastrocnemii muscles increased significantly ($p < 0.001$) from the slow to maximum walking speed (Table 4-4). At the knee joint, the negative work increased, and the positive work decreased by increasing walking speed ($p < 0.05$, Table 4-4). As a result, the net mechanical work of the gastrocnemii at the knee joint increased in negative values as a function of speed ($p < 0.001$). The negative ($p = 0.098$), positive ($p = 0.149$), and net ($p = 0.323$) mechanical work of the gastrocnemii MTU did not show a significant speed effect (Table 4-4).

There were four characteristic phases during the stance phase of walking where the unique property of the biarticular gastrocnemii muscles to act simultaneously at the ankle and knee joints influenced the net mechanical work at the ankle joint despite the unchanged net mechanical work of their MTU (Figures 2B,C and 4I–L). First, at the beginning of the stance phase and during the knee flexion, power and energy were transferred from the dorsiflexed ankle joint to the knee joint (phase T1, energy-transfer mechanism). Second, in the phase where the ankle joint continued the dorsiflexion and the knee joint was extended, the gastrocnemii absorbed energy in both the ankle and knee joint (phase C1, joint-coupling mechanism). Third, during a simultaneous plantar flexion and knee extension, particularly in the transition and maximum walking speeds, energy was transferred from the knee to the ankle joint (phase T2, energy-transfer mechanism). Fourth, at the end of the stance phase and during the synchronous plantar flexion and knee flexion, the gastrocnemii generated work in both the ankle and knee joint (phase C2, joint-coupling mechanism). Figure 4-5A visualizes the four phases, showing the mechanical power performed by the biarticular gastrocnemii muscles at the knee joint during the maximum walking speed. The mechanical knee joint work of the gastrocnemii muscles in the four phases and their net knee work during all walking speeds are shown in Figure 4-5B.

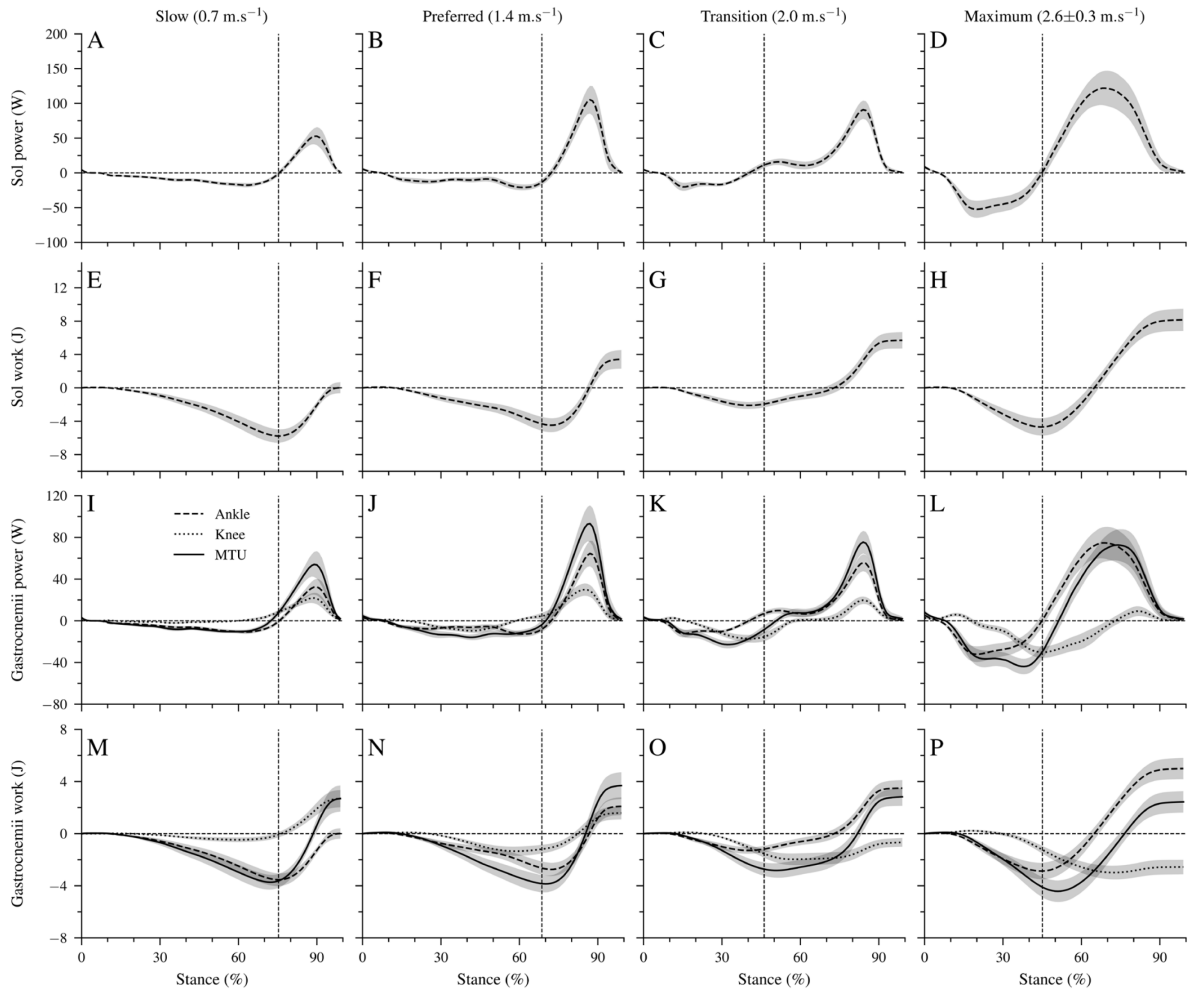

Figure 4-4 Mechanical power (**A**–**D**) and work (**E**–**H**) of the soleus (Sol) muscle at the ankle joint, mechanical power (**I**–**L**) and work (**M**–**P**) of the gastrocnemii muscles at the ankle and knee joints, and the mechanical power/work of the gastrocnemii muscle-tendon unit (MTU). Negative values in the mechanical power indicate energy absorption at the ankle joint during dorsiflexion, energy absorption at the knee joint during knee extension, and energy absorption of the MTU during lengthening. Positive power values indicate energy production during ankle plantar flexion, knee flexion, and MTU shortening. All investigated parameters are presented for the stance phase of walking at slow (0.7 $m.s^{-1}$), preferred (1.4 $m.s^{-1}$), transition (2.0 $m.s^{-1}$), and maximum speed (2.6 ± 0.3 $m.s^{-1}$) as mean ± standard error (average of fifteen participants with nine gait cycles). The vertical dashed line shows the separation between dorsiflexion and plantar flexion.

4.10. Discussion

Our results show that an increase in walking speed is associated with increased net ATF mechanical work, despite a decrease in the maximum AT force in the transition and maximum compared to the preferred speed. We demonstrated that the enhanced musculotendinous energy production of the monoarticular Sol and biarticular mechanisms of the gastrocnemii muscles contributed to the speed-related increase of net ATF mechanical work. Furthermore, our

findings show that in the two higher walking speeds, an earlier plantar flexion due to a rapid increase in the EMG-activity of the Sol and GM muscles was accompanied by a knee extension. The consequence was a knee-to-ankle joint energy transfer via the biarticular gastrocnemii muscles and earlier mechanical energy production of the Sol MTU compared to the slow and preferred speeds. The continued elongation of the AT in the two higher speeds shows that a part of this energy was transferred to the tendon despite the initiation of the plantar flexion. In line with our hypothesis, the results show a different mechanistic participation of the monoarticular Sol muscle and the biarticular gastrocnemii in the speed-related increase of net ATF mechanical work.

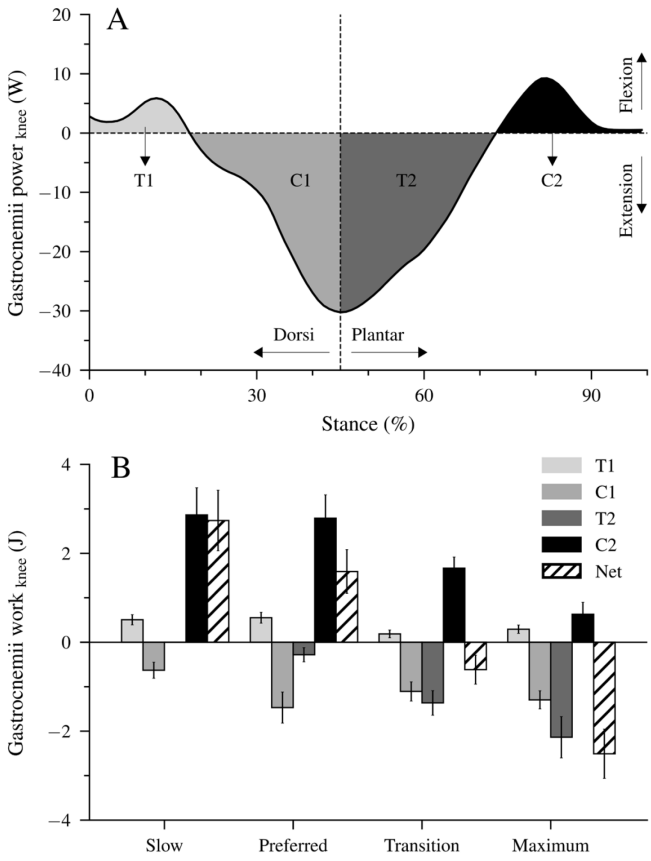

Figure 4-5 Mechanical power (**A**) and work (**B**) of the biarticular gastrocnemii muscles at the knee joint illustrate the transfer (T) and joint-coupling mechanisms (C). T1: ankle-to-knee joint energy transfer, C1: energy absorption at the knee joint during dorsiflexion and knee extension, T2: knee-to-ankle joint energy transfer, C2: energy production at the knee joint during plantar flexion and knee flexion, Net: net work at the knee joint. The values are mean ± standard error (average of fifteen participants with nine gait cycles).

Similarly to earlier studies (Neptune et al., 2008), we found a continuous decrease in stance and swing times and an increase in step length and cadence as a function of walking speed. The duty factor in all investigated speeds was >0.5, showing a double contact time at all speeds.

The maximum AT forces ranged between 1.616 and 2.174 kN and were very close to the measured values in comparable walking speeds reported by Finni et al. (Finni et al., 1998) using optic fiber methodology. The maximum AT force reduced by 21% in the two higher speeds compared to the preferred one, despite the higher EMG activity of the Sol and GM muscles, which confirms the predictions from musculoskeletal models at comparable walking speeds (Neptune & Sasaki, 2005). The increase of net ATF work with speed can result from both an increased net mechanical work of the contractile elements of the Sol, GM, and GL muscles and a modulation of the biarticular mechanisms. The most voluminous monoarticular Sol muscle can produce power and work only at the ankle joint. Based on the physiological cross-sectional area within the Sol, GM, and GL muscles (Albracht et al., 2008), we assumed a 38% contribution of the gastrocnemii to the AT force. This means that most of the speed-related increased net ATF work is done by the Sol muscle (i.e., 62%) or, more specifically, by the Sol contractile element, as the elastic element cannot produce positive net work. The unchanged net mechanical work of the gastrocnemii MTU indicates a similar net mechanical work of their contractile elements within the four investigated speeds. This implies that the contractile elements of the gastrocnemii muscles did not contribute to the speed-related increased net ATF work.

The two gastrocnemii are biarticular muscles and, thus, are able to generate power and work in both the ankle and knee joints. Due to their biarticularity, two additional mechanisms can affect the net ATF work in addition to the work output of their contractile elements. The net mechanical work of the gastrocnemii muscles at the ankle joint showed a continuous increase from slow to the maximum speed of 4.3 ± 0.8 J, demonstrating relevant participation of the biarticular mechanisms. This speed-related increase of the biarticular net work at the ankle joint without changes in the net work of the gastrocnemii MTU was due to the speed-related increase negative net mechanical work of the gastrocnemii at the knee joint. These findings provide first-time evidence that the biarticular gastrocnemii muscles modulate their energy output within the two joints towards an increased output at the ankle joint at higher walking speeds. Thus, the current study demonstrates that both the monoarticular Sol and the biarticular gastrocnemii contribute to the speed-related increase of net mechanical work carried out at the ankle joint. However, the energetic processes and the mechanisms for this phenomenon differ between the two synergistic muscles. The Sol muscle increased the net mechanical work at the ankle joint by a speed-related increase of contractile work production (62% contribution), while the gastrocnemii muscles increased their work output at the ankle joint by an increased contribution of biarticular mechanisms (38%). The largest energy transfer from the knee to the

ankle joint occurred at the maximum speed. More than three decades ago, van Ingen Schenau (van Ingen Schenau, 1989) mentioned that the timing of the coupling between knee extension and plantar flexion could influence the effectivity of the knee-to-ankle joint energy transfer via the biarticular gastrocnemii muscles. The greater knee-to-ankle joint energy transfer in the maximum walking speed indicates a more effective coupling between knee extension and plantar flexion concerning energy production at the ankle joint compared to the transition and preferred speeds.

The earlier initiation of the plantar flexion in the two higher speeds (47% of the stance phase) compared to the slow and preferred ones (72% of the stance phase) was associated with a rapid increase in the EMG-activity of the Sol and GM muscles and with a knee- to-ankle joint energy transfer via the biarticular gastrocnemii muscles (Video S1 in the Supplementary Materials). Interestingly, the dorsiflexion and plantar flexion duration intersected at the transition speed, indicating a different coordination at the ankle joint as well as between ankle and knee joints in the two higher walking speeds that promote the increase of the ATF work. The earlier initiation of the plantar flexion (relative to the stance phase) combined with a rapid increase in the EMG-activity of the Sol and GM resulted in an increase of the AT force in the two higher walking speeds during the first part of the plantar flexion, whereas in the slow and preferred speed the plantar flexion was associated with a continuous and rapid decline of AT force. The result was an invariant (p = 0.295) average AT force in all speeds during the plantar flexion phase (slow: 1035 ± 148 N, preferred: 1175 ± 143 N, transition: 1016 ± 102 N, maximum: 985 ± 128 N). The similar average AT force with the increased plantar flexion RoM resulted to a greater positive ATF work at the maximum walking speed. The lower negative ATF work at the transition speed and the higher positive ATF work at the maximum speed caused the increase of net ATF work despite the decrease of maximum AT force in the two higher speeds. This earlier initiation of the plantar flexion occurred at a low AT operating strain (Figure 4-6). At the beginning of the plantar flexion, the AT strain was 2.6 ± 0.2% in the transition and 3.3 ± 0.3% in the maximum walking speed, and both were clearly lower in comparison during slow 3.9 ± 0.3% and preferred 4.1 ± 0.3% walking speeds. The low AT strain values in the two higher speeds indicate that the initiation of the plantar flexion and, thus, the production of mechanical work at the ankle joint occurred when the AT operates closer to or even within the toe region of the tendon force-elongation relationship, where the tendon may be elongated with rather low increments of muscle force. The energy transfer from the knee-to-ankle joint via the biarticular gastrocnemii muscles and the rapid increase in Sol and GM muscle activation at a low level of muscle forces (26 ± 0.4% of the MVC) facilitated the muscles' force generation

and storage of the elastic strain energy on the AT even during the plantar flexion. The simultaneous plantar flexion and AT elongation during the transition and maximum speeds show, at least for the monoarticular Sol muscle, a transfer of contractile energy production to the AT. Furthermore, the knee-to-ankle joint energy transfer via the gastrocnemii muscles indicates energy transfer from the proximal quadriceps muscles to the AT.

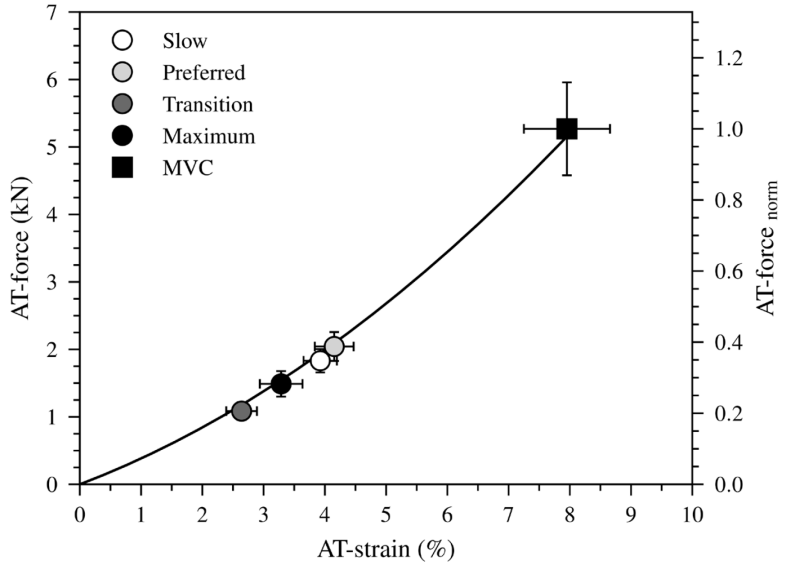

Figure 4-6 The force-strain relationship of the Achilles tendon (AT) during a maximum voluntary contraction (MVC). The markers show the operating AT force and strain values at the beginning of the plantar flexion during walking at slow (0.7 $m.s^{-1}$), preferred (1.4 $m.s^{-1}$), transition (2.0 $m.s^{-1}$) and maximum speed (2.6 ± 0.3 $m.s^{-1}$, Max) as means ± standard error (average of fifteen participants with nine gait cycles).

The biarticular net work at the ankle joint increased as a function of walking speed and was greater than the net mechanical work of the gastrocnemii MTU, particularly at the two higher speeds. In addition, the monoarticular Sol muscle contractile energy production was greater in the transition and maximum walking speed compared to the preferred one. Although, the contractile energy production of the monoarticular Sol and the participation of the biarticular mechanisms of the gastrocnemii muscles may increase the net mechanical work done at the ankle joint during the two higher speeds, and thus walking performance is metabolically costly. Contractile work during shortening increases the active muscle volume and thus the metabolic costs. The enormous increased EMG activity of the investigated muscles in the transition and maximum walking speeds predict a higher active muscle volume. In the biarticular knee-to-ankle joint energy-transfer mechanism, the more proximal quadriceps muscles are involved, and part of their contractile work can be transferred to the ankle joint (M. F. Bobbert et al., 1986; Gregoire et al., 1984). Due to the greater muscle volume of the quadriceps compared to the distal Sol, GM, and GL muscles (Mersmann et al., 2014; Mersmann et al., 2015), they can

produce more muscular power and work. However, due to their longer fibers, a unit of force generation is metabolically more expensive compared to the shorter Sol, GM, and GL muscles (Biewener et al., 1998; Bohm et al., 2021). Therefore, the knee-to-ankle joint energy transfer at the two higher speeds might increase the metabolic costs of walking. Studies that measured the metabolic cost of walking show that the energy cost increased at speeds higher than the preferred and at speeds above 2.2 $m.s^{-1}$, e.g., our maximum speed, (2.6 $m.s^{-1}$), it is even higher than during running (Minetti et al., 1994).

The quantification of AT force in vivo is challenging, and there are some limitations associated with the approach used in the present study that need to be considered when interpreting the results. The anatomical structure of the AT comprises bundles of fascicles originating from Sol, GM, and GL muscles (Franz et al., 2015; Szaro et al., 2009). This structure allows a certain degree of inter-fascicle sliding, which may result in different regional displacement gradients within the AT during loading (Franz et al., 2015). Contraction dynamics of the Sol, GM, and GL muscles may affect the inter-fascicle sliding within the AT during walking, which would affect the accuracy of the AT force quantification. On the other hand, there is also evidence that the myotendinous structures of the Sol, GM, and GL do not work independently but are mechanically connected (Bojsen-Møller et al., 2010; Finni et al., 2017). Myotendinous force transmission through contiguous extramuscular connective tissue structures influences the mechanical linkage of adjacent MTUs during muscle contraction (Huijing, 2009; Kinugasa et al., 2013) and promotes a synchronous movement of connective tissues between the Sol, GM, and GL muscles (Bojsen-Møller et al., 2010; Finni et al., 2017). Force transmission mechanisms through the connective tissue network of the MTUs may redistribute the forces within the AT in order to minimize peak stresses (Maas & Finni, 2018) and thus, heterogeneous regional displacement gradients. Similar AT force–elongation curves have been reported when using either the myotendinous junction of the GM or GL as measured points (Morrison et al., 2015; Obst et al., 2016), and were independent of the ankle angle, i.e., rest length of the AT (Ackermans et al., 2016; Morrison et al., 2015). Consequently, although a certain degree of heterogeneous displacement within the AT length is possible during walking (which may, to some extent, influence the accuracy of the AT force quantification) it is unlikely to change the main findings and conclusions.

In this study, the AT force contribution of each individual muscle was assumed to be proportional to its relative PCSA. However, the individual muscle force also depends on the respective force–length–velocity potential (i.e., fraction of maximum force according to the force–length and force–velocity curves) and muscle activation. During human walking, the

force–length–velocity potential of the Sol and GM was found to be between 0.6 and 0.8 (Monte et al., 2023; Rubenson et al., 2012). We performed a sensitivity analysis by varying the force-length–velocity potential of the Sol and gastrocnemii separately in 0.1 intervals between 0.6 and 0.8. Since a similar fascicle shortening behavior of the GM and GL has been found during the stance phase of walking (Hamard et al., 2021), we assumed a similar force–length–velocity potential for the two muscles. To estimate muscular activation, we used the average normalized EMG-activity for the Sol and GM muscles we measured during walking. Some studies (Hamard et al., 2021; Hug et al., 2021) reported distinct activation patterns of the GM and GL during walking. Hamard et al. (Hamard et al., 2021) reported a ratio of the GM EMG-activity to the sum of GM and GL EMG-activity between 0.44 and 0.68 across participants. Since we did not measure the EMG-activity of the GL, an activity-ratio of GM from 0.4 to 0.7 in 0.1 increments was used for the sensitivity analysis. In total, 36 different combinations were considered. The new distribution coefficients (*ki*) used for the sensitivity analysis were calculated with Equation 4-3:

$$k_i = (\lambda_i^{l,v} \cdot \alpha_i \cdot r_i^{PCSA}) \Big/ \sum_{i}^{3} (\lambda_i^{l,v} \cdot \alpha_i \cdot r_i^{PCSA}) \qquad \text{Equation 4-3}$$

with *i*: Sol, GM, GL; $\lambda l,v$: force–length–velocity potential of the muscle *i*; αi: activation of *i* muscle *i*; *rPCSA*: relative *PCSA* of muscle *i*. *i*. The Tables S1–S4 in the Supplementary Materials show the results of the sensitivity analysis on the net work of the Sol and gastrocnemii at the ankle joint as well as the net work of the gastrocnemii at the knee joint, which represents the contribution of the biarticular mechanisms to the increase of net ankle work. Different force potentials and ratios of the GM EMG activity affect the absolute values in all three parameters. Nevertheless, in all combinations, the contribution of the Sol to the net mechanical work at the ankle joint was higher than the gastrocnemii. Both the energy production of the monoarticular Sol and the contribution of the biarticular mechanisms (i.e., increased net ankle work) increased with walking speed. Thus, the sensitivity analysis clearly demonstrates that the main findings and conclusions generally hold true even under the assumption of varying force–length–velocity potentials and activation of the individual muscles.

In conclusion, an increase in the net mechanical work at the ankle joint from the Sol and gastrocnemii muscles is needed to increase walking speed. The net mechanical work at the ankle joint can be affected by the contractile energy production of the three muscles and by the biarticular mechanisms of the gastrocnemii muscles. In the current study, we focused on the contribution of monoarticular and biarticular muscle mechanisms for the needed greater net

ATF work from slow to maximum walking speeds. Our findings show that both the contractile energy production of the monoarticular Sol muscle and the biarticular mechanisms of the gastrocnemii muscles contributed to the speed-related increased net mechanical work at the ankle joint. Although the contribution of the contractile work of the Sol was greater, biarticular mechanisms of the gastrocnemii accounted for a relevant part of the increased net ankle joint mechanical work with speed. An earlier plantar flexion initiated by a rapidly increased activation of the Sol and GM muscles increased the net ATF mechanical work 1.7 and 2.4-fold in the transition and maximum walking speeds, respectively, compared to the preferred one, despite a decrease in maximum AT force.

4.11. Supplementary Materials:

The following supporting information can be downloaded at: https://www.mdpi.com/article/10.3390/biology12060872/s1, Tables S1–S4: Sensitivity analysis; Video S1: Energy transfer.

4.12. Author Contributions:

Design, experimentation, data analysis, writing—first draft, M.K.; coordination, design, experiment, writing—review and editing, S.B.; experimentation, data acquisition, writing—review and editing, C.T.; writing—review and editing, F.M.; conceptualization, design, coordination, writing—first draft, A.A. All authors have read and agreed to the published version of the manuscript.

4.13. Funding:

This research received no external funding.

4.14. Institutional Review Board Statement:

The study was conducted in accordance with the Declaration of Helsinki, and approved by the Institutional Ethics Committee.

4.15. Informed Consent Statement:

Informed consent was obtained from all subjects involved in the study.

4.16. Data Availability Statement:

https://doi.org/10.6084/m9.figshare.21075907.v3.

4.17. Acknowledgments:

We acknowledge the German Research Foundation (DFG) support and the Open Access Publication Fund of the Humboldt-Universität zu Berlin.

4.18. Conflicts of Interest:

The authors declare no competing interests.

4.19. Abbreviations

The following abbreviations are used in this manuscript:

AT	Achilles tendon
ATF power/work/moment	Power, work, or moment of the AT at the ankle joint
EMG	Electromyographic activity
Sol	Soleus
GM	Gastrocnemius medialis
GL	Gastrocnemius lateralis
TA	Tibialis anterior
MVC	Maximum voluntary isometric contraction
GM-MTG	Gastrocnemius medialis muscle–tendon junction
MTU	Muscle–tendon unit
PCSA	Physiological cross-section area
First energy-transfer mechanism	Phase T1
First joint-coupling mechanism	Phase C1
Second energy-transfer mechanism	Phase T2
Second joint-coupling mechanism	Phase C2

5. Third study: A Simplified Method for Considering Achilles Tendon Curvature in the Assessment of Tendon Elongation

Authors:

Mohamadreza Kharazi [1,2]
Sebastian Bohm [1,2]
Christos Theodorakis [1,2]
Falk Mersmann [1,2]
Adamantios Arampatzis [1,2]

[1] Department of Training and Movement Sciences, Humboldt-Universität zu Berlin, Germany.
[2] Berlin School of Movement Science, Berlin, Humboldt-Universität zu Berlin, Germany.

Published in:
Sensors 2021, 21:7387; https://doi.org/10.3390/s21217387
(reprinted with permission by MDPI)

5.1. Abstract

The consideration of the Achilles tendon (AT) curvature is crucial for the precise determination of AT length and strain. We previously established an ultrasound-kinematic-based method to quantify the curvature, using a line of reflective foil skin markers covering the AT from origin to insertion. The current study aimed to simplify the method by reducing the number of markers while maintaining high accuracy. Eleven participants walked (1.4 m/s) and ran (2.5, 3.5 m/s) on a treadmill, and the AT curvature was quantified using reflective foil markers aligned with the AT between the origin on the gastrocnemius myotendinous-junction (tracked by ultrasound) and a marker on the calcaneal insertion. Foil markers were then systematically removed, and the introduced error on the assessment of AT length and strain was calculated. We found a significant main effect of marker number on the measurement error of AT length and strain ($p < 0.001$). Using more than 30% of the full marker-set for walking and 50% for running, the R2 of the AT length error saturated, corresponding to average errors of <0.1 mm and <0.15% strain. Therefore, a substantially reduced marker-set, associated with a marginal error, can be recommended for considering the AT curvature in the determination of AT length and strain.

Keywords: Achilles tendon; tendon elongation; tendon strain; walking and running; ultrasound

5.2. Introduction

The Achilles tendon (AT) length is an important parameter to assess its mechanical properties and to understand the muscle-tendon interaction within the triceps surae muscle-tendon unit during functional tasks of daily life or athletic performance, such as walking (Ishikawa et al., 2005), running (Albracht & Arampatzis, 2013; Wang et al., 2013), sprinting (Lai et al., 2015), jumping/landing (Kümmel et al., 2018; Lichtwark & Wilson, 2005; Werkhausen et al., 2017), and cycling (Dick et al., 2016; Dick & Wakeling, 2017). AT length-changes upon loading can also be used to estimate tendon forces and strain energy (Kharazi et al., 2021), tendon stiffness (Arampatzis, Karamanidis, & Albracht, 2007), the decoupling within the muscle-tendon unit (Dick & Wakeling, 2017), and tendon hysteresis (Lichtwark & Wilson, 2005). Furthermore, tendon strain (length-changes normalized to resting length) has been suggested as a predictor for tendon injury risk (Pizzolato et al., 2019), a regulator of tendon adaptation (Arampatzis et al., 2010; Wang et al., 2013), and, in this regard, an important marker for subject-specific

tendon exercise prescriptions (Arampatzis et al., 2020). Thus, the accurate assessment of AT length is crucial for the field of human tendon biomechanics.

A simple planimetric model (Fukunaga et al., 2001) is often used for the determination of in vivo AT length but may not reflect the complex in vivo condition (Herzog, 2019). For more sophisticated measures of the AT length, a combination of ultrasound and motion capture has been established previously (Lichtwark & Wilson, 2005; Matijevich et al., 2018; Werkhausen et al., 2017). Using this approach, the gastrocnemius medialis muscle-tendon junction (GM MTJ) commonly defines the AT origin and is tracked by ultrasound and transferred to the global coordinate system. The insertion is given by a reflective marker on the calcaneus bone in the same global coordinate system. The AT length is then calculated as the linear distance between the AT origin and insertion. The assumption to this method is that the AT follows a straight line from the origin to insertion and does not change its alignment, i.e., curvature, during the movement tasks. In fact, the AT features a concave curvature that can alter during contractions and functional movements (Kinugasa et al., 2018; Maganaris et al., 2000), calling the straight length method into question. In a previous study (De Monte et al., 2006), we provided an approach to consider the AT curvature for the AT length determination using a line of reflective foil markers (i.e., self-adhesive retro-reflective tape circles with 5 mm in diameter) placed in small spatial intervals on the skin covering the AT from origin to insertion. We showed that when including the instant AT curvature, the AT elongation was significantly lower by 1.2 ± 0.4 mm compared to the AT length measured with the straight AT length method (i.e., no curvature consideration) during a maximal isometric voluntary contraction (Arampatzis et al., 2008). The error was found to be substantially higher during more dynamic tasks, e.g., 9.0 ± 5.4 mm during ankle joint rotations (15º dorsiflexion to 30º plantar flexion) (Fukutani et al., 2014) and 5.0 ± 1.3 mm during hopping (Stosic & Finni, 2011). Together these reports provide evidence that the consideration of the AT curvature is crucial for the precise measurement of AT length and strain. However, using many foil markers on the path of the AT to reconstruct its curvature is experimentally effortful (Kharazi et al., 2021). The increased need for hardware (i.e., number of cameras for high-quality marker tracking) and high time-demand for post-data processing (marker labeling, gap filling and checking for potential foil markers distortion) hamper the practicability and applicability of this method. A simplified AT length assessment using a reduced marker-set may, however, be appropriate to detect the AT length and strain magnitudes and might be of interest when implemented in a diagnostic approach to monitor the mechanical demand of a tendon and control for strain ranges to stimulate adaptation (4.5% to 6.5%) (Arampatzis, Karamanidis, & Albracht, 2007; Arampatzis

et al., 2020; Bohm et al., 2015; Bohm et al., 2014). A reduced marker-set as a straightforward approach could increase the feasibility of the foil marker-based method to reconstruct the AT curvature while maintaining the associated error in a reasonable range. However, it has not been systematically investigated yet how many foil markers are required for a precise AT length determination during locomotion. Furthermore, changes in AT curvature during locomotion and thus the required markers for reconstruction may depend on the gait phase (stance vs. swing), gait mode (walking vs. running), and gait speed (slow vs. fast) because of different contraction intensities and ankle joint range of motions that are involved.

The purpose of the present study was to measure the AT length under consideration of its curvature using a modified number of foil markers compared to our previously proposed method (Kharazi et al., 2021) during walking and running at different speeds. The error on the AT length and maximum strain introduced by a given marker number with respect to the length calculated with all markers was investigated by systematically eliminating markers from the curved length. We hypothesized significant inaccuracies in the AT tendon length measurement across gait phases, gait modes and gait speeds of the AT straight compared to AT curved approach. We further hypothesized that the AT length and strain could be determined with a tolerable error by a reduced marker-set, i.e., fewer markers than all available markers.

5.3. Materials and Methods

5.3.1. Experimental Design

In this study, 11 young, healthy individuals participated (age 28.0 ± 2.6 years, height 175.0 ± 7.1 cm, body mass 75.0 ± 12.0 kg). All participants gave written informed consent to the experimental procedure, which was approved by the ethics committee of the Humboldt-Universität zu Berlin (HU-KSBF-EK_2018_0005) and in accordance with the Declaration of Helsinki. After 10 min of familiarization, participants walked at 1.4 m/s and ran at 2.5 m/s

(slow running) and 3.5 m/s (fast running) on a treadmill (Daum electronic, ergorun premium8, Fürth, Germany).

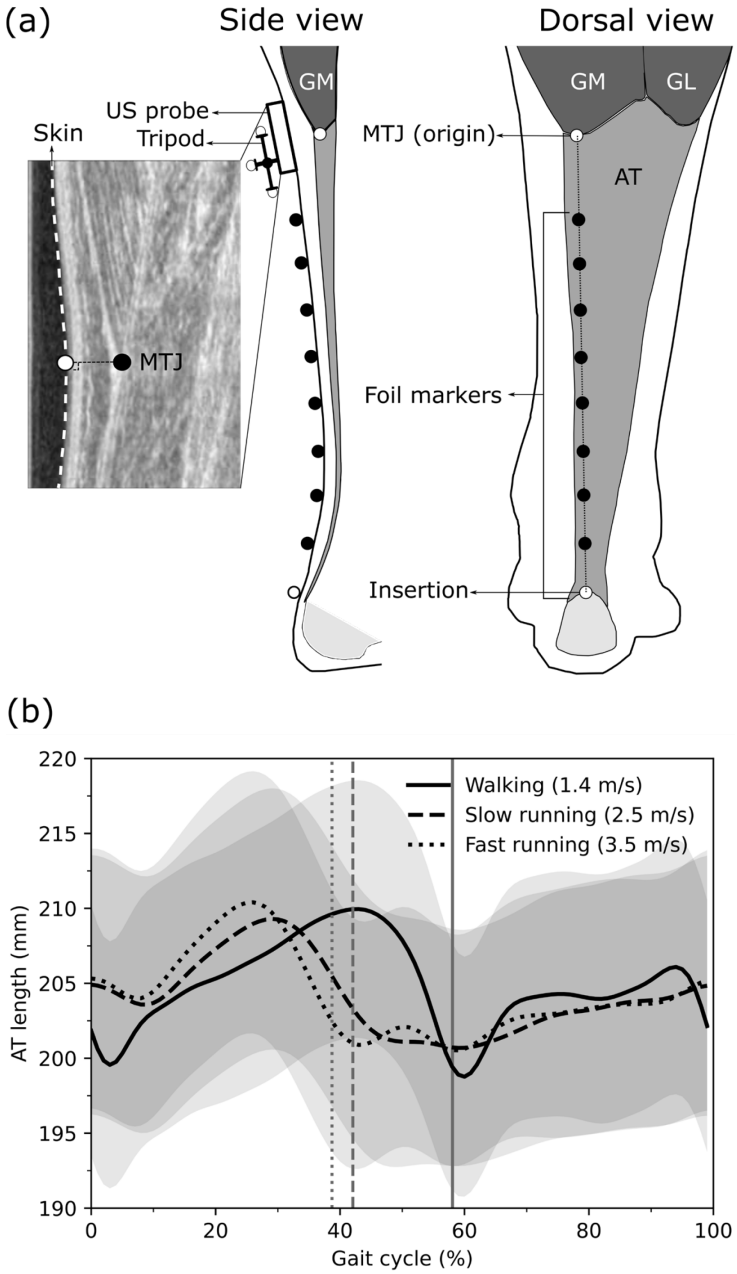

Figure 5-1 (a) Experimental setup for determining the Achilles tendon (AT) length during walking and running. Reflective foil markers on the skin were used to reconstruct the curvature of the AT (black markers) from origin to insertion (white markers). The gastrocnemius medialis (GM) myotendinous junction (MTJ), as the AT origin, was projected to the skin surface, and the coordinates of the ultrasound images were transferred to the global coordinate system using a tripod that was mounted on the ultrasound probe. (b) The length of the AT with all foil makers during walking, slow running and fast running throughout the gait cycle. Vertical lines separate stance and swing phases. GL: gastrocnemius lateralis, US: Ultrasound.

During gaits, the length of the AT was defined as the distance between the origin on the GM MTJ and the insertion on the calcaneus bone, under consideration of the concave curvature of

the AT in the longitudinal axis (Figure 5-1a). The insertion position was captured by a reflective foil marker placed on the notch of the calcaneus bone (Figure 5-1a). The curvature was assessed using several of the same reflective foil markers placed along the curved length of the AT on the skin (Figure 5-1a). The position of the GM MTJ was determined using ultrasound and a projection to the skin surface, which was then transformed to the global coordinate system to align insertion, foil, and origin markers (Figure 5-1a). For the simplification of the AT length determination with a reduced number of reflective foil markers, we then assessed the deviation of AT length that would be introduced when removing one or more reflective foil markers between origin and insertion by calculating the absolute length error compared to the reference criterion, i.e., the AT length determined by all reflective markers. Furthermore, we calculated the straight length of the AT as a Euclidean distance between AT origin and insertion.

5.3.2. Gait Event Detection

During walking, the touchdown of the right foot was determined as the minimal vertical position of the heel marker (Fellin et al., 2010) and during running as the first maximum extension of the knee angle (Dingwell et al., 2001). The foot-off was defined as the reversal of the anterior–posterior velocity of the toe marker during walking and as the second maximum extension of the knee angle during running (Alvim et al., 2015). For this purpose, the right leg ankle and knee joint kinematics were assessed by six reflective markers placed on the tip of the toe, medial and lateral malleolus, medial and lateral epicondyle of the femur, and the greater trochanter. The marker trajectories were filtered with a fourth-order, low pass, and zero-phase shift Butterworth filter with a cutoff frequency of 12 Hz.

5.3.3. Achilles Tendon Length and Strain Assessment

For the AT length determination during gaits, a reflective marker-based motion capture approach was implemented and combined with ultrasonography (Kharazi et al., 2021). The position of the AT insertion on the notch of the calcaneus bone (identified by means of ultrasound) as well as the curvature of the AT between origin and insertion were captured using a line of reflective foil markers placed on the skin (distal marker on calcaneus notch, 20 mm intervals, 5 mm in diameter) using a motion capture system (Vicon Motion Systems, Oxford, UK) integrating 14 cameras at a sampling frequency of 250 Hz. The GM MTJ, as the AT origin, was defined as the most distal ending of the GM and tracked during gaits using a 6 cm linear

ultrasound transducer operating at 146 Hz (Aloka UST-5713T, Hitachi Prosound, alpha 7, Japan), which was aligned with the reflective foil marker path (Figure 5-1a). The GM MTJ was tracked using a semi-automatic tracking algorithm from the stack of the US images (Kharazi et al., 2021).

The position of the GM MTJ was then transferred to the skin surface, which was detected by using the 'Canny edge detection algorithm' (Canny, 1987) in the same actual ultrasound image. The transformation of GM MTJ to the skin surface was done as the shortest distance of the GM MTJ to skin (Figure 5-1a). The position and the orientation of the ultrasound transducer in 3D space were captured employing a mounted custom marker tripod and the motion capture system (Figure 5-1a). For the transformation of the defined coordinate system in the ultrasound image to the global coordinate system, a custom-made calibration tool was used in order to digitize the four corners of the protective front layer of the ultrasound transducer and then a coordinate system was defined on the left-center of the front protective layer. During a separate static preparation trial, the position of the tripod on the probe was determined relative to the defined coordinate system on the front protective layer of the transducer. The AT length was then calculated as the sum of Euclidean distances between all foil markers from the insertion to the origin (GM MTJ). The averaged AT length from all participants, calculated by all possible reflective foil markers along the AT curve during walking, slow running and fast running over the gait cycle, is shown in Figure 5-1b. A manual trigger was used to synchronize the ultrasound device and the motion capture system. Ten complete gait cycles in each gait speed per individual were captured for the kinematic and AT length assessments and used for further analysis. The entire methodology, including the GM MTJ projection to motion capture coordination system and validation of the semi-automatic tracking algorithm, has been described in detail previously (Kharazi et al., 2021). Furthermore, the AT strain during walking and running was calculated by dividing the instantaneous difference of AT length and AT resting length, which was measured at rest in 20◦ plantar flexion, where tendon slackness has been reported previously (De Monte et al., 2006).

5.3.4. Reduction of Reflective Foil Marker Number for Achilles Tendon Curvature Determination

The number of reflective foil markers on the AT path (i.e., all reflective markers excluding the insertion and the origin of the AT) to assess its curvature varied because of the individuals' GM MTJ position, which could be more or less distal on the shank (Figure 5-1a). The

individuals with the same number of foil markers were clustered, i.e., P5: individuals with five foil markers (two participants), P6: six foil markers (two participants), P7: seven foil markers (four participants), P8: eight foil markers (two participants), and P9: nine foil makers (one participant).

The AT length was first calculated without any foil marker as a straight length, connecting the origin (GM MTJ) and insertion (calcaneus marker). The AT length was also calculated with all foil markers as the reference criterion (i.e., reference length). Then the number of foil markers was systematically reduced one by one, where MS8 (marker-set) to MS1 indicates the number of used

foil markers for each participant. The AT length in each of the available marker-sets was calculated considering all possible combinations (i.e., the order does not matter) of the foil makers (i.e., different markers positioned on the AT curved path) using Equation 5-1:

$$\mathrm{n}c_{ji} = \frac{\mathrm{n_j}!}{(\mathrm{n_j} - r_i)!\ r_i!} \qquad \text{Equation 5-1}$$

where *j* is the index of the participant, *i* refers to the marker-set (i.e., MS1-8), *nc* is the total number of combinations of the different foil marker positions, *n* is the total number of foil markers, and *r* is the selected number of foil markers depending on the used marker-set (i.e., from 1 to 8). The calculated AT length in each individuals' combination of each marker-set (nc_i) over the whole stride was compared to the reference length by means of the root mean square error (RMSE). The combination with the lowest RMSE was selected as the optimal combination for the selected marker-set for each participant and expressed for further analysis as absolute AT length error, i.e., the AT length difference to the reference curved length in mm. Further, we analyzed the error of the foil marker reduction on the AT maximum strain with respect to the AT maximum strain calculated with all foil markers in order to analyze the error effect associated with length changes of the AT during gaits normalized to the individual AT resting length.

5.4. Statistics

A Wilcoxon signed-rank test was used to test for differences between AT length and maximum strain determined by either the curved length approach or straight length approach, including all gait speeds and phases. A linear mixed model was conducted to test for the main effects of marker-set (MS1-8), gait speed (walking, slow and fast running) and gait phase (swing vs. stance) on the phase-averaged AT length error and AT maximum strain error. In case of a

significant interaction effect, a post hoc analysis was performed, and Benjamini-Hochberg corrected *p*-values will be reported. The normal distribution of the linear mixed model residuals of the AT length and maximum strain error was tested using the Shapiro-Wilk test and revealed non-normal distribution ($p < 0.001$). However, since linear mixed models are robust against violations of this assumption, we adhered to this concept (Jacqmin-Gadda et al., 2007). The significance level was set to $\alpha = 0.05$, and all values are reported as means and standard deviation. The statistical analyses were conducted using R v4.0.1 (R foundation for statistical computing, Vienna, Austria. Packages, 'nlme package' was used for the linear mixed model and 'emmeanse' was used for post hoc testing). To assess at which percentage of all used markers the measurement accuracy is not substantially decreased by removing further markers, the absolute length difference averaged over both phases between the AT curved length and AT length including a reduced relative foil marker number were calculated. The AT length measurement error of each individual was interpolated linearly to 100 points, and then a linear regression was fitted to all data points in 1% intervals starting from 0% (i.e., straight length) to 100% (i.e., reference length). The resultant $R2$ values of each interval were then calculated in each step. The percentage of remaining markers where the
average $R2$ curve saturated was used as an indicator of a sufficient marker number, i.e., the addition of more markers would not significantly improve the accuracy. For this specific percentage of remaining markers, we calculated the respective locations of the foil markers as an average of the individual best marker combination (lowest RMSE) across phases and participants, to provide a recommendation for the application of a reduced marker-set. The positions were expressed as the percentage of the AT length during upright standing relative to the calcaneus marker (i.e., 0%). The length-error for each individual that is introduced when applying the average marker position and not the individual optimal position was also calculated as length-difference (RMSE over the whole stride).

5.5. Results

The reference AT length throughout the entire gait cycle ranged between 197 ± 25 mm and 210 ± 27 mm during walking; 199 ± 26 mm and 210 ± 27 mm during slow running; and 199 ± 25 mm and 211 ± 27 mm during fast running (Figure 5-1b). On average, the curved reference length of the AT was significantly longer than the straight length across all gait speeds and gait phases with individual maximum differences of up to 4.3 ± 1.0 mm during walking, 5.4 ± 1.1 mm during slow running, and 5.7 ± 1.2 mm during fast running (Figure 5-2). The AT length

measurement error for each marker-set with respect to the reference length during the entire gait cycle of walking, slow running and fast running is illustrated in Figure 5-2.

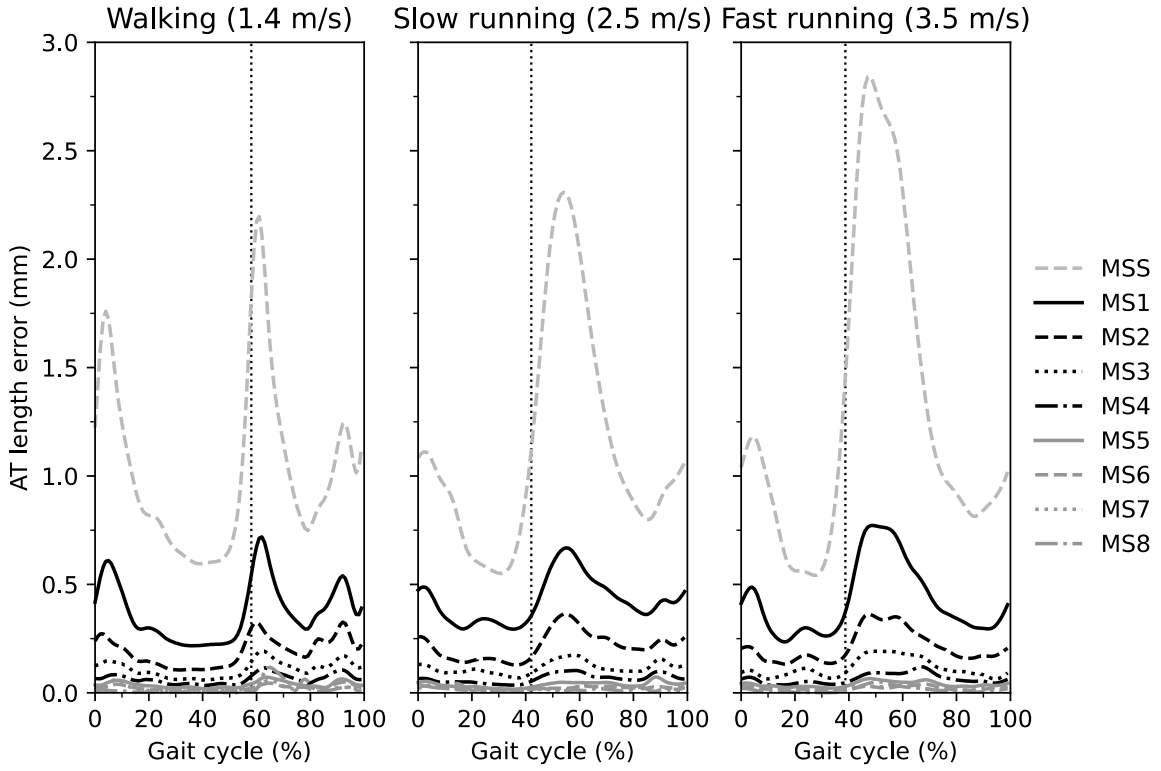

Figure 5-2 The absolute error of the Achilles tendon (AT) length measurement as the difference between the different marker-sets (MS) in comparison to the curved AT length (reference value) throughout the gait cycle. MSS is the straight AT length, and MS1-8 indicates the marker-set with one to eight foil markers. The vertical dashed line separates the stance and swing phase.

In all three gait speeds, the AT length measurement error was larger for marker- sets with fewer foil markers compared to those with a greater number over the entire gait cycle. Increased AT length measurement errors were observed at the initial stance phase and during the first half of the swing phase in all three gait speeds, yet most prominent in MS1 and MS2 (Figure 5-2). For the phase-averaged AT length measurement error, the linear mixed model revealed a significant main effect of marker-set ($p < 0.001$) and gait phase ($p < 0.001$) but not of gait speed ($p = 0.752$, Figure 5-3a). The swing phase-averaged AT length measurement error was larger than the stance phase-averaged error (Figure 5-3a,b).

The analysis also showed a significant interaction effect of marker-set and gait phase ($p < 0.0001$). The post hoc analysis for the comparison of marker-set between swing and stance phases revealed significantly lower errors for MS1-3 ($p < 0.001$, $p < 0.001$, and $p = 0.012$, respectively) during the stance phase compared to the swing phase and no significant differences between phases for MS4-8 ($p = 0.126$, 0.443, 0.665, 0.777; Figure 5-3a,b).

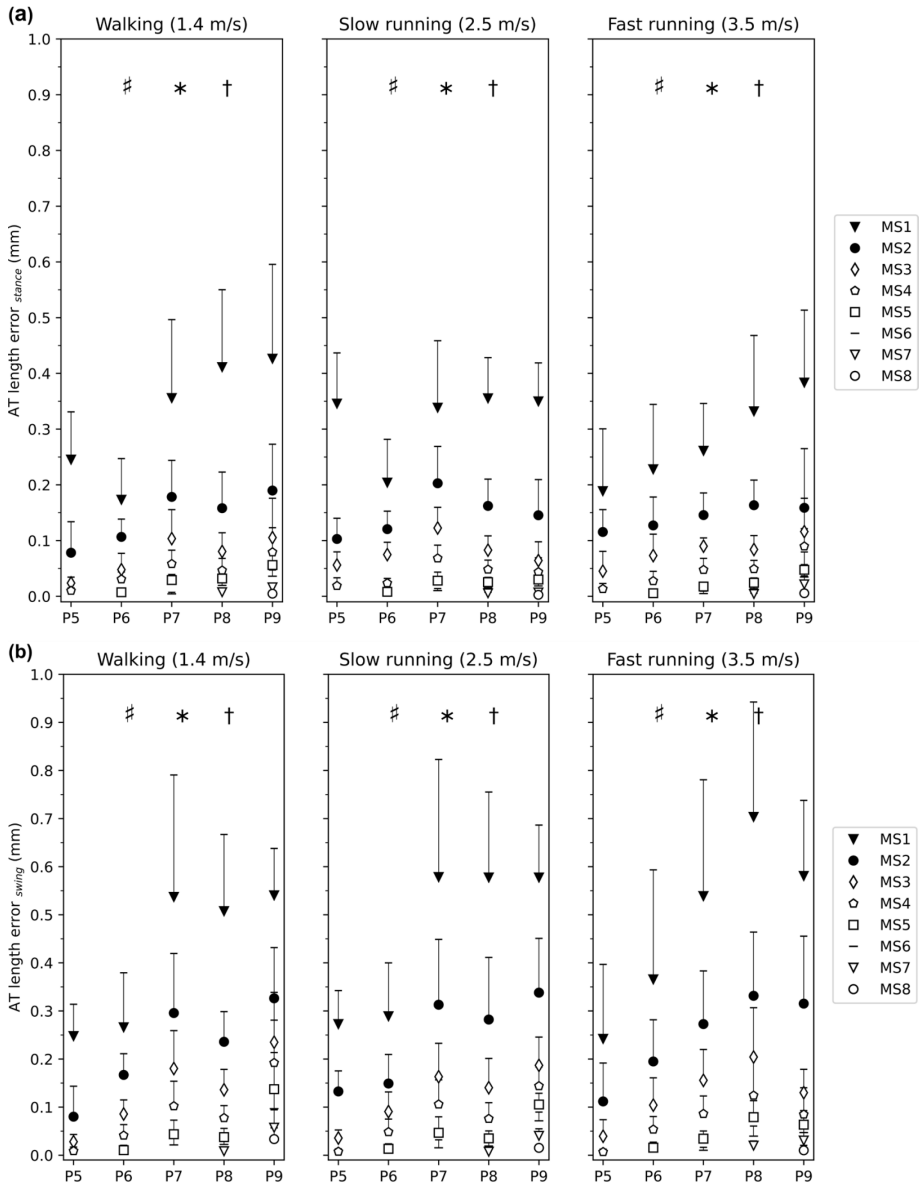

Figure 5-3 Averaged Achilles tendon (AT) length measurement error for each marker-set with respect to the curved reference length of the AT during the (a) stance phase and (b) swing phase of walking, slow and fast running. The marker-set with i number of foil markers (MSi) is the AT length with i = 1 to 8 foil markers. P5 to P9 are the clustered participants with the same number of foil markers. The error bars express the standard deviation of the AT length error throughout the phase (stance, swing), showing the variance over each phase and then averaged among individuals within each cluster. ∗ main effect of phase ($p < 0.001$), † main effect of marker-set ($p < 0.001$), # interaction effect of phase and marker-set ($p < 0.001$). The post hoc analysis for the comparison of marker-set between swing and stance phases revealed significant lower errors for MS1-3 ($p < 0.001$, $p < 0.0001$ and $p = 0.012$, respectively) during the stance phase and no significant phase differences for MS4-8 ($p = 0.126, 0.443, 0.665, 0.777$).

The AT length measurement error averaged over the entire gait cycle for the calculated percentage of remaining markers, and the corresponding $R2$ is shown in Figure 5-4a,b. High inter-individual variability was obtained at values below 30% of the remaining markers (Figure

5-4a). Qualitatively, the $R2$ reached and maintained a plateau at a value of 30% of markers for walking and 50% for running (Figure 5-4b). The average error of the AT length measurement was below 0.13 mm at 30% and 0.06 mm at 50% of the full marker-set in walking and running, respectively (Figure 5-4a).

The maximum AT strain occurred during the stance phase and was in the magnitude of 4.0 ± 1.2% during walking, 4.5 ± 1.4% during slow running and 4.9 ± 1.2% during fast running. AT maximum strain measured by the curved length method was significantly lower by 0.76 ± 0.17% than the straight AT length method across all gait speeds and phases ($p < 0.001$).

The AT maximum strain measurement error showed a significant main effect of marker-set ($p < 0.001$), indicating that the AT maximum strain measurement error was higher with a reduced number of foil markers (from MS1 to MS8 Figure 5-5). No further significant main or interaction effects were found for the AT maximum strain measurement error (gait speed $p = 0.443$, gait speed by marker-set interaction $p = 1.000$). The maximum strain measurement error when using 30% of the markers was below 0.15% for walking and below 0.08% with 50% of the markers during both slow and fast running.

The average location of the foil markers for marker-set 2 to 4 is presented in Table 5-1. The averaged overall error associated when using this reduced average marker positions across participants and gait phases was for marker-set 2: walking 0.26 mm, slow running 0.28 mm, and fast running 0.29 mm; marker-set 3: walking 0.18 mm, slow running 0.17 mm, and fast running 0.18 mm; and marker-set 4: walking 0.15 mm, slow running 0.14 mm, and fast running 0.14 mm.

5.6. Discussion

Here we investigated the reconstruction of the in vivo AT curvature during locomotion using a various number of reflective foil markers on the line connecting the AT insertion and origin. We found a significantly longer length of the AT measured with the reference curved length approach compared to the straight length approach. The AT length and maximum strain measurement error decreased in marker-sets with more reflective markers. When using a minimalistic marker-set with only 30% of the markers of the reference marker-set during walking and 50% during running, the involved measurement error of AT maximum length and maximum strain were lower than 0.35 mm and 0.15% strain, respectively. The results suggest the feasibility of the reduced marker-set that involved only a marginal error for the in vivo AT length and strain determination during locomotion.

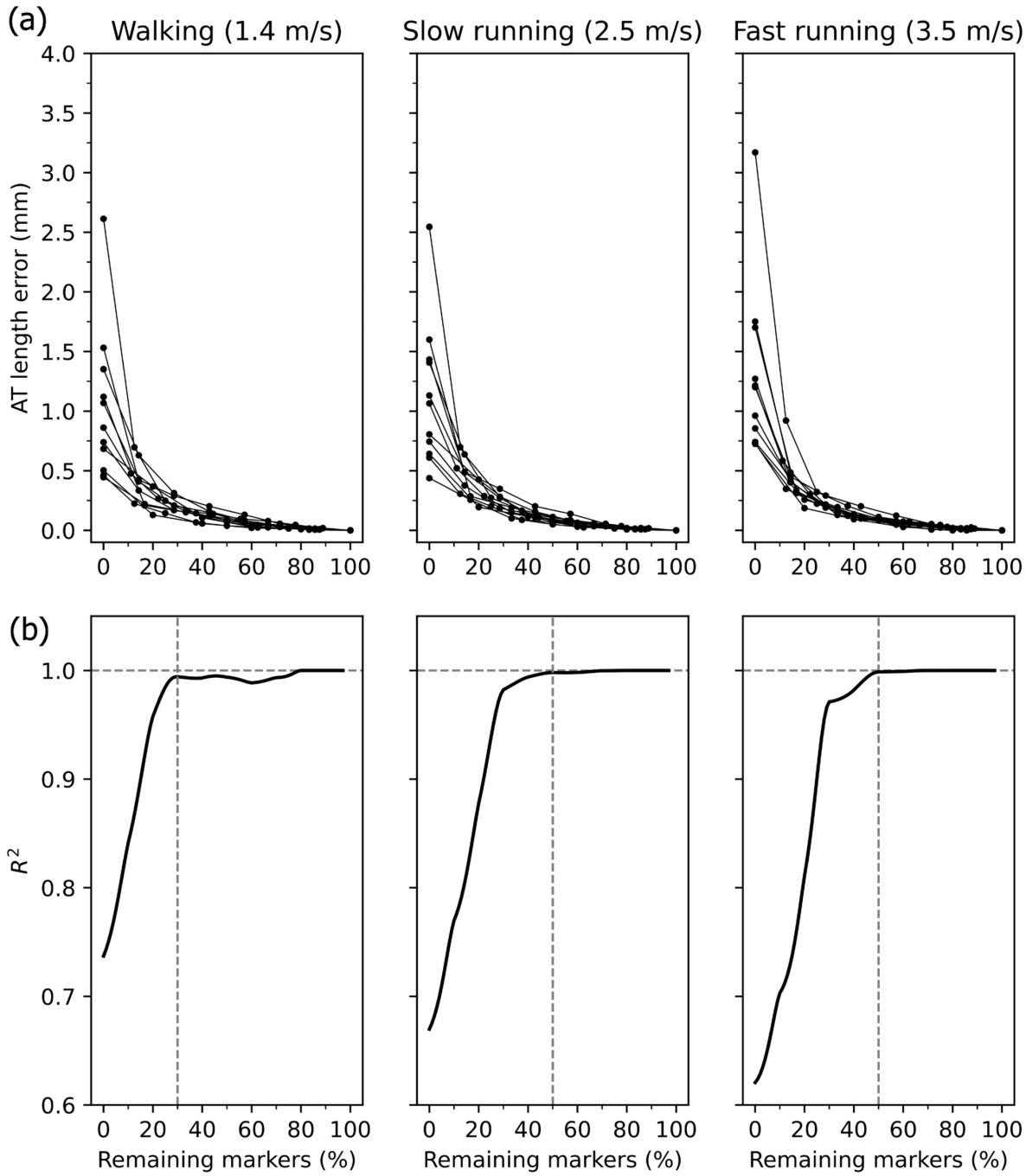

Figure 5-4 (a) Individual Achilles tendon (AT) length measurement error with respect to the reference length (i.e., the AT length with all foil makers) as a function of relative marker number. The 0% indicates the straight AT length, and 100% the curved reference AT length. Note the different number of markers between individuals. (b) The resultant R^2 of the linear regression on the data presented in panel (a) in % intervals from 0% to 100% of the remaining markers.

It has previously been recognized (De Monte et al., 2006) that the AT curvature changes duringcontractionss of the triceps surae muscles, ankle joint rotations, and different functional movement tasks (Kinugasa et al., 2018; Maganaris et al., 2000) and, thus, need to be considered for an accurate AT length determination. For instance, Fukutani et al. (Fukutani et al., 2014)

reported a maximum difference of 9.0 ± 5.4 mm between curved and straight AT length during passive ankle joint rotations.

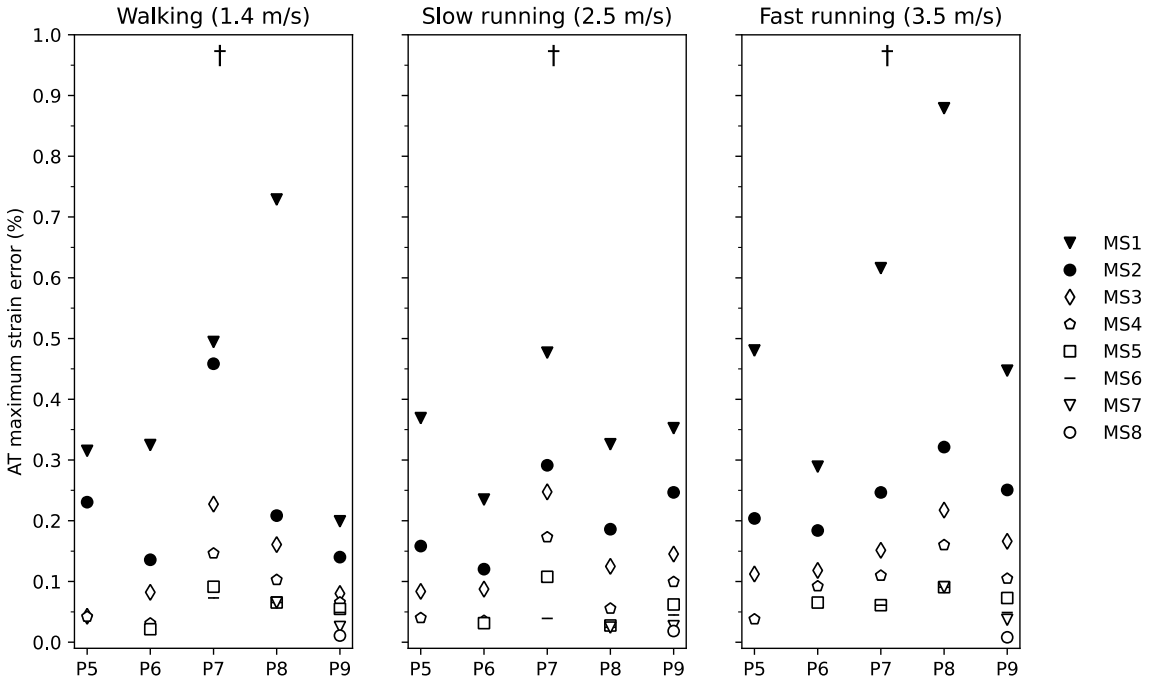

Figure 5-5 Maximum strain error of the Achilles tendon (AT) during walking, slow and fast running for marker-set 1-8 (markers-set (MS) with 1 to 8 foil markers) with respect to the marker-set with all possible foil reflective markers. Participants were clustered into five groups of P5-9 (participants with 5 foil makers to participants with 9 foil markers). † main effect of marker-set ($p < 0.001$).

Furthermore, it has been shown that the AT curved length and strain during hopping differed by 5.0 ± 1.3 mm and1.3 ± 0.7%, respectively, compared to the straight
length and strain (Stosic & Finni, 2011). In agreement with the earlier studies, we found a significant difference of the straight length and maximum strain to the curved length and maximum strain of the AT over the three gait speeds and both gait phases. The straight length approach underestimated the AT length and showed a high individual variability in the resultant error. In our investigated participants, the observed maximum differences between the curved and straight length assessment ranged from 0.1 to 5.7 mm, i.e., 0.2% to 1.6% strain. Considering that the AT maximum strain
during the stance phase was 4.0%–4.9% across gait modes (walking and running), our results evidence that the straight length method may introduce important artifacts (5% to 40%) in maximum tendon strain measurements during walking and running.

The reconstruction of the AT curvature by an increasing number of foil markers continuously reduced the average and maximum AT length and maximum strain error. The findings showed that when including already 30% of the maximum available markers for walking and 50% for

running, the $R2$ of the AT length measurement error reached and maintained a very high value ($R2 > 0.99$). Furthermore, the achieved steady-state in $R2$ shows that a higher percentage of marker number (above the mentioned thresholds) would not significantly increase the measurement accuracy. The remaining errors in the maximum AT length and strain measurement were for walking 0.35 ± 0.11 mm and 0.15 ± 0.06%, for slow running 0.15 ± 0.08 mm and 0.06 ± 0.04%, and for fast running 0.17 ± 0.04 mm and 0.08 ± 0.02%. The magnitude of these errors is arguably negligible when considering a given average AT length change of 7.8 ± 2.6 mm and average maximum strains between 4.0% and 4.9% across speeds and phases. Therefore, for the investigated participants and depending on the individual AT length, 2 to 4 markers between the origin and insertion of the AT are sufficient to determine the AT curvature across speeds and gait phases. Using the reduced marker-set instead of all markers would significantly simplify the assessment protocol in terms of cameras needed for marker capturing and post-processing and thus improve the feasibility of the method. For practical application purposes and based on the present results, Table 5-1 provides the position of markers in MS2 to MS4 (averaged among three gait speeds and two gait phases), expressed as relative positions with respect to the individual AT length during upright standing. According to a given individual AT length, an appropriate marker-set for a simplified assessment protocol can be chosen from Table 5-1. The presented average positions for markers in Table 5-1 do not affect the individual variability of the participants because there was no significant difference between marker positions in the different gait speeds ($p = 0.674$) and gait phases ($p = 0.723$, tested using a repeated-measures ANOVA). In addition, the final associated overall error when applying the average markers positions of the reduced marker-sets 2 to 4 was 0.20 ± 0.05 mm on average similarly during walking, slow running and fast running.

Table 5-1 Location of foil markers in the percentage of Achilles tendon (AT) length during quite upright standing relative to the AT insertion marker on the calcaneus bone for each marker-set. The locations refer to the reduced marker-set (i.e., 50% of all markers according to the individual AT length, thus, 2 to 4 markers) across the three gait speeds (1.4, 2.5, and 3.5 m/s) and two phases (stance and swing).

	FM1(%)	FM2(%)	FM3(%)	FM4(%)
MS2	22	56		
MS3	15	35	65	
MS4	10	31	47	66

The AT length measurement error was significantly greater during the swing phase than the stance phase, indicated by the significant main effect, but the magnitude was rather small. Furthermore, this difference diminished at marker-sets with a greater foil marker number (<MS4). It is reasonable to assume that the greater error with fewer markers during swing arises from the high plantar flexion angles after toe-off, which affects the AT curvature. The gait speed showed no significant effect on the AT length measurement error, indicating a comparable curvature behavior between speeds and gait modes, suggesting that the same marker-set can be used for different gait speeds and modes.

5.7. Conclusions

In conclusion, we investigated the effect of foil marker reduction on the reconstructed AT curvature. Our results indicate that reducing the number of foil markers by 70% during walking and 50% during running would result in a marginal error and thus a negligible effect on the AT length and maximum strain measurement across gait phases and gait speeds. Therefore, a reduced marker-set can be recommended for future applications. The marker positions for each marker-set suggested here can be used to choose an appropriate marker-set for the individual AT length in a simplified assessment protocol.

5.8. Author Contributions

M.K., S.B., and A.A.; methodology; software, M.K.; validation, analysis, M.K., S.B., and C.T.; data curation, M.K., and S.B.; writing original draft preparation, M.K., F.M., A.A., and S.B.; writing—review and editing, visualization, M.K., and S.B.; supervision, A.A., and S.B.; project administration, A.A., and S.B.; funding acquisition, A.A. All authors have read and agreed to the published version of the manuscript.

5.9. Acknowledgments

We thank our colleague Arno Schroll for his help during the data analysis.

6. Main findings and conclusions

The main objectives of the present thesis were firstly to develop a new and robust method for quantifying the AT strain and force in vivo during locomotion, secondly to enhance our understanding of the facilitation mechanisms in high-speed human walking. Finally, it was tried to simplify the proposed method in the study 1 in terms of considering the length of the AT curve shape with reduced number of the foil reflective markers.

In the first study, it was showed that two methodological issues, namely the projection of the GM-MTJ to the skin and skin-to-bone displacement (i.e., the skin movement artifact on top of the calcaneus), significantly affect the measurement of AT length and strain. The new in vivo assessment of the AT mechanical loading and strain during locomotion revealed that the AT mechanical loading during submaximal running is lower than previously reported, which could explain why there are no detectable differences in AT stiffness between runners and non-runners. Lastly, the study presented the first evidence of an early elastic strain energy rebound of the AT while running (i.e., rearfoot runners), which might be functionally relevant for running economy.

In my second study, we utilized our established method to investigate how the soleus muscle, as a monoarticular muscle, and the gastrocnemii muscles, as biarticular muscles, contribute to compensatory mechanisms during fast human walking speed. We found that to increase walking speed, the triceps surae muscles have to produce more net mechanical work at the ankle joint. The contractile energy generation ability of the triceps surae muscles and the biarticular processes of the gastrocnemii muscles can affect the net mechanical effort at the ankle joint. Our study mainly focused on the contribution of monoarticular and biarticular muscle processes to the increased net triceps surae muscle work required from moderate to maximum walking speeds. Our results showed that the speed-related increased net mechanical work at the ankle joint was a result of contractile energy generation in the monoarticular soleus muscle and the biarticular mechanism of the gastrocnemii muscles. While the monoarticular soleus muscle contributed more contractile work, the biarticular mechanisms of the gastrocnemii muscles accounted for a significant portion of the increased net ankle joint mechanical work with speed. Despite a decrease in maximum AT force, an earlier onset of plantar flexion, with a quickly increased activation of the triceps surae muscles, improved the net triceps surae muscle mechanical work by 1.7-fold and 2.4-fold at the transition (2.0 m/s)

and maximum walking (2.6±.03 m/s) speeds, respectively, compared to normal walking speed (1.4 m/s).

Finally in third study, we examined the impact of reducing the number of foil markers, which are responsible for considering the AT curve-path, on the reconstructed AT curvature. Our results indicated that decreasing the number of foil markers by 70% during walking and 50% during running had a negligible effect on the accuracy of AT length and maximum strain measurements across various gait phases and speeds. Therefore, a smaller set of markers may be recommended for future use, and a simplified process can be followed to select an appropriate marker placement for each marker-set, based on the individual's AT length.

6.1. Limitations

The method used in the present thesis was conducted in two separate sessions, one in a seated position and another during locomotion. During the seated position, dynamometry, ultrasound, and motion capture cameras were used, and during locomotion, ultrasound and motion capture systems were used. The AT-force was calculated from the ankle joint moment, taking into account various factors such as inertia of the leg and dynamometer arm, axes misalignment, antagonistic muscle coactivation, and passive forces of connective tissues. However, the contribution of synergistic muscles to the plantar flexion moment, such as m. tibialis posterior and m. flexor halucis longus, was not considered in the methods used. Nonetheless, these muscles have smaller cross-sectional areas and lever arms than the triceps surae muscles, indicating that they contribute less to the produced moment. This effect is constant across all measurements and should not significantly impact the findings of the thesis.

The method used in the thesis to compute the Achilles tendon lever arm during the seated position was based on the ratio of the displacement of the gastrocnemius medialis-Achilles tendon junction to the equivalent angular excursion of the ankle joint. However, it should be noted that this approach assumes that the Achilles tendon is inflexible, which may not be entirely accurate as the tendon does exhibit some degree of flexibility. Nonetheless, this approach has been widely used in previous studies and is considered to an acceptable accuracy in estimating the Achilles tendon lever arm during walking and running (Fath et al., 2010). The tendon does indeed lengthen as dorsal flexion increases (De Monte et al., 2006), hence the lever arm values could be too low compared to the actual tendon lever arm values. However, De Monte et al. (De Monte et al., 2006) found that the amount of tendon elongation caused by the change in ankle angle was extremely little (between 85 and 100 °), and as a result, the effect

of non-rigidity should be minimal. Additionally, due to a tendon alignment, tendon lever arm values rise with increased muscle activity (Maganaris et al., 1998, 2000). In the current experiment, this shift in the lever arm values wasn't explicitly measured, but it was taken into account using proposed correction factors (Maganaris et al., 1998).

During the locomotion trials the AT lever arm was measured as the perpendicular distance between the AT curve middle line and the middle of the malleoli (i.e., detected by two reflective markers on the left and right side). This method was different in the calibration measure of the AT force during the seated position as discussed above (tendon excursion method). Using two different approaches to measure the AT lever arm might introduce some inaccuracy in AT loading values. The comparison of the two approaches to measure the AT lever arm have not yet been investigated, thus, the amount of error produced is unknown.

6.2. Future studies

All three studies provide valuable insights into the biomechanics of the Achilles tendon and triceps surae muscles during locomotion. However, there are still many unanswered questions that warrant future investigation. One possible avenue for future research is to investigate the effects of varying terrain on AT mechanical loading, strain energy and energy transfer from more proximal muscles to distal joints. Another potential area of study is the impact of footwear and orthotics on AT mechanics during walking and running. Additionally, further research is needed to explore the relationships between AT mechanics, muscle mechanics, joint mechanics, and how these relationships may change with aging, injury, or disease. Moreover, there is a need to investigate the effects of specific interventions, such as resistance training or stretching, on AT mechanics and their potential role in injury prevention and rehabilitation. Finally, advances in imaging techniques, such as magnetic resonance imaging (MRI) and ultrasound elastography with combination of artificial intelligence, may provide new opportunities for non-invasive and more precise quantification of AT mechanical properties during locomotion.

At present, it is commonly accepted that the aponeurosis, tendon, and three sub-tendons of the AT should be evaluated and analyzed separately due to their distinct mechanical properties and behavior. However, it is important to acknowledge that these structures are interconnected through a complex three-dimensional connective network, which has a significant impact on their behavior. Consequently, there is a need to investigate the AT at various hierarchical levels and in conjunction with adjacent connective and contractile tissues. In the future, it is possible

that researchers will attempt to estimate not only the total forces acting on the AT but also the distribution of forces and strain rates across the sub-tendons. The integration of advanced experimental methodologies and modeling techniques should enable future investigations to account for viscoelasticity, slack length, and inter-individual variability in the structure and material properties of the AT. These developments hold the potential to generate innovative hypotheses and facilitate the design of personalized training and rehabilitation strategies.

References

Ackermans, T. M. A., Epro, G., McCrum, C., Oberländer, K. D., Suhr, F., Drost, M. R., Meijer, K., & Karamanidis, K. (2016). Aging and the effects of a half marathon on Achilles tendon force–elongation relationship. *European Journal of Applied Physiology*, *116*, 2281-2292.

Ait-Haddou, R., Jinha, A., Herzog, W., & Binding, P. (2004). Analysis of the force-sharing problem using an optimization model. *Mathematical biosciences*, *191*(2), 111-122.

Albracht, K., & Arampatzis, A. (2013). Exercise-induced changes in triceps surae tendon stiffness and muscle strength affect running economy in humans. *European Journal of Applied Physiology*, *113*(6), 1605-1615.

Albracht, K., Arampatzis, A., & Baltzopoulos, V. (2008). Assessment of muscle volume and physiological cross-sectional area of the human triceps surae muscle in vivo. *Journal of Biomechanics*, *41*(10), 2211-2218.

Aleshinsky, S. Y. (1986). An energy 'sources' and 'fractions' approach to the mechanical energy expenditure problem—I. Basic concepts, description of the model, analysis of a one-link system movement. *Journal of Biomechanics*, *19*(4), 287-293.

Alexander, R., & Ker, R. (1990). The architecture of leg muscles. In *Multiple muscle systems* (pp. 568-577). Springer.

Alexander, R. M. (1984). Elastic energy stores in running vertebrates. *American Zoologist*, *24*(1), 85-94.

Alexander, R. M. (1988). *Elastic mechanisms in animal movement* (Vol. 404). Cambridge University Press Cambridge.

Alexander, R. M. (1991). Energy-saving mechanisms in walking and running. *Journal of Experimental Biology*, *160*(1), 55-69.

Alexander, R. M. (1995). Leg design and jumping technique for humans, other vertebrates and insects. *Philosophical Transactions of the Royal Society of London. Series B: Biological Sciences*, *347*(1321), 235-248.

Alexander, R. M., & Bennet-Clark, H. (1977). Storage of elastic strain energy in muscle and other tissues. *Nature*, *265*(5590), 114-117.

Alexander, R. M., & Vernon, A. (1975). The mechanics of hopping by kangaroos (Macropodidae). *Journal of Zoology*, *177*(2), 265-303. https://doi.org/https://doi.org/10.1111/j.1469-7998.1975.tb05983.x

Almonroeder, T., Willson, J. D., & Kernozek, T. W. (2013). The effect of foot strike pattern on Achilles tendon load during running. *Annals of Biomedical Engineering*, *41*(8), 1758-1766. (Annals of Biomedical Engineering)

Alvim, F., Cerqueira, L., Netto, A. D. A., Leite, G., & Muniz, A. (2015). Comparison of five kinematic-based identification methods of foot contact events during treadmill walking and running at different speeds. *Journal of applied biomechanics*, *31*(5), 383-388.

An, K., Takahashi, K., Harrigan, T., & Chao, E. (1984). Determination of muscle orientations and moment arms.

Andres, K., Von Düring, M., & Schmidt, R. (1985). Sensory innervation of the Achilles tendon by group III and IV afferent fibers. *Anatomy and embryology*, *172*(2), 145-156.

Andriacchi, T. P., Johnson, T. S., Hurwitz, D. E., & Natarajan, R. N. (2005). Musculoskeletal dynamics, locomotion, and clinical applications. *Basic orthopaedic biomechanics and mechano-biology*, *3*, 91-121.

Arampatzis, A., De Monte, G., & Karamanidis, K. (2008). Effect of joint rotation correction when measuring elongation of the gastrocnemius medialis tendon and aponeurosis. *Journal of Electromyography and Kinesiology*, *18*(3), 503-508.

Arampatzis, A., Karamanidis, K., & Albracht, K. (2007). Adaptational responses of the human Achilles tendon by modulation of the applied cyclic strain magnitude. *Journal of Experimental Biology*, *210*(15), 2743-2753.

Arampatzis, A., Karamanidis, K., Morey-Klapsing, G., De Monte, G., & Stafilidis, S. (2007). Mechanical properties of the triceps surae tendon and aponeurosis in relation to intensity of sport activity. *Journal of Biomechanics*, *40*(9), 1946-1952.

Arampatzis, A., Mademli, L., De Monte, G., & Walsh, M. (2007). Changes in fascicle length from rest to maximal voluntary contraction affect the assessment of voluntary activation. *Journal of Biomechanics*, *40*(14), 3193-3200.

Arampatzis, A., Mersmann, F., & Bohm, S. (2020). Individualized Muscle-Tendon Assessment and Training. *Frontiers in Physiology*, *11*.

Arampatzis, A., Morey-Klapsing, G., Karamanidis, K., DeMonte, G., Stafilidis, S., & Brüggemann, G.-P. (2005). Differences between measured and resultant joint moments during isometric contractions at the ankle joint. *Journal of Biomechanics*, *38*(4), 885-892.

Arampatzis, A., Peper, A., Bierbaum, S., & Albracht, K. (2010). Plasticity of human Achilles tendon mechanical and morphological properties in response to cyclic strain. *Journal of Biomechanics*, *43*(16), 3073-3079.

Arampatzis, A., Stafilidis, S., DeMonte, G., Karamanidis, K., Morey-Klapsing, G., & Brüggemann, G. (2005). Strain and elongation of the human gastrocnemius tendon and aponeurosis during maximal plantarflexion effort. *Journal of Biomechanics*, *38*(4), 833-841.

Arnoczky, S. P., Lavagnino, M., Whallon, J. H., & Hoonjan, A. (2002). In situ cell nucleus deformation in tendons under tensile load; a morphological analysis using confocal laser microscopy. *Journal of Orthopaedic Research*, *20*(1), 29-35.

Arnoczky, S. P., Tian, T., Lavagnino, M., Gardner, K., Schuler, P., & Morse, P. (2002). Activation of stress-activated protein kinases (SAPK) in tendon cells following cyclic strain: the effects of strain frequency, strain magnitude, and cytosolic calcium. *Journal of Orthopaedic Research*, *20*(5), 947-952.

Arnold, A. S., Salinas, S., Hakawa, D. J., & Delp, S. L. (2000). Accuracy of muscle moment arms estimated from MRI-based musculoskeletal models of the lower extremity. *Computer Aided Surgery*, *5*(2), 108-119.

Babič, J. (2012). Biarticular Actuation of Robotic Systems. In *Robotic Systems-Applications, Control and Programming*. IntechOpen.

Ballal, M., Walker, C., & Molloy, A. (2014). The anatomical footprint of the Achilles tendon: a cadaveric study. *The bone & joint journal*, *96*(10), 1344-1348.

Barber, L., Barrett, R., & Lichtwark, G. (2009). Validation of a freehand 3D ultrasound system for morphological measures of the medial gastrocnemius muscle. *Journal of Biomechanics*, *42*(9), 1313-1319. https://doi.org/https://doi.org/10.1016/j.jbiomech.2009.03.005

Barfod, K. W., Riecke, A. F., Boesen, A., Hansen, P., Maier, J. F., Døssing, S., & Troelsen, A. (2015). Validation of a novel ultrasound measurement of Achilles tendon length. *Knee Surgery, Sports Traumatology, Arthroscopy*, *23*(11), 3398-3406.

Baxter, J. R., Corrigan, P., Hullfish, T. J., O'Rourke, P., & Silbernagel, K. G. (2021). Exercise Progression to Incrementally Load the Achilles Tendon. *Medicine and Science in Sports and Exercise*, *53*(1), 124-130.

Benjamin, M., Kaiser, E., & Milz, S. (2008). Structure-function relationships in tendons: a review. *Journal of anatomy*, *212*(3), 211-228. https://doi.org/https://doi.org/10.1111/j.1469-7580.2008.00864.x

Bennet-Clark, H. (1975). The Energetics of the Jump of the Locust Shistocerca Gregaria. *J Exp. Biol.*, *63*, 52.

Bennet-Clark, H., & Lucey, E. (1967). The jump of the flea: a study of the energetics and a model of the mechanism. *Journal of Experimental Biology*, *47*(1), 59-76.

Bennett1, M., Ker1, R., Imery, N. J., & Alexander1, R. M. (1986). Mechanical properties of various mammalian tendons. *Journal of Zoology*, *209*(4), 537-548.

Biewener, A. A. (2016). Locomotion as an emergent property of muscle contractile dynamics. *Journal of Experimental Biology*, *219*(2), 285-294.

Biewener, A. A., Konieczynski, D. D., & Baudinette, R. V. (1998). In vivo muscle force-length behavior during steady-speed hopping in tammar wallabies. *Journal of Experimental Biology*, *201*(11), 1681-1694.

Biewener, A. A., & Roberts, T. J. (2000). Muscle and tendon contributions to force, work, and elastic energy savings: a comparative perspective. *Exercise and sport sciences reviews*, *28*(3), 99-107.

Binding, P., Jinha, A., & Herzog, W. (2000). Analytic analysis of the force sharing among synergistic muscles in one-and two-degree-of-freedom models. *Journal of Biomechanics*, *33*(11), 1423-1432.

Blitz, N. M., & Eliot, D. J. (2007). Anatomical aspects of the gastrocnemius aponeurosis and its insertion: a cadaveric study. *The Journal of foot and ankle surgery*, *46*(2), 101-108.

Bobbert, M., Mackay, M., Schinkelshoek, D., Huijing, P., & van Ingen Schenau, G. (1986). Biomechanical analysis of drop and countermovement jumps. *European journal of applied physiology and occupational physiology*, *54*(6), 566-573.

Bobbert, M. F., Huijing, P. A., & van Ingen Schenau, G. J. (1986). An estimation of power output and work done by the human triceps surae musle-tendon complex in jumping. *Journal of Biomechanics*, *19*(11), 899-906.

Bobbert, M. F., & van Ingen Schenau, G. J. (1988). Coordination in vertical jumping. *Journal of Biomechanics*, *21*(3), 249-262.

bohm, S. (2015). Human tendon adaptation in response to mechanical loading. *Thesis*.

Bohm, S., Mersmann, F., & Arampatzis, A. (2015). Human tendon adaptation in response to mechanical loading: a systematic review and meta-analysis of exercise intervention studies on healthy adults. *Sports medicine-open*, *1*(1), 7.

Bohm, S., Mersmann, F., Santuz, A., & Arampatzis, A. (2019). The force–length–velocity potential of the human soleus muscle is related to the energetic cost of running. *Proceedings of the Royal Society B*, *286*(1917), 20192560.

Bohm, S., Mersmann, F., Santuz, A., Schroll, A., & Arampatzis, A. (2021). Muscle-specific economy of force generation and efficiency of work production during human running.

Bohm, S., Mersmann, F., Tettke, M., Kraft, M., & Arampatzis, A. (2014). Human Achilles tendon plasticity in response to cyclic strain: effect of rate and duration. *Journal of Experimental Biology*, *217*(22), 4010-4017.

Bohs, L. N., & Trahey, G. E. (1991). A novel method for angle independent ultrasonic imaging of blood flow and tissue motion. *IEEE Transactions on Biomedical Engineering*, *38*(3), 280-286.

Bojsen-Møller, J., Schwartz, S., Kalliokoski, K. K., Finni, T., & Magnusson, S. P. (2010). Intermuscular force transmission between human plantarflexor muscles in vivo. *Journal of Applied Physiology*, *109*(6), 1608-1618.

Broker, J. P., & Gregor, R. J. (1994). Mechanical energy management in cycling: source relations and energy expenditure. *Medicine and Science in Sports and Exercise*, *26*(1), 64-74.

Brouwer, E. F., Myhrvold, S. B., Benth, J. Š., & Hoelsbrekken, S. E. (2018). Ultrasound measurements of Achilles tendon length using skin markings are more reliable than extended-field-of-view imaging. *Knee Surgery, Sports Traumatology, Arthroscopy*, *26*(7), 2088-2094.

Browning, R. C., Baker, E. A., Herron, J. A., & Kram, R. (2006). Effects of obesity and sex on the energetic cost and preferred speed of walking. *Journal of Applied Physiology*, *100*(2), 390-398.

Buchanan, T. S., & Shreeve, D. A. (1996). An evaluation of optimization techniques for the prediction of muscle activation patterns during isometric tasks. *Journal of biomechanical engineering*, *118*(4), 565-574.

Buford, W. L., Ivey, F. M., Malone, J. D., Patterson, R. M., Pearce, G., Nguyen, D. K., & Stewart, A. A. (1997). Muscle balance at the knee-moment arms for the normal knee and the ACL-minus knee. *IEEE Transactions on Rehabilitation Engineering*, *5*(4), 367-379.

Buschmann, J., Puippe, G., Bürgisser, G. M., Bonavoglia, E., Giovanoli, P., & Calcagni, M. (2014). Correspondence of high-frequency ultrasound and histomorphometry of healing rabbit Achilles tendon tissue. *Connective tissue research*, *55*(2), 123-131.

Buschmann, T., Ewald, A., von Twickel, A., & Bueschges, A. (2015). Controlling legs for locomotion—Insights from robotics and neurobiology. *Bioinspiration & biomimetics*, *10*(4), 041001.

Butler, D. L., Grood, E. S., Noyes, F. R., Zernicke, R. F., & Brackett, K. (1984). Effects of structure and strain measurement technique on the material properties of young human tendons and fascia. *Journal of Biomechanics*, *17*(8), 579-596.

Caldwell, G. E., & Forrester, L. W. (1992). Estimates of mechanical work and energy transfers: demonstration of a rigid body power model of the recovery leg in gait. *Medicine and Science in Sports and Exercise*, *24*(12), 1396-1412.

Calow, L. J., & Alexander, R. M. (1973). A mechanical analysis of a hind leg of a frog (Rana temporaria). *Journal of Zoology*, *171*(3), 293-321.

Canny, J. (1987). A computational approach to edge detection. In *Readings in computer vision* (pp. 184-203). Elsevier.

Carr, J. A., Ellerby, D. J., & Marsh, R. L. (2011). Function of a large biarticular hip and knee extensor during walking and running in guinea fowl (Numida meleagris). *Journal of Experimental Biology*, *214*(20), 3405-3413. https://doi.org/10.1242/jeb.060335

Carr, J. A., Ellerby, D. J., Rubenson, J., & Marsh, R. L. (2011). Mechanisms producing coordinated function across the breadth of a large biarticular thigh muscle. *Journal of Experimental Biology*, *214*(20), 3396-3404. https://doi.org/10.1242/jeb.060319

Carrier, D. R., Gregersen, C. S., & Silverton, N. A. (1998). Dynamic gearing in running dogs. *Journal of Experimental Biology*, *201*(23), 3185-3195.

Carroll, A. M., & Biewener, A. A. (2009). Mono-versus biarticular muscle function in relation to speed and gait changes: in vivo analysis of the goat triceps brachii. *Journal of Experimental Biology*, *212*(20), 3349-3360.

Cavagna, G., & Kaneko, M. (1977). Mechanical work and efficiency in level walking and running. *The Journal of physiology*, *268*(2), 467-481.

Chen, T. M., Rozen, W. M., Pan, W. r., Ashton, M. W., Richardson, M. D., & Taylor, G. I. (2009). The arterial anatomy of the Achilles tendon: anatomical study and clinical implications. *Clinical Anatomy: The Official Journal of the American Association of Clinical Anatomists and the British Association of Clinical Anatomists*, *22*(3), 377-385.

Chiel, H. J., & Beer, R. D. (1997). The brain has a body: adaptive behavior emerges from interactions of nervous system, body and environment. *Trends in Neurosciences*, *20*(12), 553-557. https://doi.org/https://doi.org/10.1016/S0166-2236(97)01149-1

Child, S., Bryant, A. L., Clark, R. A., & Crossley, K. M. (2010). Mechanical properties of the achilles tendon aponeurosis are altered in athletes with achilles tendinopathy. *The American journal of sports medicine*, *38*(9), 1885-1893.

Cleather, D. J., Southgate, D. F., & Bull, A. M. (2015). The role of the biarticular hamstrings and gastrocnemius muscles in closed chain lower limb extension. *Journal of theoretical biology*, *365*, 217-225.

Cleland, J. (1867). On the actions of muscles passing over more than one joint. *Journal of anatomy and physiology*, *1*(1), 85.

Cohen, J. C. (2009). Anatomy and biomechanical aspects of the gastrocsoleus complex. *Foot and ankle clinics*, *14*(4), 617-626.

Craig, J. J. (2005). *Introduction to robotics: mechanics and control* (Vol. 3). Pearson/Prentice Hall Upper Saddle River, NJ, USA:.

Cronin, N. J., & Lichtwark, G. (2013). The use of ultrasound to study muscle–tendon function in human posture and locomotion. *Gait & posture*, *37*(3), 305-312.

Cumins, E., Anson, B., Carr, B., Wright, R., & Hauser, E. (1946). The structure of the calcaneal (Achilles) tendon in relation to orthopaedic surgery. *Surg Gynaecol Obst*, *83*, 107.

David, L., Grood, E. S., Noyes, F. R., & Zernicke, R. E. (1978). Biomechanics of ligaments and tendons. *Exercise and sport sciences reviews*, *6*(1), 125-182.

Davy, D., & Audu, M. (1987). A dynamic optimization technique for predicting muscle forces in the swing phase of gait. *Journal of Biomechanics*, *20*(2), 187-201.

Dawson, T. J., & Taylor, C. R. (1973). Energetic cost of locomotion in kangaroos. *Nature*, *246*, 313-314.

de David, A. C., Carpes, F. P., & Stefanyshyn, D. (2015). Effects of changing speed on knee and ankle joint load during walking and running. *Journal of sports sciences*, *33*(4), 391-397.

De Monte, G., Arampatzis, A., Stogiannari, C., & Karamanidis, K. (2006). In vivo motion transmission in the inactive gastrocnemius medialis muscle–tendon unit during ankle and knee joint rotation. *Journal of Electromyography and Kinesiology*, *16*(5), 413-422.

Delp, S. L., & Loan, J. P. (2000). A computational framework for simulating and analyzing human and animal movement. *Computing in Science & Engineering*, *2*(5), 46-55.

Delp, S. L., Loan, J. P., Hoy, M. G., Zajac, F. E., Topp, E. L., & Rosen, J. M. (1990). An interactive graphics-based model of the lower extremity to study orthopaedic surgical procedures. *IEEE Transactions on Biomedical Engineering*, *37*(8), 757-767.

Devaprakash, D., Graham, D. F., Barrett, R. S., Lloyd, D. G., Obst, S. J., Kennedy, B., Adams, K. L., Kiely, R. J., Hunter, A., Vlahovich, N., Pease, D. L., Shim, V. B., Besier, T. F., Zheng, M., Cook, J. L., & Pizzolato, C. (2022). Free Achilles tendon strain during selected rehabilitation, locomotor, jumping, and landing tasks. *Journal of Applied Physiology*, *132*(4), 956-965. https://doi.org/10.1152/japplphysiol.00662.2021

Devaprakash, D., Lloyd, D. G., Barrett, R. S., Obst, S. J., Kennedy, B., Adams, K. L., Hunter, A., Vlahovich, N., Pease, D. L., & Pizzolato, C. (2019). Magnetic resonance imaging and freehand 3-D ultrasound provide similar estimates of free Achilles tendon shape and 3-D geometry. *Ultrasound in medicine & biology*, *45*(11), 2898-2905.

Dick, T. J., Arnold, A. S., & Wakeling, J. M. (2016). Quantifying Achilles tendon force in vivo from ultrasound images. *Journal of Biomechanics*, *49*(14), 3200-3207.

Dick, T. J., & Wakeling, J. M. (2017). Shifting gears: dynamic muscle shape changes and force-velocity behavior in the medial gastrocnemius. *Journal of Applied Physiology*, *123*(6), 1433-1442.

Dingwell, J., Cusumano, J. P., Cavanagh, P., & Sternad, D. (2001). Local dynamic stability versus kinematic variability of continuous overground and treadmill walking. *Journal of biomechanical engineering*, *123*(1), 27-32.

Doral, M. N., Alam, M., Bozkurt, M., Turhan, E., Atay, O. A., Dönmez, G., & Maffulli, N. (2010). Functional anatomy of the Achilles tendon. *Knee Surgery, Sports Traumatology, Arthroscopy*, *18*(5), 638-643.

Dowling, J. J., & Vamos, L. (1993). Identification of kinetic and temporal factors related to vertical jump performance. *Journal of applied biomechanics*, *9*(2), 95-110.

Edama, M., Kubo, M., Onishi, H., Takabayashi, T., Inai, T., Yokoyama, E., Hiroshi, W., Satoshi, N., & Kageyama, I. (2015). The twisted structure of the human A chilles tendon. *Scandinavian journal of medicine & science in sports*, *25*(5), e497-e503.

Elftman, H. (1939a). Forces and energy changes in the leg during walking. *American Journal of Physiology-Legacy Content*, *125*(2), 339-356.

Elftman, H. (1939b). The function of muscles in locomotion. *American Journal of Physiology-Legacy Content*, *125*(2), 357-366.

Erickson, B. J., Cvetanovich, G. L., Nwachukwu, B. U., Villarroel, L. D., Lin, J. L., Bach, B. R., & McCormick, F. M. (2014). Trends in the Management of Achilles Tendon Ruptures in the United States Medicare Population, 2005-2011. *Orthopaedic Journal of Sports Medicine*, *2*(9), 232596711454994. https://doi.org/10.1177/2325967114549948

Farris, D. J., & Sawicki, G. S. (2012). Human medial gastrocnemius force–velocity behavior shifts with locomotion speed and gait. *Proceedings of the National Academy of Sciences*, *109*(3), 977-982.

Farris, D. J., & Sawicki, G. S. (2012). The mechanics and energetics of human walking and running: a joint level perspective. *J R Soc Interface*, *9*(66), 110-118. https://doi.org/10.1098/rsif.2011.0182

Fath, F., Blazevich, A. J., Waugh, C. M., Miller, S. C., & Korff, T. (2010). Direct comparison of in vivo Achilles tendon moment arms obtained from ultrasound and MR scans. *Journal of Applied Physiology*, *109*(6), 1644-1652.

Fellin, R. E., Rose, W. C., Royer, T. D., & Davis, I. S. (2010). Comparison of methods for kinematic identification of footstrike and toe-off during overground and treadmill running. *Journal of Science and Medicine in Sport*, *13*(6), 646-650.

Fenn, W. O. (1924). The relation between the work performed and the energy liberated in muscular contraction. *The Journal of physiology*, *58*(6), 373.

Finni, T., Cronin, N., Mayfield, D., Lichtwark, G., & Cresswell, A. (2017). Effects of muscle activation on shear between human soleus and gastrocnemius muscles. *Scandinavian journal of medicine & science in sports*, *27*(1), 26-34.

Finni, T., Komi, P., & Lukkariniemi, J. (1998). Achilles tendon loading during walking: application of a novel optic fiber technique. *European journal of applied physiology and occupational physiology*, *77*(3), 289-291. (European journal of applied physiology and occupational physiology)

Finni, T., & Vanwanseele, B. (2023). Towards modern understanding of the Achilles tendon properties in human movement research. *Journal of Biomechanics*, *152*, 111583. https://doi.org/https://doi.org/10.1016/j.jbiomech.2023.111583

Franz, J. R., Slane, L. C., Rasske, K., & Thelen, D. G. (2015). Non-uniform in vivo deformations of the human Achilles tendon during walking. *Gait & posture*, *41*(1), 192-197.

Franz, J. R., & Thelen, D. G. (2015). Depth-dependent variations in Achilles tendon deformations with age are associated with reduced plantarflexor performance during walking. *Journal of Applied Physiology*, *119*(3), 242-249.

Fraysse, F., Dumas, R., Cheze, L., & Wang, X. (2009). Comparison of global and joint-to-joint methods for estimating the hip joint load and the muscle forces during walking. *Journal of Biomechanics*, *42*(14), 2357-2362.

FUGL-MEYER, A. R., MILD, K. H., & HÖRNSTEN, J. (1982). Output of skeletal muscle contractions A study of isokinetic plantar flexion in athletes. *Acta Physiologica Scandinavica*, *115*(2), 193-199.

Fukashiro, S., & Komi, P. (1987). Joint moment and mechanical power flow of the lower limb during vertical jump. *International Journal of Sports Medicine*, *8*(S 1), S15-S21.

Fukunaga, T., Kubo, K., Kawakami, Y., Fukashiro, S., Kanehisa, H., & Maganaris, C. N. (2001). In vivo behaviour of human muscle tendon during walking. *Proceedings of the Royal Society of London. Series B: Biological Sciences*, *268*(1464), 229-233.

Fukutani, A. (2014). New method for measuring the Achilles tendon length by ultrasonography. *Current Medical Imaging*, *10*(4), 259-265. (Current Medical Imaging)

Fukutani, A., Hashizume, S., Kusumoto, K., & Kurihara, T. (2014). Influence of neglecting the curved path of the Achilles tendon on Achilles tendon length change at various ranges of motion. *Physiological reports*, *2*(10), e12176.

Fung, Y.-c. (2013). *Biomechanics: mechanical properties of living tissues*. Springer Science & Business Media.

Gambaryan, P. P. (1974). How mammals run. *Anatomical Adaptations*.

Gee, A., Prager, R., Treece, G., Cash, C., & Berman, L. (2004). Processing and visualizing three-dimensional ultrasound data. *The British journal of radiology*, *77*(suppl_2), S186-S193.

Giddings, V. L., Beaupre, G. S., Whalen, R. T., & Carter, D. R. (2000). Calcaneal loading during walking and running. *Medicine & Science in Sports & Exercise*, *32*(3), 627-634.

Gregersen, C. S., & Carrier, D. R. (2004). Gear ratios at the limb joints of jumping dogs. *Journal of Biomechanics*, *37*(7), 1011-1018.

Gregoire, L., Veeger, H., Huijing, P., & van Ingen Schenau, G. (1984). Role of mono-and biarticular muscles in explosive movements. *International Journal of Sports Medicine*, *5*(06), 301-305.

Günther, M., Ishida, H., Kumakura, H., & Nakano, Y. (1991). The jump as a fast mode of locomotion in arboreal and terrestrial biotopes. *Zeitschrift für Morphologie und Anthropologie*, 341-372.

Günther, M. M. (1985). Biomechanische Voraussetzungen beim Absprung des Senegalgalagos. *Zeitschrift für Morphologie und Anthropologie*, 287-306.

Gushue, D. L., Houck, J., & Lerner, A. L. (2005). Rabbit knee joint biomechanics: motion analysis and modeling of forces during hopping. *Journal of Orthopaedic Research*, *23*(4), 735-742.

Hamard, R., Aeles, J., Kelp, N. Y., Feigean, R., Hug, F., & Dick, T. J. (2021). Does different activation between the medial and the lateral gastrocnemius during walking translate into different fascicle behavior? *Journal of Experimental Biology*, *224*(12), jeb242626.

Handsfield, G., Slane, L., & Screen, H. (2016). Nomenclature of the tendon hierarchy: An overview of inconsistent terminology and a proposed size-based naming scheme with terminology for multi-muscle tendons. *Journal of Biomechanics*, *49*(13), 3112-3124.

Handsfield, G. G., Inouye, J. M., Slane, L. C., Thelen, D. G., Miller, G. W., & Blemker, S. S. (2017). A 3D model of the Achilles tendon to determine the mechanisms underlying nonuniform tendon displacements. *Journal of Biomechanics*, *51*, 17-25.

Hansen, P., Aagaard, P., Kjaer, M., Larsson, B., & Magnusson, S. P. (2003). Effect of habitual running on human Achilles tendon load-deformation properties and cross-sectional area. *Journal of Applied Physiology*, *95*(6), 2375-2380.

Hardt, D. E. (1978). Determining muscle forces in the leg during normal human walking—an application and evaluation of optimization methods.

Harkness-Armstrong, C., Debelle, H. A., Maganaris, C. N., Walton, R., Wright, D. M., Bass, A., Baltzopoulos, V., & O'Brien, T. D. (2020). Effective Mechanical Advantage About the Ankle Joint and the Effect of Achilles Tendon Curvature During Toe-Walking. *Frontiers in Physiology*, *11*, 407.

Hatze, H. (1977). A complete set of control equations for the human musculo-skeletal system. *Journal of Biomechanics*, *10*(11-12), 799-805.

Hatze, H. (1980). Neuromusculoskeletal control systems modeling--A critical survey of recent developments. *IEEE Transactions on Automatic Control*, *25*(3), 375-385.

Hatze, H. (2000). The inverse dynamics problem of neuromuscular control. *Biological cybernetics*, *82*(2), 133-141.

Hatze, H., & Baca, A. (1993). Contact-free determination of human body segment parameters by means of videometric image processing of an anthropomorphic body model. Applications of digital image processing XV,

Haut, R. (1983). Age-dependent influence of strain rate on the tensile failure of rat-tail tendon.

Heinemeier, K., Langberg, H., Olesen, J. L., & Kjaer, M. (2003). Role of TGF-β1 in relation to exercise-induced type I collagen synthesis in human tendinous tissue. *Journal of Applied Physiology*, *95*(6), 2390-2397.

Herzog, W. (1996). Force-sharing among synergistic muscles: theoretical considerations and experimental approaches. *Exercise and sport sciences reviews*, *24*(1), 173-202.

Herzog, W. (2019). The problem with skeletal muscle series elasticity. *BMC Biomedical Engineering*, *1*(1), 1-14.

Herzog, W., & Leonard, T. (1991). Validation of optimization models that estimate the forces exerted by synergistic muscles. *Journal of Biomechanics*, *24*, 31-39.

Hess, G. P., Cappiello, W. L., Poole, R. M., & Hunter, S. C. (1989). Prevention and treatment of overuse tendon injuries. *Sports medicine*, *8*(6), 371-384.

HIRANO, M., & ROME, L. C. (1984). Jumping performance of frogs (Rana pipiens) as a function of muscle temperature. *Journal of Experimental Biology*, *108*(1), 429-439.

Hof, A. (2001). The force resulting from the action of mono-and biarticular muscles in a limb. *Journal of Biomechanics*, *34*(8), 1085-1089.

Hof, A. L., Van Zandwijk, J. P., & Bobbert, M. (2002). Mechanics of human triceps surae muscle in walking, running and jumping. *Acta Physiologica Scandinavica*, *174*(1), 17-30.

Hreljac, A. (1993). Preferred and energetically optimal gait transition speeds in human locomotion. *Medicine and Science in Sports and Exercise*, *25*(10), 1158-1162.

Hudson, P. E., Corr, S. A., Payne-Davis, R. C., Clancy, S. N., Lane, E., & Wilson, A. M. (2011). Functional anatomy of the cheetah (Acinonyx jubatus) hindlimb. *Journal of anatomy*, *218*(4), 363-374.

Hudson, P. E., Corr, S. A., & Wilson, A. M. (2012). High speed galloping in the cheetah (Acinonyx jubatus) and the racing greyhound (Canis familiaris): spatio-temporal and kinetic characteristics. *Journal of Experimental Biology*, *215*(14), 2425-2434.

Hug, F., Vecchio, A. D., Avrillon, S., Farina, D., & Tucker, K. (2021). Muscles from the same muscle group do not necessarily share common drive: evidence from the human triceps surae. *Journal of Applied Physiology*, *130*(2), 342-354. https://doi.org/10.1152/japplphysiol.00635.2020

Huijing, P. A. (2009). Epimuscular myofascial force transmission: a historical review and implications for new research. International Society of Biomechanics Muybridge Award Lecture, Taipei, 2007. *Journal of Biomechanics*, *42*(1), 9-21.

Huttunen, T. T., Kannus, P., Rolf, C., Felländer-Tsai, L., & Mattila, V. M. (2014). Acute Achilles tendon ruptures: incidence of injury and surgery in Sweden between 2001 and 2012. *The American journal of sports medicine*, *42*(10), 2419-2423.

Ishikawa, M., Komi, P. V., Grey, M. J., Lepola, V., & Bruggemann, G.-P. (2005). Muscle-tendon interaction and elastic energy usage in human walking. *Journal of Applied Physiology*, *99*(2), 603-608.

Ivanenko, Y. P., Cappellini, G., Dominici, N., Poppele, R. E., & Lacquaniti, F. (2007). Modular control of limb movements during human locomotion. *Journal of Neuroscience*, *27*(41), 11149-11161.

Jacobs, R., Bobbert, M. F., & van Ingen Schenau, G. J. (1996). Mechanical output from individual muscles during explosive leg extensions: the role of biarticular muscles. *Journal of Biomechanics*, *29*(4), 513-523.

Jacqmin-Gadda, H., Sibillot, S., Proust, C., Molina, J.-M., & Thiébaut, R. (2007). Robustness of the linear mixed model to misspecified error distribution. *Computational Statistics & Data Analysis*, *51*(10), 5142-5154.

Jinha, A., Ait-Haddou, R., Binding, P., & Herzog, W. (2006). Antagonistic activity of one-joint muscles in three-dimensions using non-linear optimisation. *Mathematical biosciences*, *202*(1), 57-70.

Johnson, R. T., Hafer, J. F., Wedge, R. D., & Boyer, K. A. (2020). Comparison of measurement protocols to estimate preferred walking speed between sites. *Gait & posture*, *77*, 171-174.

Jozsa, L., & Kannus, P. (1997). Histopathological findings in spontaneous tendon ruptures. *Scandinavian journal of medicine & science in sports*, *7*(2), 113-118.

Junius, K., Moltedo, M., Cherelle, P., Rodriguez-Guerrero, C., Vanderborght, B., & Lefeber, D. (2017). Biarticular elements as a contributor to energy efficiency: biomechanical review and application in bio-inspired robotics. *Bioinspiration & biomimetics*, *12*(6), 061001.

Kannus, P. (2000). Structure of the tendon connective tissue. *Scandinavian journal of medicine & science in sports*, *10*(6), 312-320. https://doi.org/https://doi.org/10.1034/j.1600-0838.2000.010006312.x

Kar, D., Issac, K. K., & Jayarajan, K. (2003). Gaits and energetics in terrestrial legged locomotion. *Mechanism and machine theory*, *38*(4), 355-366.

Karamanidis, K., & Arampatzis, A. (2005). Mechanical and morphological properties of different muscle–tendon units in the lower extremity and running mechanics: effect of aging and physical activity. *Journal of Experimental Biology*, *208*(20), 3907-3923.

Karamanidis, K., & Epro, G. (2020). Monitoring muscle-tendon adaptation over several years of athletic training and competition in elite track and field jumpers. *Frontiers in Physiology*, *11*.

Kaufman, K. (1999). Future directions in gait analysis. *Gait analysis in the science of rehabilitation*.

Kautz, S., Hull, M., & Neptune, R. (1994). A comparison of muscular mechanical energy expenditure and internal work in cycling. *Journal of Biomechanics*, *27*(12), 1459-1467.

Kautz, S. A., Neptune, R. R., & Zajac, F. E. (2000). General coordination principles elucidated by forward dynamics: minimum fatigue does not explain muscle excitation in dynamic tasks. *Motor control*, *4*(1), 75-80.

Kelly, L. A., Lichtwark, G., & Cresswell, A. G. (2015). Active regulation of longitudinal arch compression and recoil during walking and running. *Journal of The Royal Society Interface*, *12*(102), 20141076.

Ker, R., Bennett, M., Bibby, S., Kester, R., & Alexander, R. (1987a). The spring in the arch of the human foot. *Nature*, *325*(6100), 147-149.

Ker, R., Bennett, M., Bibby, S., Kester, R., & Alexander, R. M. (1987b). The spring in the arch of the human foot. *Nature*, *325*(6100), 147-149.

Ker, R. F. (1981). Dynamic tensile properties of the plantaris tendon of sheep (Ovis aries). *Journal of Experimental Biology*, *93*(1), 283-302.

Kharazi, M., Bohm, S., Theodorakis, C., Mersmann, F., & Arampatzis, A. (2021). Quantifying mechanical loading and elastic strain energy of the human Achilles tendon during walking and running. *Scientific reports*, *11*(1), 5830. https://doi.org/10.1038/s41598-021-84847-w

Kinugasa, R., Oda, T., Komatsu, T., Edgerton, V. R., & Sinha, S. (2013). Interaponeurosis shear strain modulates behavior of myotendinous junction of the human triceps surae. *Physiological reports*, *1*(6), e00147.

Kinugasa, R., Taniguchi, K., Yamamura, N., Fujimiya, M., Katayose, M., Takagi, S., Edgerton, V. R., & Sinha, S. (2018). A multi-modality approach towards elucidation of the mechanism for human achilles tendon bending during passive ankle rotation. *Scientific reports*, *8*(1), 1-13.

Komi, P. V. (1990). Relevance of in vivo force measurements to human biomechanics. *Journal of Biomechanics*, *23*, 23-34.

Komi, P. V., Fukashiro, S., & Järvinen, M. (1992). Biomechanical loading of Achilles tendon during normal locomotion. *Clinics in sports medicine*, *11*(3), 521-531.

Kongsgaard, M., Nielsen, C., Hegnsvad, S., Aagaard, P., & Magnusson, S. (2011). Mechanical properties of the human Achilles tendon, in vivo. *Clinical biomechanics*, *26*(7), 772-777.

Kubo, K., Kanehisa, H., & Fukunaga, T. (2003). Gender differences in the viscoelastic properties of tendon structures. *European Journal of Applied Physiology*, *88*(6), 520-526.

Kubo, K., Tabata, T., Ikebukuro, T., Igarashi, K., Yata, H., & Tsunoda, N. (2010). Effects of mechanical properties of muscle and tendon on performance in long distance runners. *European Journal of Applied Physiology*, *110*(3), 507-514.

Kümmel, J., Cronin, N. J., Kramer, A., Avela, J., & Gruber, M. (2018). Conditioning hops increase triceps surae muscle force and Achilles tendon strain energy in the stretch-shortening cycle. *Scandinavian journal of medicine & science in sports*, *28*(1), 126-137.

Kuo, A. D. (1998). A least-squares estimation approach to improving the precision of inverse dynamics computations. *Journal of biomechanical engineering*, *120*(1), 148-159.

Kurokawa, S., Fukunaga, T., & Fukashiro, S. (2001). Behavior of fascicles and tendinous structures of human gastrocnemius during vertical jumping. *Journal of Applied Physiology*.

Kvist, M. (1994). Achilles tendon injuries in athletes. *Sports medicine*, *18*(3), 173-201.

Lai, A., Lichtwark, G. A., Schache, A. G., Lin, Y.-C., Brown, N. A., & Pandy, M. G. (2015). In vivo behavior of the human soleus muscle with increasing walking and running speeds. *Journal of Applied Physiology*, *118*(10), 1266-1275.

Lai, A., Schache, A. G., Lin, Y.-C., & Pandy, M. G. (2014). Tendon elastic strain energy in the human ankle plantar-flexors and its role with increased running speed. *Journal of Experimental Biology*, *217*(17), 3159-3168. (Journal of Experimental Biology)

Lai, A. K., Lichtwark, G. A., Schache, A. G., & Pandy, M. G. (2018). Differences in in vivo muscle fascicle and tendinous tissue behavior between the ankle plantarflexors during running. *Scandinavian journal of medicine & science in sports*, *28*(7), 1828-1836.

Lavagnino, M., Arnoczky, S. P., Kepich, E., Caballero, O., & Haut, R. C. (2008). A finite element model predicts the mechanotransduction response of tendon cells to cyclic tensile loading. *Biomechanics and modeling in mechanobiology*, *7*(5), 405-416.

Lavagnino, M., Arnoczky, S. P., Tian, T., & Vaupel, Z. (2003). Effect of amplitude and frequency of cyclic tensile strain on the inhibition of MMP-1 mRNA expression in tendon cells: an in vitro study. *Connective tissue research*, *44*(3-4), 181-187.

Lee, J., Hwangbo, J., Wellhausen, L., Koltun, V., & Hutter, M. (2020). Learning quadrupedal locomotion over challenging terrain. *Science Robotics*, *5*(47), eabc5986.

Lee, K. K., Ling, S. K., & Yung, P. S. (2019). Controlled trial to compare the Achilles tendon load during running in flatfeet participants using a customized arch support orthoses vs an orthotic heel lift. *BMC musculoskeletal disorders*, *20*(1), 1-12.

Li, Y.-Y., Mao, K., Zhao, C., Zhang, R.-F., Zhao, X.-Y., Zhang, H.-L., Shu, H.-R., & Hao, Y.-J. (2013). Molecular cloning of cryptochrome 1 from apple and its functional characterization in Arabidopsis. *Plant Physiology and Biochemistry*, *67*, 169-177. https://doi.org/https://doi.org/10.1016/j.plaphy.2013.02.031

Lian, Ø., Dahl, J., Ackermann, P. W., Frihagen, F., Engebretsen, L., & Bahr, R. (2006). Pronociceptive and antinociceptive neuromediators in patellar tendinopathy. *The American journal of sports medicine*, *34*(11), 1801-1808.

Lichtwark, G., Bougoulias, K., & Wilson, A. (2007). Muscle fascicle and series elastic element length changes along the length of the human gastrocnemius during walking and running. *Journal of Biomechanics*, *40*(1), 157-164.

Lichtwark, G., & Wilson, A. (2005). In vivo mechanical properties of the human Achilles tendon during one-legged hopping. *Journal of Experimental Biology*, *208*(24), 4715-4725.

Lichtwark, G., & Wilson, A. (2006). Interactions between the human gastrocnemius muscle and the Achilles tendon during incline, level and decline locomotion. *Journal of Experimental Biology*, *209*(21), 4379-4388.

Lichtwark, G., & Wilson, A. (2008). Optimal muscle fascicle length and tendon stiffness for maximising gastrocnemius efficiency during human walking and running. *Journal of theoretical biology*, *252*(4), 662-673.

Lombard, W. P. (1903). The action of two-joint muscles. *American Physical Education Review*, *8*(3), 141-145.

Lombard, W. P., & Abbott, F. (1907). The mechanical effects produced by the contraction of individual muscles of the thigh of the frog. *American Journal of Physiology-Legacy Content*, *20*(1), 1-60.

Lutz, G. J., & Rome, L. C. (1994). Built for jumping: the design of the frog muscular system. *Science*, *263*(5145), 370-372.

Maas, H., & Finni, T. (2018). Mechanical coupling between muscle-tendon units reduces peak stresses. *Exercise and sport sciences reviews*, *46*(1), 26-33.

Mademli, L., & Arampatzis, A. (2014). Lower safety factor for old adults during walking at preferred velocity. *Age*, *36*(3), 1359-1365.

Mademli, L., Arampatzis, A., Morey-Klapsing, G., & Brüggemann, G.-P. (2004). Effect of ankle joint position and electrode placement on the estimation of the antagonistic moment during maximal plantarflexion. *Journal of Electromyography and Kinesiology*, *14*(5), 591-597. (Journal of Electromyography and Kinesiology)

Maffulli, N. (1999). Current concepts review-rupture of the Achilles tendon. *JBJS*, *81*(7), 1019-1036.

Maganaris, C. N., Baltzopoulos, V., & Sargeant, A. J. (1998). Changes in Achilles tendon moment arm from rest to maximum isometric plantarflexion: in vivo observations in man. *The Journal of physiology*, *510*(3), 977-985.

Maganaris, C. N., Baltzopoulos, V., & Sargeant, A. J. (2000). In vivo measurement-based estimations of the human Achilles tendon moment arm. *European Journal of Applied Physiology*, *83*(4-5), 363-369.

Maganaris, C. N., Narici, M. V., & Maffulli, N. (2008). Biomechanics of the Achilles tendon. *Disabil Rehabil*, *30*(20-22), 1542-1547.

Magnusson, S. P., Hansen, P., Aagaard, P., Brønd, J., Dyhre-Poulsen, P., Bojsen-Moller, J., & Kjaer, M. (2003). Differential strain patterns of the human gastrocnemius aponeurosis and free tendon, in vivo. *Acta Physiologica Scandinavica*, *177*(2), 185-195. https://doi.org/https://doi.org/10.1046/j.1365-201X.2003.01048.x

Magnusson, S. P., Langberg, H., & Kjaer, M. (2010). The pathogenesis of tendinopathy: balancing the response to loading. *Nature Reviews Rheumatology*, *6*(5), 262-268.

Maharaj, J. N., Cresswell, A. G., & Lichtwark, G. A. (2019). Tibialis anterior tendinous tissue plays a key role in energy absorption during human walking. *Journal of Experimental Biology*, *222*(11).

Margaria, R., Cerretelli, P., Aghemo, P., & Sassi, G. (1963). Energy cost of running. *Journal of Applied Physiology*, *18*(2), 367-370.

Martin, P. E., Rothstein, D. E., & Larish, D. D. (1992). Effects of age and physical activity status on the speed-aerobic demand relationship of walking. *Journal of Applied Physiology*, *73*(1), 200-206. (Journal of applied physiology)

Matijevich, E. S., Branscombe, L. M., & Zelik, K. E. (2018). Ultrasound estimates of Achilles tendon exhibit unexpected shortening during ankle plantarflexion. *Journal of Biomechanics*, *72*, 200-206.

McDonald, K. A., Cusumano, J. P., Hieronymi, A., & Rubenson, J. (2022). Humans trade off whole-body energy cost to avoid overburdening muscles while walking. *Proceedings of the Royal Society B*, *289*(1985), 20221189.

McGowan, C. P., Baudinette, R. V., & Biewener, A. A. (2005). Joint work and power associated with acceleration and deceleration in tammar wallabies (Macropus eugenii). *Journal of Experimental Biology*, *208*(1), 41-53.

Mersmann, F., Bohm, S., & Arampatzis, A. (2017). Imbalances in the development of muscle and tendon as risk factor for tendinopathies in youth athletes: a review of current evidence and concepts of prevention. *Frontiers in Physiology*, *8*, 987.

Mersmann, F., Bohm, S., Schroll, A., & Arampatzis, A. (2014). Validation of a simplified method for muscle volume assessment. *Journal of Biomechanics*, *47*(6), 1348-1352.

Mersmann, F., Bohm, S., Schroll, A., Boeth, H., Duda, G., & Arampatzis, A. (2015). Muscle shape consistency and muscle volume prediction of thigh muscles. *Scandinavian journal of medicine & science in sports*, *25*(2), e208-e213.

Mersmann, F., Bohm, S., Schroll, A., Boeth, H., Duda, G., & Arampatzis, A. (2017). Muscle and tendon adaptation in adolescent athletes: a longitudinal study. *Scandinavian journal of medicine & science in sports*, *27*(1), 75-82.

Mian, O. S., Thom, J. M., Ardigò, L. P., Minetti, A. E., & Narici, M. V. (2007). Gastrocnemius muscle–tendon behaviour during walking in young and older adults. *Acta physiologica*, *189*(1), 57-65.

Minetti, A., & Alexander, R. M. (1997). A theory of metabolic costs for bipedal gaits. *Journal of theoretical biology*, *186*(4), 467-476.

Minetti, A., Ardigo, L., & Saibene, F. (1994). The transition between walking and running in humans: metabolic and mechanical aspects at different gradients. *Acta Physiologica Scandinavica*, *150*(3), 315-323.

Mo, X., Ge, W., Miraglia, M., Inglese, F., Zhao, D., Stefanini, C., & Romano, D. (2020). Jumping locomotion strategies: from animals to bioinspired robots. *Applied Sciences*, *10*(23), 8607.

Monte, A., Baltzopoulos, V., Maganaris, C. N., & Zamparo, P. (2020). Gastrocnemius Medialis and Vastus Lateralis in vivo muscle-tendon behavior during running at increasing speeds. *Scandinavian journal of medicine & science in sports*.

Monte, A., Tecchio, P., Nardello, F., Bachero-Mena, B., Ardigò, L. P., & Zamparo, P. (2023). The interplay between gastrocnemius medialis force–length and force–velocity potentials, cumulative EMG activity and energy cost at speeds above and below the walk to run transition speed. *Experimental physiology*, *108*(1), 90-102.

Moritz, C. T., & Farley, C. T. (2005). Human hopping on very soft elastic surfaces: implications for muscle pre-stretch and elastic energy storage in locomotion. *Journal of Experimental Biology*, *208*(5), 939-949.

Morrison, S. M., Dick, T. J., & Wakeling, J. M. (2015). Structural and mechanical properties of the human Achilles tendon: Sex and strength effects. *Journal of Biomechanics*, *48*(12), 3530-3533.

Müller, S. A., Evans, C. H., Heisterbach, P. E., & Majewski, M. (2018). The role of the paratenon in Achilles tendon healing: a study in rats. *The American journal of sports medicine*, *46*(5), 1214-1219.

Muramatsu, T., Muraoka, T., Takeshita, D., Kawakami, Y., Hirano, Y., & Fukunaga, T. (2001). Mechanical properties of tendon and aponeurosis of human gastrocnemius muscle in vivo. *Journal of Applied Physiology*, *90*(5), 1671-1678.

Murray, W., Buchanan, T., & Delp, S. (1926). Scaling of peak moment arms of elbow muscles with dimensions of the upper extremity. *J. Biomech*, *35*, 2002.

Németh, G., & Ohlsén, H. (1985). In vivo moment arm lengths for hip extensor muscles at different angles of hip flexion. *Journal of Biomechanics*, *18*(2), 129-140.

Neptune, R., & Hull, M. (1998). Evaluation of performance criteria for simulation of submaximal steady-state cycling using a forward dynamic model.

Neptune, R., & Van Den Bogert, A. (1997). Standard mechanical energy analyses do not correlate with muscle work in cycling. *Journal of Biomechanics*, *31*(3), 239-245.

Neptune, R. R., & Kautz, S. (2001). Muscle activation and deactivation dynamics: the governing properties in fast cyclical human movement performance? *Exercise and sport sciences reviews*, *29*(2), 76-81.

Neptune, R. R., & Sasaki, K. (2005). Ankle plantar flexor force production is an important determinant of the preferred walk-to-run transition speed. *Journal of Experimental Biology*, *208*(5), 799-808.

Neptune, R. R., Sasaki, K., & Kautz, S. A. (2008). The effect of walking speed on muscle function and mechanical energetics. *Gait & posture*, *28*(1), 135-143.

Nikolaidou, M. E., Marzilger, R., Bohm, S., Mersmann, F., & Arampatzis, A. (2017). Operating length and velocity of human M. vastus lateralis fascicles during vertical jumping. *Royal Society Open Science*, *4*(5), 170185.

Nilsson, J., & Thorstensson, A. (1987). Adaptability in frequency and amplitude of leg movements during human locomotion at different speeds. *Acta Physiologica Scandinavica*, *129*(1), 107-114.

Nishikawa, K., Biewener, A. A., Aerts, P., Ahn, A. N., Chiel, H. J., Daley, M. A., Daniel, T. L., Full, R. J., Hale, M. E., Hedrick, T. L., Lappin, A. K., Nichols, T. R., Quinn, R. D., Satterlie, R. A., & Szymik, B. (2007). Neuromechanics: an integrative approach for understanding motor control. *Integrative and comparative biology*, *47*(1), 16-54. https://doi.org/10.1093/icb/icm024

Nobel, B., Metz, K., Pandolf, K., Bell, C., Cafarelli, E., & WE, S. (1973). Perceived exertion during walking and running-II: Med. sci. *Sports*, *5*, 116-120.

Novacheck, T. F. (1998). The biomechanics of running. *Gait & posture*, *7*(1), 77-95.

O'Brien, M. (2005). The anatomy of the Achilles tendon. *Foot and ankle clinics*, *10*(2), 225-238.

O'Donnell, M., Skovoroda, A. R., Shapo, B. M., & Emelianov, S. Y. (1994). Internal displacement and strain imaging using ultrasonic speckle tracking. *IEEE transactions on ultrasonics, ferroelectrics, and frequency control*, *41*(3), 314-325.

Obst, S., Newsham-West, R., & Barrett, R. (2016). Changes in A chilles tendon mechanical properties following eccentric heel drop exercise are specific to the free tendon. *Scandinavian journal of medicine & science in sports*, *26*(4), 421-431.

Obst, S. J., Heales, L. J., Schrader, B. L., Davis, S. A., Dodd, K. A., Holzberger, C. J., Beavis, L. B., & Barrett, R. S. (2018). Are the mechanical or material properties of the achilles and patellar tendons altered in tendinopathy? A systematic review with meta-analysis. *Sports medicine*, *48*(9), 2179-2198.

Ophir, J., Cespedes, I., Ponnekanti, H., Yazdi, Y., & Li, X. (1991). Elastography: a quantitative method for imaging the elasticity of biological tissues. *Ultrasonic imaging*, *13*(2), 111-134.

Pal, S., Langenderfer, J. E., Stowe, J. Q., Laz, P. J., Petrella, A. J., & Rullkoetter, P. J. (2007). Probabilistic modeling of knee muscle moment arms: effects of methods, origin–insertion, and kinematic variability. *Annals of Biomedical Engineering*, *35*, 1632-1642.

Pandy, M., & Zajac, F. (1989). Dependence of jumping performance on muscle strength, muscle-fiber speed, and tendon compliance. Issues in the modeling and control of biomechanical systems, 1989 ASME winter annual meeting in San Francisco (ed. JL Stein, JA Ashton-Miller & MG Pandy). New York, NY: The American Society of Mechanical Engineers,

Pandy, M. G., & Zajac, F. E. (1991). Optimal muscular coordination strategies for jumping. *Journal of Biomechanics*, *24*(1), 1-10.

Pandy, M. G., Zajac, F. E., Sim, E., & Levine, W. S. (1990). An optimal control model for maximum-height human jumping. *Journal of Biomechanics*, *23*(12), 1185-1198.

Pedotti, A., Krishnan, V., & Stark, L. (1978). Optimization of muscle-force sequencing in human locomotion. *Mathematical biosciences*, *38*(1-2), 57-76.

Perry, J., & Davids, J. R. (1992). Gait analysis: normal and pathological function. *Journal of pediatric orthopaedics*, *12*(6), 815.

Pizzolato, C., Lloyd, D. G., Zheng, M. H., Besier, T. F., Shim, V. B., Obst, S. J., Newsham-West, R., Saxby, D. J., & Barrett, R. S. (2019). Finding the sweet spot via personalised Achilles tendon training: the future is within reach. In: BMJ Publishing Group Ltd and British Association of Sport and Exercise Medicine.

Pizzolato, C., Shim, V. B., Lloyd, D. G., Devaprakash, D., Obst, S. J., Newsham-West, R., Graham, D. F., Besier, T. F., Zheng, M. H., & Barrett, R. S. (2020). Targeted Achilles tendon training and rehabilitation using personalized and real-time multiscale models of the neuromusculoskeletal system. *Frontiers in Bioengineering and Biotechnology*, *8*, 878. (Frontiers in Bioengineering and Biotechnology)

Pollock, C. M., & Shadwick, R. E. (1994). Relationship between body mass and biomechanical properties of limb tendons in adult mammals. *American Journal of Physiology-Regulatory, Integrative and Comparative Physiology*, *266*(3), R1016-R1021.

Pons, J. L. (2008). *Wearable robots: biomechatronic exoskeletons*. John Wiley & Sons.

Prager, R. W., Rohling, R. N., Gee, A., & Berman, L. (1998). Rapid calibration for 3-D freehand ultrasound. *Ultrasound in medicine and biology*, *24*(6), 855-869.

Prilutsky, B. I., & Gregor, R. J. (2001). Swing-and support-related muscle actions differentially trigger human walk–run and run–walk transitions. *Journal of Experimental Biology*, *204*(13), 2277-2287.

Prilutsky, B. I., Herzog, W., & Leonard, T. (1996). Transfer of mechanical energy between ankle and knee joints by gastrocnemius and plantaris muscles during cat locomotion. *Journal of Biomechanics*, *29*(4), 391-403.

Prilutsky, B. I., & Zatsiorsky, V. M. (1994). Tendon action of two-joint muscles: transfer of mechanical energy between joints during jumping, landing, and running. *Journal of Biomechanics*, *27*(1), 25-34.

Prilutsky, B. I. (2000). Coordination of two-and one-joint muscles: functional consequences and implications for motor control. *Motor control*, *4*(1), 1-44.

Raasch, C. C., Zajac, F. E., Ma, B., & Levine, W. S. (1997). Muscle coordination of maximum-speed pedaling. *Journal of Biomechanics*, *30*(6), 595-602.

Rajagopal, A., Dembia, C. L., DeMers, M. S., Delp, D. D., Hicks, J. L., & Delp, S. L. (2016). Full-body musculoskeletal model for muscle-driven simulation of human gait. *IEEE Transactions on Biomedical Engineering*, *63*(10), 2068-2079.

Ralston, H. J. (1958). Energy-speed relation and optimal speed during level walking. *Internationale Zeitschrift für Angewandte Physiologie Einschliesslich Arbeitsphysiologie*, *17*(4), 277-283.

Rasske, K., & Franz, J. R. (2018). Aging Effects on the Achilles Tendon Moment Arm during Walking. *Journal of Biomechanics*.

Rasske, K., Thelen, D. G., & Franz, J. R. (2017). Variation in the human Achilles tendon moment arm during walking. *Computer methods in biomechanics and biomedical engineering*, *20*(2), 201-205.

Riley, G. (2005). Chronic tendon pathology: molecular basis and therapeutic implications. *Expert reviews in molecular medicine*, *7*(5), 1-25.

Roberts, T. J., & Azizi, E. (2011). Flexible mechanisms: the diverse roles of biological springs in vertebrate movement. *Journal of Experimental Biology*, *214*(3), 353-361.

Roberts, T. J., Marsh, R. L., Weyand, P. G., & Taylor, C. R. (1997). Muscular force in running turkeys: the economy of minimizing work. *Science*, *275*(5303), 1113-1115.

Rosario, M. V., & Roberts, T. J. (2020). Loading rate has little influence on tendon fascicle mechanics. *Frontiers in Physiology*, *11*, 255.

Rosendo, A., & Iida, F. (2016). Energy efficient hopping with Hill-type muscle properties on segmented legs. *Bioinspiration & biomimetics*, *11*(3), 036002.

Rubenson, J., Pires, N. J., Loi, H. O., Pinniger, G. J., & Shannon, D. G. (2012). On the ascent: the soleus operating length is conserved to the ascending limb of the force–length curve across gait mechanics in humans. *Journal of Experimental Biology*, *215*(20), 3539-3551. https://doi.org/10.1242/jeb.070466

Rugg, S., Gregor, R., Mandelbaum, B., & Chiu, L. (1990). In vivo moment arm calculations at the ankle using magnetic resonance imaging (MRI). *Journal of Biomechanics*, *23*(5), 495-501.

Samson, M. M., Crowe, A., De Vreede, P. L., Dessens, J. A. G., Duursma, S. A., & Verhaar, H. J. J. (2001). Differences in gait parameters at a preferred walking speed in healthy subjects due to age, height and body weight. *Aging Clinical and Experimental Research*, *13*(1), 16-21. https://doi.org/10.1007/bf03351489

Santander, R. G., Arriba, M. P., Cuadrado, G. M., Alonso, A. L., Martinez, M. G.-S., Alonso, F. M., Monteagudo, M., & Lobo, M. T. (1999). Intracellular biogenesis of collagen fibrils in 'activated fibroblasts' of tendo Achillis: AN ULTRASTRUCTURAL STUDY IN THE NEW ZEALAND RABBIT. *The Journal of Bone and Joint Surgery. British volume*, *81*(3), 522-530.

Sarfaty, O., & Ladin, Z. (1993). A video-based system for the estimation of the inertial properties of body segments. *Journal of Biomechanics*, *26*(8), 1011-1016.

Sasaki, K., & Neptune, R. R. (2006). Muscle mechanical work and elastic energy utilization during walking and running near the preferred gait transition speed. *Gait & posture*, *23*(3), 383-390.

Schatzmann, L., Brunner, P., & Stäubli, H. (1998). Effect of cyclic preconditioning on the tensile properties of human quadriceps tendons and patellar ligaments. *Knee Surgery, Sports Traumatology, Arthroscopy*, *6*(1), S56-S61.

Schechtman, H., & Bader, D. L. (1997). In vitro fatigue of human tendons. *Journal of Biomechanics*, *30*(8), 829-835. https://doi.org/https://doi.org/10.1016/S0021-9290(97)00033-X

Scholz, M. N., D'Août, K., Bobbert, M. F., & Aerts, P. (2006). Vertical jumping performance of bonobo (Pan paniscus) suggests superior muscle properties. *Proceedings of the Royal Society B: Biological Sciences*, *273*(1598), 2177-2184.

Schubert, T. E., Weidler, C., Lerch, K., Hofstaedter, F., & Straub, R. (2005). Achilles tendinosis is associated with sprouting of substance P positive nerve fibres. *Annals of the rheumatic diseases*, *64*(7), 1083-1086.

Schulze, F., Mersmann, F., Bohm, S., & Arampatzis, A. (2012). A wide number of trials is required to achieve acceptable reliability for measurement patellar tendon elongation in vivo. *Gait & posture*, *35*(2), 334-338.

Schumacher, C., Sharbafi, M., Seyfarth, A., & Rode, C. (2020). Biarticular muscles in light of template models, experiments and robotics: a review. *J R Soc Interface*, *17*(163), 20180413. https://doi.org/10.1098/rsif.2018.0413

Schumacher, G. v., & Wolff, E. (1966). Trockengewicht und physiologischer querschnitt der menschlichen skelettmuskulatur. II. Physiologische querschnitte. *Anat Anz*, *119*(259), I7.

Schwaner, M. J., Lin, D. C., & McGowan, C. P. (2018). Jumping mechanics of desert kangaroo rats. *Journal of Experimental Biology*, *221*(22). https://doi.org/10.1242/jeb.186700

Screen, H., Bader, D., Lee, D., & Shelton, J. (2004). Local strain measurement within tendon. *Strain*, *40*(4), 157-163.

Shadwick, R. E. (1990). Elastic energy storage in tendons: mechanical differences related to function and age. *Journal of Applied Physiology*, *68*(3), 1033-1040.

Shim, V. B., Fernandez, J. W., Gamage, P. B., Regnery, C., Smith, D. W., Gardiner, B. S., Lloyd, D. G., & Besier, T. F. (2014). Subject-specific finite element analysis to characterize the influence of geometry and material properties in Achilles tendon rupture. *Journal of Biomechanics*, *47*(15), 3598-3604. https://doi.org/https://doi.org/10.1016/j.jbiomech.2014.10.001

Siegler, S., & Liu, W. (1997). Inverse dynamics in human locomotion. *Three-dimensional analysis of human locomotion*, 191-209.

Silva, M. F., & Machado, J. T. (2006). Energy efficiency of quadruped gaits. Climbing and Walking Robots: Proceedings of the 8th International Conference on Climbing and Walking Robots and the Support Technologies for Mobile Machines (CLAWAR 2005),

Silver, F. H., Freeman, J. W., & Seehra, G. P. (2003). Collagen self-assembly and the development of tendon mechanical properties. *Journal of Biomechanics*, *36*(10), 1529-1553.

Spoor, C., Van Leeuwen, J., Meskers, C., Titulaer, A., & Huson, A. (1990). Estimation of instantaneous moment arms of lower-leg muscles. *Journal of Biomechanics*, *23*(12), 1247-1259.

Stenum, J., & Choi, J. T. (2016). Neuromuscular effort predicts walk–run transition speed in normal and adapted human gaits. *Journal of Experimental Biology*, *219*(18), 2809-2813.

Stilwell Jr, D. L. (1957). The innervation of tendons and aponeuroses. *American Journal of Anatomy*, *100*(3), 289-317.

Stosic, J., & Finni, T. (2011). Gastrocnemius tendon length and strain are different when assessed using straight or curved tendon model. *European Journal of Applied Physiology*, *111*(12), 3151-3154.

Suzuki, T., Ogane, R., Yaeshima, K., & Kinugasa, R. (2019). Forefoot running requires shorter gastrocnemius fascicle length than rearfoot running. *Journal of sports sciences*, 1-9. (Journal of sports sciences)

Szaro, P., Witkowski, G., Śmigielski, R., Krajewski, P., & Ciszek, B. (2009). Fascicles of the adult human Achilles tendon–an anatomical study. *Annals of Anatomy-Anatomischer Anzeiger*, *191*(6), 586-593.

Thorstensson, A., & Roberthson, H. (1987). Adaptations to changing speed in human locomotion: speed of transition between walking and running. *Acta Physiologica Scandinavica*, *131*(2), 211-214. (Acta Physiologica Scandinavica)

Treece, G. M., Prager, R. W., Gee, A. H., & Berman, L. (1999). Fast surface and volume estimation from non-parallel cross-sections, for freehand three-dimensional ultrasound. *Medical image analysis*, *3*(2), 141-173.

van Ingen Schenau, G. J. (1989). From rotation to translation: Constraints on multi-joint movements and the unique action of bi-articular muscles. *Human Movement Science*, *8*(4), 301-337.

van Ingen Schenau, G. J., Bobbert, M. F., Huijing, P. A., & Woittiez, R. D. (1985). The instantaneous torque-angular velocity relation in plantar flexion during jumping. *Medicine and Science in Sports and Exercise*, *17*(4), 422-426.

van Ingen Schenau, G. v., Bobbert, M., & Rozendal, R. (1987). The unique action of bi-articular muscles in complex movements. *Journal of anatomy*, *155*, 1.

Van Soest, A., & Casius, L. (2000). Which factors determine the optimal pedaling rate in sprint cycling? *Medicine and Science in Sports and Exercise*, *32*(11), 1927-1934.

Varghese, T. (2009). Quasi-static ultrasound elastography. *Ultrasound clinics*, *4*(3), 323.

Visser, J., Hoogkamer, J., Bobbert, M., & Huijing, P. (1990). Length and moment arm of human leg muscles as a function of knee and hip-joint angles. *European journal of applied physiology and occupational physiology*, *61*, 453-460.

Voigt, M., Bojsen-Møller, F., Simonsen, E. B., & Dyhre-Poulsen, P. (1995). The influence of tendon Youngs modulus, dimensions and instantaneous moment arms on the efficiency of human movement. *Journal of Biomechanics*, *28*(3), 281-291.

Wakeling, J. M., Blake, O. M., Wong, I., Rana, M., & Lee, S. S. (2011). Movement mechanics as a determinate of muscle structure, recruitment and coordination. *Philosophical Transactions of the Royal Society B: Biological Sciences*, *366*(1570), 1554-1564.

Wang, S., Van Dijk, W., & van der Kooij, H. (2011). Spring uses in exoskeleton actuation design. 2011 IEEE International Conference on Rehabilitation Robotics,

Wang, T., Lin, Z., Day, R. E., Gardiner, B., Landao-Bassonga, E., Rubenson, J., Kirk, T. B., Smith, D. W., Lloyd, D. G., & Hardisty, G. (2013). Programmable mechanical stimulation influences tendon homeostasis in a bioreactor system. *Biotechnology and bioengineering*, *110*(5), 1495-1507.

Wells, R. (1988). Mechanical energy costs of human movement: an approach to evaluating the transfer possibilities of two-joint muscles. *Journal of Biomechanics*, *21*(11), 955-964.

Werkhausen, A., Albracht, K., Cronin, N. J., Meier, R., Bojsen-Møller, J., & Seynnes, O. R. (2017). Modulation of muscle–tendon interaction in the human triceps surae during an energy dissipation task. *Journal of Experimental Biology*, *220*(22), 4141-4149.

Werkhausen, A., Albracht, K., Cronin, N. J., Paulsen, G., Bojsen-Møller, J., & Seynnes, O. R. (2018). Effect of training-induced changes in achilles tendon stiffness on muscle–tendon behavior during landing. *Frontiers in Physiology*, *9*, 794.

Werkhausen, A., Cronin, N. J., Albracht, K., Bojsen-Møller, J., & Seynnes, O. R. (2019). Distinct muscle-tendon interaction during running at different speeds and in different loading conditions. *Journal of Applied Physiology*, *127*(1), 246-253.

Wertheim, G. (1847). *Mémoire sur l'élasticité et la cohésion des principaux tissus du corps humain*.

Whittle, M. W. (2014). *Gait analysis: an introduction*. Butterworth-Heinemann.

Wiesinger, H.-P., Kösters, A., Müller, E., & Seynnes, O. R. (2015). Effects of increased loading on in vivo tendon properties: a systematic review. *Medicine and Science in Sports and Exercise*, *47*(9), 1885.

Wiesinger, H.-P., Rieder, F., Kösters, A., Müller, E., & Seynnes, O. R. (2016). Are sport-specific profiles of tendon stiffness and cross-sectional area determined by structural or functional integrity? *PloS one*, *11*(6), e0158441.

Wilson, A. M., McGuigan, M. P., Su, A., & van den Bogert, A. J. (2001). Horses damp the spring in their step. *Nature*, *414*(6866), 895-899. https://doi.org/10.1038/414895a

Winter, D. A. (1995). Human balance and posture control during standing and walking. *Gait & posture*, *3*(4), 193-214.

Winter, D. A. (2009). *Biomechanics and motor control of human movement*. John Wiley & Sons.

Wretenberg, P., Nemeth, G., Lamontagne, M., & Lundin, B. (1996). Passive knee muscle moment arms measured in vivo with MRI. *Clinical biomechanics*, *11*(8), 439-446.

Yang, G., Crawford, R. C., & Wang, J. H. (2004). Proliferation and collagen production of human patellar tendon fibroblasts in response to cyclic uniaxial stretching in serum-free conditions. *Journal of Biomechanics*, *37*(10), 1543-1550.

Yettram, A., & Camilleri, N. (1993). The forces acting on the human calcaneus. *Journal of Biomedical Engineering*, *15*(1), 46-50.

Yin, N.-H., Fromme, P., McCarthy, I., & Birch, H. L. (2021). Individual variation in Achilles tendon morphology and geometry changes susceptibility to injury. *Elife*, *10*, e63204.

Zajac, F. E. (1993). Muscle coordination of movement: a perspective. *Journal of Biomechanics*, *26*, 109-124.

Zajac, F. E., Neptune, R. R., & Kautz, S. A. (2002). Biomechanics and muscle coordination of human walking: Part I: Introduction to concepts, power transfer, dynamics and simulations. *Gait & posture*, *16*(3), 215-232.

Zajac, F. E., & Winters, J. M. (1990). Modeling musculoskeletal movement systems: joint and body segmental dynamics, musculoskeletal actuation, and neuromuscular control. *Multiple muscle systems: Biomechanics and movement organization*, 121-148.

Zarrugh, M., Todd, F., & Ralston, H. (1974). Optimization of energy expenditure during level walking. *European journal of applied physiology and occupational physiology*, *33*(4), 293-306.

Zhang, G., Young, B., Ezura, Y., Favata, M., Soslowsky, L., Chakravarti, S., & Birk, D. E. (2005). Development of tendon structure and function: regulation of collagen fibrillogenesis. *J Musculoskelet Neuronal Interact*, *5*(1), 5-21.

Zhang, Q., Adam, N. C., Nasab, S. H., Taylor, W. R., & Smith, C. R. (2020). Techniques for In Vivo Measurement of Ligament and Tendon Strain: A Review. *Annals of Biomedical Engineering*, 1-22.

Acknowledgments

I would like to express my sincere gratitude to my supervisor, Prof. Adamatios Arampatzis, for his invaluable guidance, expertise, and unwavering support throughout my Ph.D. studies. His mentorship has been instrumental in shaping my academic journey and instilling in me the values of Persistence, Teamwork, and Innovation, not just in words but in action.

I would also like to extend my heartfelt thanks to my colleagues and friends in the training and movement science department of Humboldt University of Berlin, whose kindness and endless support have been a source of motivation and inspiration.

I am deeply grateful to my siblings, my kind mother, and my patient father for their unending love, support, and belief in me, which has been a constant source of strength throughout my academic pursuit.

Finally, I would like to acknowledge the financial support of my Ph.D. studies by the German Academic Exchange Service (DAAD), which has enabled me to pursue my academic and research goals with greater confidence and focus.

Selbstständigkeitserklärung

Statement of authorship

Ich erkläre ausdrücklich, dass es sich bei der von mir eingereichten Arbeit um eine von mir selbstständig und ohne fremde Hilfe verfasste Arbeit handelt.

I expressly declare that the work I have submitted was written independently and without external help.

Ich erkläre ausdrücklich, dass ich sämtliche in der oben genannten Arbeit verwendeten fremden Quellen, auch aus dem Internet (einschließlich Tabellen, Grafiken u. Ä.) als solche kenntlich gemacht habe. Insbesondere bestätige ich, dass ich ausnahmslos sowohl bei wörtlich übernommenen Aussagen bzw. unverändert übernommenen Tabellen, Grafiken o. Ä. (Zitaten) als auch bei in eigenen Worten wiedergegebenen Aussagen bzw. von mir abgewandelten Tabellen, Grafiken o.Ä. anderer Autorinnen und Autoren die Quelle angegeben habe.

I expressly declare that all sources used in the abovementioned work – including those from the Internet (including tables, graphic and suchlike) – have been marked as such. In particular, I declare that I have, without exception, stated the source for any statements quoted verbatim and/or unmodified tables, graphics etc. (i.e. quotations) of other authors.

Mir ist bewusst, dass Verstöße gegen die Grundsätze der Selbstständigkeit als Täuschung betrachtet und entsprechend geahndet werden.

I am aware that violations against the principles of academic independence are considered deception and are punished accordingly.

Berlin, 26 May 2023

Mohamadreza Kharazi